1-1-2003

Synthesis and solid-state NMR characterization of long-chain aliphatic polyesters with regularly spaced "defects".

Maria Gabriele Menges
University of Massachusetts Amherst

SYNTHESIS AND SOLID-STATE NMR CHARACTERIZATION OF LONG-CHAIN ALIPHATIC POLYESTERS WITH REGULARLY SPACED "DEFECTS"

A Dissertation Presented

by

MARIA GABRIELE MENGES

Submitted to the Graduate School of the
University of Massachusetts Amherst in partial fulfillment
of the requirements for the degree of

DOCTOR OF PHILOSOPHY

September 2003

Polymer Science and Engineering

SYNTHESIS AND SOLID-STATE NMR CHARACTERIZATION OF LONG-CHAIN ALIPHATIC POLYESTERS WITH REGULARLY SPACED "DEFECTS"

A Dissertation Presented

by

MARIA GABRIELE MENGES

Approved as to style and content by:

Jacques Penelle, Co-Chair

Klaus Schmidt-Rohr, Co-Chair

Dhandapani Venkataraman, Member

Thomas J. McCarthy, Department Head
Polymer Science and Engineering

DEDICATION

Für meine Eltern

ACKNOWLEDGMENTS

My sincere gratitude is expressed towards my co-advisors Profs. Jacques Penelle and Klaus Schmidt-Rohr. I am very grateful that I had two advisors with such different fields of expertise. This gave me the opportunity to not only strengthen my chemistry background but also to explore a completely new field of polymer characterization, solid-state NMR spectroscopy. I am indebted to them for being excellent and patient teachers, providing me with countless opportunities to present my research, and for challenging me to see beyond the realm of synthetic chemistry. Prof. Schmidt-Rohr has left a lasting impression on me for transforming me from a synthetic chemist to a polymer scientist with a true appreciation for the power and beauty of solid-state NMR. I also want to thank Prof. Dhandapani Venkataraman, the third member of my committee, for valuable advice and helpful suggestions for my project throughout my entire graduate career.

Dr. L. Charles Dickinson is gratefully acknowledged for his tremendous help in keeping the solid-state NMR in great shape and for helping me to solve hardware problems, even after Prof. Schmidt-Rohr's move to Iowa. I am also indebted to Prof. Alan Jonas, Cédric Le Fevere de Ten Hove, and Benoit de Meersman for their in-depth X-ray analysis and their helpful discussions regarding manuscripts.

My fellow group members are acknowledged here for providing a productive and enjoyable work environment. Regarding the Penelle group, I'm particularly grateful to Cédric Le Fevere de Ten Hove who pioneered the research on branched polyesters in our group, and who has been a model for hard work and dedication. All members of the Schmidt-Rohr group, past and present, are gratefully acknowledged for helping me find my way into a new field, and making me comfortable with running the NMR experiments

on my own. Especially, Dan Mowery is acknowledged here for countless hours of teaching me on the spectrometer.

I would like to express thanks to the exceptional support staff in the department. Training provided by Dr. Dickinson (NMR) and Dr. Waddon (X-ray diffraction) was critical for many of the experiments described here. I would also like to thank the secretarial staff, Sophie, Ann, Eleanor, and especially Eileen, who has been tremendously helpful with paperwork. I would also like to thank Andre Mel'cuk for help with any computer problems I ran into, and his tremendous patience with my less than helpful descriptions of those problems.

On a more personal note, I would like to thank the few true friends I have made here, with whom I hope to stay in contact long after graduate school. Namely, I would like to thank Michael Pollard, who lived with me for the first two years and went through all the stages of cumulative exams with me. His friendship and advice during this period was very helpful. Donna Wrublewski has been incredibly supportive through the really hard times, and I will always be indebted to her for her understanding and unlimited patience with me. I would also like to thank my work-out buddy Melissa Light, as well as Greg Constable, Ticora Jones, Lachelle Arnt, and Julie Leiston for friendship and support.

All this would never have been possible was it not for my family. Although my parents cannot share in celebrating the completion of my university education, I am convinced they are watching over me and I will always strive to make them proud. I am incredibly grateful to my sisters Eva and Hiltrud who have accompanied me all the way

through undergraduate and graduate school. They are my worst critics, but also my best friends, advisors, and models for success.

Finally, I would like to thank my loving husband Dave Flanagan. Meeting him 7 1/2 years ago started the adventure of a new life on a different continent, and he has never made me regret it. Without him, I would have given up numerous times along the way, and I have no words describing my love and thanks to him for his continued love, devotion, and support during the good as well as the really bad times. Thank you!

ABSTRACT

SYNTHESIS AND SOLID-STATE NMR CHARACTERIZATION OF LONG-CHAIN ALIPHATIC POLYESTERS WITH REGULARLY SPACED "DEFECTS"

SEPTEMBER 2003

MARIA GABRIELE MENGES,

Diplom JOHANNES GUTENBERG UNIVERSITÄT MAINZ GERMANY

M.S. UNIVERSITY OF MASSACHUSETTS AMHERST

Ph. D. UNIVERSITY OF MASSACHUSETTS AMHERST

Directed by: Professors Jacques Penelle and Klaus Schmidt-Rohr

In order to gain a better understanding of structure-property relationships, particularly the influence of regular versus random branching on the crystallization and polymer morphology of polyethylene, and to obtain chemical control over chain folding and lamellar thickness, model polyesters were synthesized and thoroughly characterized by solid-state NMR. Polyesters with perfectly regular placement of defects along the backbone were obtained by melt polycondensation of long-chain aliphatic α,ω-diols and ^{13}C-labeled short-chain branched and non-branched diacids, diluting the amount of ester functionalities along the backbone by steadily increasing the length of the employed diols from 22 to 32 and then 46 methylene units.

Wide-angle X-ray diffraction established that the minimum diol length necessary to produce polyethylene-like orthorhombic crystal structures is 32 methylene units. A non-branched system used as a benchmark for comparison of long-chain polyesters to polyethylene showed polyesters to possess a polyethylene-like crystal structure with

diester layers. This shows that these long-chain polyesters are valid model systems for polyethylene. However, chain dynamics in the polyester crystallites were found to greatly differ from those in polyethylene. This must be attributed to the diester layering prohibiting chain diffusion.

Small-angle x-ray diffraction of regularly branched polyesters showed the desired control over lamellar thickness, which is invariable under varying crystallization conditions and thermal treatment. The regular placement of the non-crystallizable defects enforces quantization of the length of non-crystalline chain folds. The resulting marked length difference between tight and loose loops affects the crystallinity significantly. Crystallinities determined by solid-state direct polarization NMR were found to be well above 50 %, proving tight chain folds. The location of ester moieties and their mobility was probed by ^{1}H spin diffusion and wideline separation NMR, showing ester groups to be located either on the crystalline/amorphous interface or in the amorphous regions, depending on the length of the diacid segment. Finally, diacid segment conformations were probed by DOQSY NMR, which showed specific conformations of ester moieties compatible with tight chain folds. Future research on this topic should focus on the variation of side groups, incorporating functional groups or reactive side groups that allow for post-polymerization modification of the crystalline/amorphous interface.

TABLE OF CONTENTS

LIST OF TABLES

LIST OF FIGURES

LIST OF SCHEMES

LIST OF ABBREVIATIONS, ACRONYMS, AND SYMBOLS

2D.....two dimensional

δ .....unit cell angle of the bc plane

a.....unit cell length

Å.....Ångstrom

ADMET .....acyclic diene metathesis

aq..... aqueous

Ar ..... argon

au.....arbitrary units

δ ..... unit cell angle of the ac plane

b.....unit cell length

δ.....unit cell angle of the ab plane

c.....unit cell length

°C .....degree Celsius

C_6D_6.....deuterated benzene

$CDCl_3$ .....deuterated chloroform

CSA.....chemical shift anisotropy

CP..... cross polarization

δ..... NMR solution chemical shift in ppm downfield with respect to tetramethylsilane

δ ..... change

δ .....heat

δT.....supercooling

d.....doublet

d_4-MeOH ..... deuterated methanol

d_6-DMSO ..... deuterated diemthylsulfoxide

dl ..... doubly labeled

DOQSY ..... double quantum spectroscopy

DP ..... direct polarization

DSC ..... differential scanning calorimetry

e. g. ..... for example

Eq ..... equation

et al. ..... and others

f_c ..... crystalline fraction

FT ..... Fourier transformation

FTS ..... Fourier transform spectroscopy

g ..... gram

G ..... Gibbs free energy

GPC ..... gel permeation chromatography

H ..... enthalpy

h ..... hours

h ..... crystallographic index (hkl)

HDPE ..... high-density polyethylene

H_f ..... enthalpy of fusion

HPLC ..... high-pressure liquid chromatography

Hz ..... Hertz

I ..... intensity

i.e. ..... that is

IR ..... infrared

J ..... coupling constant in NMR

k ..... kilo(10^3)

k ..... crystallographic index (hkl)

K ..... Kelvin

l ..... crystal thickness

l ..... liter

l ..... crystallographic index (hkl)

L_a ..... amorphous thickness

L_c ..... crystalline thickness

LDPE ..... low density polyethylene

LG CP ..... Lee-Goldburg cross polarization

lit ..... literature

LLDPE ..... linear low-density polyethylene

L_p ..... long period

μ ..... micro(10^{-6})

m ..... meter

m ..... milli(10^{-3})

m ..... multiplet (NMR)

m ..... molar

M ..... mega(10^6)

MAS ..... magic angle spinning

min ..... minute

ml ..... monolabeled

mol ..... mole

m.p. ..... melting point

M_n ..... number-average molecular weight

M_w ..... weight-average molecular weight

n ..... nano(10^{-9})

n. a. ..... not applicable

N_2 ..... nitrogen

NMR ..... nuclear magnetic resonance

NOE ..... Nuclear Overhauser Effect

p ..... para

p-TsOH ..... p-toluenesulfonic acid

PDI ..... polydispersity index

PE ..... polyethylene

PET ..... poly(ethylene terephtalate)

PL ..... Polymer Laboratories

ppm ..... parts per million

PUREX ..... pure exchange NMR

q ..... quartet (NMR)

ρ ..... density

RI ..... refractive index

RT ..... room temperature

τ ..... principal axis

τ_e ..... free energy of the fold surface

s ..... second

s ..... singlet (NMR)

S ..... entropy

SAXS ..... small-angle X-ray scattering

sec ..... second

τ_{DQ} ..... double quantum excitation and reconversion delays

T ..... temperature

T ..... Tesla

t ..... time

t ..... triplet (NMR)

$T_{1\tau}$ ..... longitudinal relaxation time in the rotating frame

$T_{1,C}$ ..... ^{13}C longitudinal relaxation time in the laboratory frame

T_2 ..... transverse relaxation time

TA ..... Thermal Analysis

T_c ..... crystallization temperature

T_d ..... decomposition temperature

T_m ..... melting temperature

TGA ..... thermogravimetric analysis

THF ..... tetrahydrofuran

TPPM ..... two-pulse phase modulation

ul ..... unlabeled

WAXS.....wide-angle X-ray scattering

WISE..... wideline separation

% .....percent

)))..... sonication

CHAPTER 1

INTRODUCTION AND BACKGROUND

1.1 Introduction

Polymers are unique among materials, and possess properties that make them arguably the most important development in materials science in the 20th century. Unlike, for example, metals or ceramics, polymers, when crystallizable, display both crystalline and amorphous regions. The amorphous regions result from the long chains of the polymer, which, for kinetic reasons, are unable to disentangle and line up to produce a thermodynamically more stable crystalline structure. It is the simultaneous presence of both crystalline and amorphous regions in the same material that is responsible for the many important macroscopic properties of semi-crystalline polymers, including melting temperature, flexibility, toughness, and strength. By studying the properties of the microstructure of semicrystalline polymers, we can learn how to further improve these properties and make even more useful polymeric materials for the 21st century. These include advanced semicrystalline materials designed by Nature such as spider silk.[1]

It is known that the structural variables that play a crucial role in the resulting macroscopic properties are the level of crystallinity, the crystal thickness distribution, and the structure and relative amount of interfacial and fully amorphous regions. Control over these variables can be achieved by systematic control over molecular structure, molecular weight, and crystallization conditions.[2] As can be imagined, it is the orchestrated combination of these variables that governs the final properties. The sheer number of combinations for these variables makes the study of polymer crystallization a

difficult and multifaceted problem that is tackled every day by both academic scientists seeking to understand the process of crystallization and by industrial researchers trying to produce improved products.[3-5]

It is the goal of this study to synthesize and thoroughly characterize systems that model polyethylene, which is the most widely used and studied semi-crystalline polymer. These model systems are designed to have polyethylene-like characteristics provided by a polymethylene backbone, but perturbed at regular distances by the inclusion of ester moieties of various types (aliphatic, aromatic, with or without additional pending groups). We propose that the inclusion of ester moieties bearing side branches will induce chain "folding", and thus provide precisely defined microstructures. These polyethylene models will permit the study of the connections between chemical microstructure and the resulting polymer crystallization, the produced crystal structure with precisely controlled chain folding, and the resulting chain dynamics. They will also be used to study the interface between amorphous and crystalline regions at the molecular level.

1.2 Crystallization Behavior of Semi-Crystalline Polymers

1.2.1 General Considerations

At the almost atomic level, crystal structures of semicrystalline polymers can be described in the same way as is done for small molecules. Through favorable interactions such as dispersion forces, hydrogen bonding, or dipole-dipole interactions, the chains pack closely together in a three-dimensional array. These close packed arrangements are described by the assignment of a repetitive unit cell of certain dimensions containing the minimum number of monomer units required to completely

describe the packing arrangement. Each unit cell is described through its three lateral dimensions a, b, and c, and three angles α, β, and γ. There are 14 translational lattices used to describe crystal arrangement, as first reported by Bravais.[8] Through the use of X-ray analysis and electron microscopy, it is often possible to determine the particular unit cell and corresponding number of chains that a given polymer will adopt. As an example, the unit cell of polyethylene is shown in Figure 1.1.

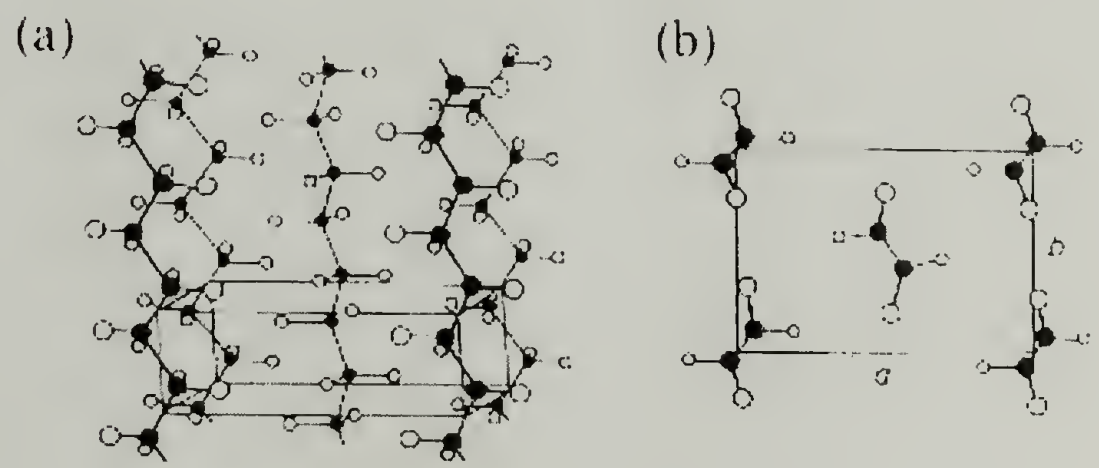

Figure 1.1 Crystal structure of orthorhombic dense packing in polyethylene.[6]

The choice of a particular unit cell is dependent on structural variables such as the monomer repeat unit, tacticity and chain architecture (branch nature and content), and any favorable interactions derived from these variables. The ability to minimize the entropic penalty associated with the ordering process, *via* some conformational pre-arrangement of small units, is also favorable. For a given semicrystalline polymer,

variables that influence the percent crystallinity and crystal size are the molecular weight, cooling rate, crystallization time and temperature.

Some trends are commonly observed for the crystallization of all semicrystalline materials. In general, crystallites consist of lamellae with thicknesses ranging from 5 nm for rapidly crystallized random copolymers to several hundred nanometers for homopolymers annealed for long periods of time.[7-11] The molecular weight has a pronounced influence on the lamellar structure and crystallinity as well, as it becomes increasingly more difficult for longer chains to disentangle and form extended structures. Random introduction of non-crystallizable co-units along the polymer backbone rapidly reduces crystallinity and ultimately yields a fully amorphous polymer microstructure.[12] The lamellae are separated by interfacial and amorphous regions containing tie chains that provide the well-known mechanical strength of polymers. For these reasons, chain folding is critical in order to understand polymer crystallization.

In 1957, Keller succeeded in preparing single crystals of polyethylene from dilute solution. These crystals possessed crystal thicknesses of 110-140 Å, whereas the contour length of the polymer was known to be on the order of 2000 Å. Keller concluded that the polymer chains had to be folded upon themselves,[13] a hypothesis that was soon confirmed by Fischer and Till.[14,15] Two main models for chain folding and reentry of chains into the crystalline region have been proposed as shown in Figure 1.2.

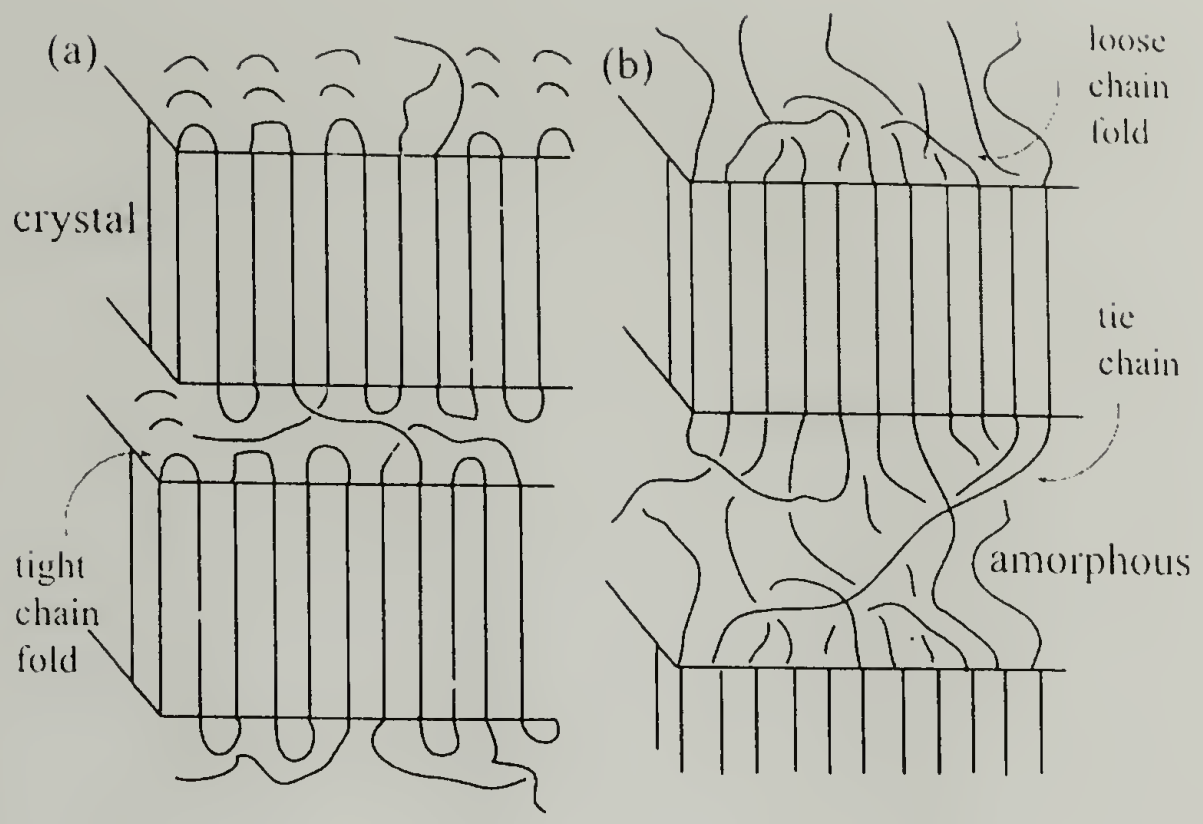

Figure 1.2 Chain-folding models: (a) adjacent reentry model (b) switchboard model.

The adjacent reentry model, proposed by Hoffman and Lauritzen, assumes chains to be folded tightly in hairpin turns, and is based on small-angle neutron scattering and infrared studies of single crystals.[16] Bulk crystallized samples, however, show a more complex behavior. To accommodate this complexity, Flory proposed a switchboard model with loose loops of variable length and tie chains connecting adjacent crystalline regions.[17] Real systems are generally expected to combine elements of both models with the evolution of from one to the other, depending on the chemical structure, branch content and crystallization mode (melt or solution).

On the next hierarchical level, lamellar structures are organized into higher-order superstructures, the most common one being spherulites. These supermolecular structures are, again, dependent on molecular weight and crystallization conditions, and can be completely absent for polymers of either very high molecular weight or having

significant non-crystallizable comonomer content.[18] Generally, crystallization from the melt leads to the formation of nuclei, from which lamellae grow radially outward until they impinge upon each another. The growth of spherulites can be followed by optical microscopy through crossed polarizers, in which the spherulites show a characteristic Maltese cross pattern. Individual lamellae are held together by tie chains. Figure 1.3 shows a schematic model for spherulite growth.

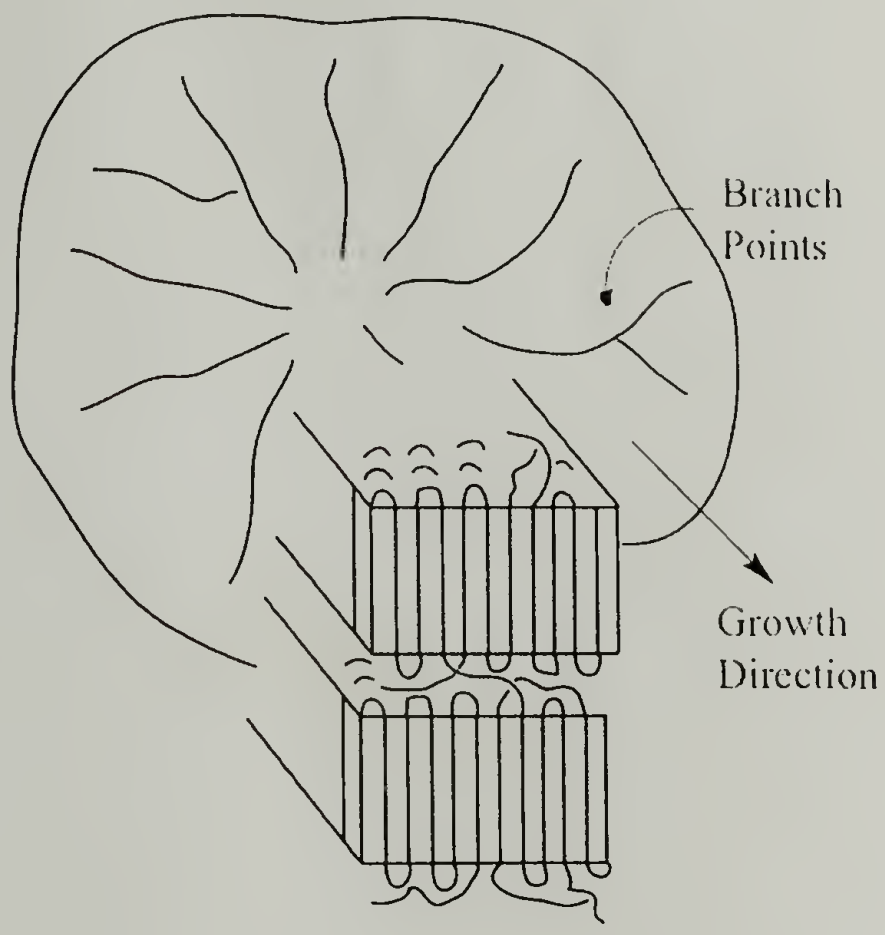

Figure 1.3 Model of spherulitic structure.

In order to better understand polymer crystallization and the presence of both crystalline and amorphous regions, the thermodynamics of crystallization have to be considered first. The difference in Gibbs free energy (ΔG) between the crystal and the

melt of any systems is related to the difference in enthalpy (ΔH) and entropy (ΔS) (Equation 1.1).

$$\Delta G = \Delta H - T\Delta S \tag{1.1}$$

Crystallization will be favored thermodynamically, if the change in enthalpy ΔH is larger than the product of temperature T and change in entropy ΔS.[6] As a result, if the polymer is cooled to a temperature below its melting point, crystallization may occur. Crystallization will lead indeed to a considerable reduction in entropy (large ΔS) offset by a large reduction in enthalpy.

These thermodynamic considerations are only strictly applicable to systems at equilibrium. This is demonstrated by the fact that the most thermodynamically favored, lowest free energy crystal would be the fully extended chain. This ideal structure, however, is virtually impossible to achieve on a practical time scale, as crystallization is governed by kinetics. In an extreme case, polymers that are rapidly cooled from the melt have no time to disentangle and align, and result in a completely amorphous structure.

According to the kinetic crystallization theory of Hoffman and Lauritzen, chain folding and lamellar formation are under kinetic control with the chain folded lamellae being metastable.[19-21] Based on this theory, a polymer will fold during crystallization if the energy penalty in forming the fold is compensated by the gain in enthalpic energy when the section of polymer with length l_c is incorporated into the cystal.[22] The obtained crystal thickness, l_c, is given by equation 1.2. It is dependent on the fold surface energy σ_e, as well as the amount of supercooling, ΔT and the enthalpy of fusion, ΔH_f.[22]

$$l_c = 2\sigma_e T_m^{\circ} (\Delta H_f(\Delta T))^{-1} \qquad (1.2)$$

In the following, the crystal structures of two classes of polymers relevant to this study, polyethylene and polyesters, will be discussed in more detail.

1.2.2 Polyethylene

Polyethylenes can be divided into three major classes, depending on the density of the material. Low-density polyethylene (LDPE) possesses densities of 0.91-0.935 g/mol and crystallinities of 30-50 %.[23] It is synthesized under high pressure and at high temperatures under free-radical conditions.[24] As a result of side reactions during the polymerization, it contains a large number of long- and short-chain branches. The short-chain branches originate from backbiting reactions, creating mostly butyl and hexyl branches. Long-chain branches are created by chain-transfer of growing polymer chains to other polymer chains. LDPE is used in a broad variety of applications, such as blown films for bags and packaging. Its use in high performance applications is limited by its poor resistance to oxidizing agents and solvents, as well as its low softening point.[23]

On the other end of the polyethylene spectrum is high-density polyethylene (HDPE), which has densities in the range of 0.92-0.99 g/mol, depending on molecular weight and crystallization conditions, and crystallinities of 35-90 %.[25] It is synthesized by metal coordination polymerization of ethylene, and has a low branch content.

In between those two classes lies linear low-density polyethylene (LLDPE). This class of polyethylene is synthesized by metal coordination copolymerization of ethylene

and α-olefins. The latter are used to introduce branches of specific lengths. The most common comonomers are 1-butene, 1-hexene, and 1-octene, leading to ethyl, n-butyl, and n-hexyl branches, respectively.[26] Conventional Ziegler-Natta catalysts yield polymers with a highly heterogeneous intermolecular distribution of comonomer units along the polymer backbone, with the branches predominantly found in the lower molecular weight chains. [12] Therefore, Ziegler-Natta LLDPE generally behaves as if it were a blend of high molecular weight HDPE and low molecular weight LDPE. The main difference between LLDPE and LDPE is the absence of long-chain branches and a narrower molecular weight distribution.

A new class of catalysts, the single-site metallocenes, were first reported as catalysts in ethylene polymerization by Breslow and Newburg[27] and have been the subject of increasingly intense academic and industrial research.[28,29] The catalysts are mainly based on group IV transition metals, predominantly titanium and zirconium, and require a coactivator such as methylaluminoxane. The polymers these catalysts produce differ significantly from conventional Ziegler-Natta LLDPE, as they possess a narrower molecular weight distribution ($M_w/M_n \sim 2$), and a random comonomer distribution along all chains.[30] For the purpose of our study, these metallocene polymers are the most similar to our regularly branched polyethylene models, and so their structure-property relationships will be discussed in more detail.

Mandelkern and co-workers performed a large number of studies on the structural properties of ethylene copolymers.[11,12,31-39] They observed similar melting temperature-composition relations for varying branch lengths, and concluded that since long and bulky side chains cannot be accommodated by the crystalline lattice of polyethylene,

ethyl and longer branches are excluded from the crystalline phase.[31] They also found that although composition and molecular weight distribution affect the crystallization behavior, the nature of the branch did not play a role as long as it is sufficiently large to be excluded from the crystalline regions.[38] It was concluded that, for a random copolymer, the crystalline phase remains "pure" and is only affected by the mole percentage of non-crystallizing units introduced into the backbone. Issues related to the validity of the two-phase model of crystalline and amorphous regions, and nature and size of interfacial regions, remained controversial.

Recent years have seen increased interest in the study of well-defined microstructures of metallocene polyethylene, as control over molecular architecture yields greater control over processing characteristics and improvement of physical properties.[40-42] Baker and Windle studied not only the influence of branch incorporation on polymer melting behavior and crystal structure, but also the short chain branch location within the polyethylene microstructure.[43-45] They found that unit cell parameters of polyethylene crystals were affected by random *vs.* heterogeneous branch distribution, and concluded that branches were partially included into the crystalline component. A third, very important observation was the existence of an intermediate, partially ordered component, which had been proposed theoretically[17,46] and observed by solid-state NMR.[47-49] This intermediate component has been reviewed by Mandelkern.[50] The nature of this component is dependent on many factors such as molecular weight, crystallization conditions, heat treatment, branch content, and branch distribution. The broad range of variables explains the variety of findings reported in the literature and the lack of definitive characterization of this partially ordered component.

Considering the still controversial questions about short-chain branch inclusion, and the nature of a third, intermediate component, it is evident that model systems allowing for exact control over one or more variables would be highly beneficial.

1.2.3 Polyesters

In the late 1920s, Carothers and coworkers at DuPont performed the first systematic structural study of polyesters.[51] In the late 1930s and early 1940s, Fuller and coworkers examined a series of polyesters derived from ethylene glycol and trimethylene glycol.[52-55] Since these early studies, a large number of investigations on specific polyesters has been performed.[56-65] Generally, short-chain polyesters (containing 2-10 methylene segment between diol and diacid functionalities) are found to crystallize in either a monoclinic unit cell containing two chains per unit cell, or an orthorhombic structure with four chains per unit cell, depending on odd-even effects as well as on gliding of ester planes.[60,66] Not surprisingly, polyester crystallization was found to be strongly influenced by dipole-dipole interactions between ester groups of neighboring chains. This yielded intermolecular forces intermediate between those of polyamides and polyethylene.[58] It was found that many of the studied short-chain polyesters had c axis cell dimensions that were significantly shortened from the expected planar extended zigzag values. Over the years, this has been attributed to specific torsional angle sequences containing a pair of gauche bonds of opposite sign separated by one or more trans bonds.[56,67] These pairs of gauche bonds were called "kinks". Liau and Boyd concluded that these kinked structures were more stable than planar all-trans structures due to comparable energy penalties for forming them as opposed to planar all-trans

structures. However, after reaching an aliphatic length of 6-10 methylene units between ester groups, the packing in planar form is less perturbed by the ester groups, and planar packing is favored as the intramolecular penalty for kink formation becomes apparent.[68] The shortening of the observed lengths of chemical repeat units from the calculated lengths of the fully extended zigzag forms in polyesters derived from ethylene glycol was ascribed to distortions in the ethylene glycol unit.[56,57,67]

Another important aspect in the crystallization of aliphatic polyesters is the observation of ester layering between chains in the crystal structure driven by dipole-dipole interactions.

In conclusion, it is generally found that, in the limit of long aliphatic segments separating the ester moieties, the crystal structures of aliphatic polyesters approach the one observed for polyethylene,[56,58,65,68] rendering them valuable as models for polyethylene chain folding, provided that aliphatic segments between ester moieties are of adequate lengths.

1.3 Objective

1.3.1 Previous Work

The study of crystallization and chain folding of polymers has long been a key focus point in polymer research. Since Keller[13] established the general concept of polymer chains becoming kinetically trapped in a chain-folded architecture during crystallization, a number of studies have been undertaken to gain control over the location and nature of these chain folds.

Tirrell and coworkers showed that periodic polypeptides of perfectly monodisperse molecular weight could be induced to form tight chain folds when crystallized in solution by incorporating a set of amino acids known to generate β-turns.[69] Lokey and Iverson introduced aromatic donor and acceptor groups based on functionalized naphtalenes to yield pleated, chain folded structures in polydisperse synthetic polymers.[70] Irwin synthesized chain folded thermotropic polyesters by incorporating a isophthaloyldiphenyl unit, which forms a resonance-stabilized 180°-folded conformation, allowing for the extended, linear segments to adopt a parallel alignment.[71]

All these previous studies indicated that control over chain folding can be achieved in synthetic polymers by incorporating short segments forcing the backbone to adopt a chain-folded conformation. Yet, control over the crystallization of polyethylene and the resulting tunability of its physical properties is still a challenging target. While control over homogeneous branch incorporation in ethylene polymerization has improved as catalysts have evolved from Ziegler-Natta to metallocene systems, branches are still distributed randomly along the polymer backbone. In order to gain control over chain folding by exclusion of sufficiently long branches into the amorphous regions, a mechanism for perfectly regular branch incorporation has to be found.

By modeling the effect of short-chain branches on chain folding behavior, both Iwata and Zhang independently found that branches larger than methyl groups were always excluded from the lamellar structure. Additionally, a critical number of branches was required to form an ideal chain folded structure. Chains with homogeneous

branching were found to form lamellae with thicknesses equal to the length between branch points.[72,73]

Using acyclic diene metathesis (ADMET), first introduced by Wagener and coworkers in 1991[74], it should be possible to gain control over placement of branches by step growth polymerization of α,ω-dienes bearing a branch point in the middle of the monomer unit. Use of this strategy for the synthesis of polyethylenes regularly substituted at short distances along the backbone indicated that achieving perfect control over methyl branch placement had a profound influence on the thermal behavior. Increasing spacing led to an increase in melting point and heat of fusion. It was also shown that the β relaxation for these methylene-substituted polyethylenes is independent on the frequency of branching.[75,76] Although these findings demonstrate the applicability and usefulness of ADMET polymerization in the synthesis of polyethylene regularly substituted by alkyl branches located at short distances, multi-step synthesis required for the monomers, made it an impractical route to systems containing branches at long distances such as the ones targeted in this study.

Research in the Penelle group on the synthesis of polyethylene-like polymers has focused on incorporation of defect units *via* polycondensation of long-chain diols and variable short-chain diacids or diisocyanates. Schall attempted to control chain folding by the incorporation of perfluorinated short-chain diacids. While it was expected that the segments would not be able to cocrystallize, it was found that stable co-crystallizing structures were formed.[77] McKiernan attempted to control chain folding in long-chain aliphatic polyurethanes by introducing intramolecular hydrogen bonds. However, even an aliphatic spacer of 46 methylene units between hydrogen bonding sites did not allow

for control over chain folding. Intermolecular, rather than intra-loop, hydrogen bonds were formed.[78] Le Feverc de Ten Hove achieved control over chain folding and lamellar thickness through the incorporation of propyl branches into a polyethylene-like polyester backbone. The lamellar thickness was found to be independent of crystallization conditions or thermal treatment, rendering it truly controlled by chemical design.[79] The further development of this approach and the in-depth characterization of the so-obtained branched structures will be discussed in the next section.

Methodologies developed by Schmidt-Rohr and coworkers has laid the groundwork in terms of solid-state NMR experiments used in this study. The development of sophisticated solid-state NMR techniques such as DOQSY NMR and ^{1}H spin diffusion will allow us to determine the specific conformation of diacid segments and assess the exact location of ester moieties.[80,81] The work performed by Hu on the determination of crystallinity[82] and by Mowery on the nature of intermediate component in the polyethylene microstructure[49] served as helpful guides in the investigations of the polyesters studied in this thesis.

1.3.2 Specific Goals

This project expands on the previous work performed by Le Fevere de Ten Hove to utilize branched polyesters as model systems to control and study polyethylene chain "folding" and crystallization. The targeted structures consisted of polyesters made of long-chain aliphatic α,ω-diols, serving to mimic polyethylene, interrupted by the placement of short-chain diacids bearing "defects". These "defects" were introduced to perturb the crystallization process in a controlled way and to affect the resulting crystal

structures. The structure of all the polyesters considered in this thesis is summarized in Scheme 1.1.

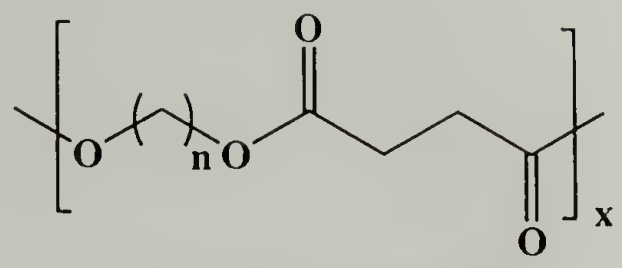

n = 22, 32/12 Succinate

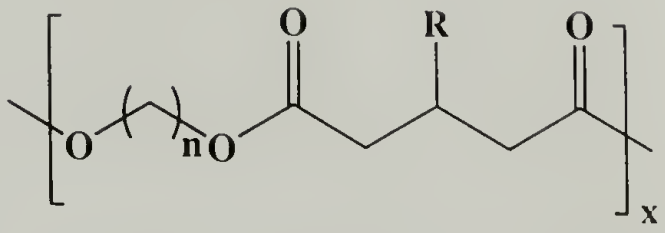

n = 22, 32, 46 R = Prop, Ph Glutarate

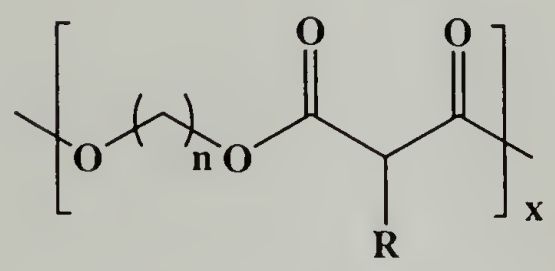

n = 22, 32, 46 R = Hex, Ph Malonate

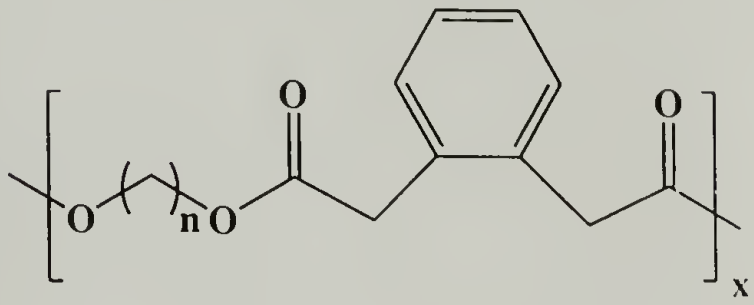

n = 22, 32, 46 1,2-Phenylenediaceate

Scheme 1. 1 Structure of the polyesters examined in this thesis.

Chapter 2 describes the synthesis of three long-chain diols of varying lengths that were used to systematically increase the aliphatic spacer between "defects" from 22 to 46 methylene units. It also describes the synthesis of a variety of ^{13}COO-labeled branched and non-branched diacids. The ^{13}C-labeling enabled the use of sophisticated solid-state NMR experiments to elucidate chain conformation and packing, as well as dynamics studies through spin diffusion and relaxation time measurements. Chapter 3 describes the two polymerization pathways utilized in this work to yield sufficiently high molecular weight polymers.

This general approach yielded polymers incorporating functional polar ester groups that obviously differentiates them from true polyethylene-like polymers. A first

objective of this study was to establish whether these polyesters constituted reasonable models for polyethylenes. Chapter 4 describes the WAXS and thermal characterization that was performed to determine the minimum aliphatic spacer length between branch points necessary for obtaining a polyethylene-like crystallization, and to probe changes in thermal behavior when systematically increasing the polyethylene-like character of these polyetsers. By relating the WAXS patterns and obtained thermal properties to the structural features introduced by varying the diol length and branch nature, some insight into structure-property relationships was gained.

In order to determine the influence of ester group incorporation on the resulting polymer crystal structure and dynamics, one specific model polyester was synthesized with varying labeling content. Chapter 5 describes the in-depth structural characterization by SAXS and solid-state NMR that allowed for the determination of similarities and discrepancies at varying length scales between long-chain polyesters and polyethylene. It was a major goal of this study to prove the validity of using polyesters as model compounds by showing that the ester groups are only minor disturbances incorporated into an otherwise polyethylene-like backbone.

As had been established by Le Fevere de Ten Hove, introduction of a propyl branch separated by a sufficiently long methylene segment (44 units) yielded a single lamellar thickness invariable with thermal treatment.[79] Exclusion of branches into the amorphous region was shown to be a strong enough driving force for chain "folding".

Chapter 6 describes a variety of polymers with branched segments of varying nature that build upon and expand that concept. SAXS and solid-state NMR confirmed that lamellae of a single thickness form, controlled by the length of the diol used in the

polyesterification. The defect location and mobility, nature of chain folds, degrees of crystallinity, and polymer dynamics were systematically studied for varying defect content and nature. The chapter examines and confirms the formation of chemically controlled lamellar thicknesses and tight chain folding.

1.4 Summary of Each Chapter

Chapter 2: Synthesis and Characterization of Diol and Diacid Monomers. A review of synthetic methodology, characterization, and overall yields is given for long-chain aliphatic α,ω-diols and ^{13}COO-labeled short-chain α,ω–diacids. The monomers are synthesized following modified but well-established literature procedures. Characterization of the long-chain aliphatic α,ω-diols shows a solid-solid phase transition attributed to a rotator phase, which has previously been observed for the long-chain diols.

Chapter 3: Synthesis of Polyethylene-like Polyesters derived from Long-Chain Diols. Two synthetic approaches to polyethylene-like polyesters, based on direct polyesterification as well as transesterification of malonates, are presented. The characterization of the resulting polyesters by ^{1}H- and ^{13}C-NMR as well as IR spectroscopy is described. Characterization of polyesters by GPC revealed the successful polymerization to molecular weights of $5\text{-}30 \cdot 10^3$ g/mol with polydispersity indices around the expected theoretical value of 2.

Chapter 4: Characterization of the Morphology of Polyethylene-like Polyesters Derived from Long-Chain Diols. Thermal characterization reveals an increase in polyethylene-like behavior with increasing diol segment lengths, manifested by an increase in observed melting points. The morphology of synthesized long-chain

polyesters is probed by WAXS. It is found that non-branched polyesters crystallize in polyethylene-like orthorhombic unit cells, independent of diol segment length Branched polyesters, however, only achieve polyethylene-like ordered crystallization when the methylene segment length is 32 or higher.

Chapter 5: Solid-State NMR Characterization of Non-Branched Long-Chain Polyesters. A detailed analysis of crystal structure and dynamics probed at various length scales for one specific non-branched polyester is presented and compared with polyethylene. It is shown by DOQSY and ^{1}H spin diffusion NMR that ester moieties can be incorporated into a polyethylene-like unit cell. Clustering of diester layers as observed for shorter chain polyesters is found, suppressing chain flips and chain diffusion as observed in polyethylene. A polymer microstructure is found that features high crystallinity and loose chain folds made of a whole diol segment.

Chapter 6: Solid-State NMR Characterization of Branched Long-Chain Polyesters. SAXS and solid-state NMR show control over chain folding and crystal thickness in branched polyesters. SAXS shows single lamellar thicknesses corresponding to a single diol segment length, that is not influenced by varying crystallization conditions or annealing. High crystallinities serve as proof of the formation of a structure with tight chain folds. Proton spin diffusion and WISE experiments show that ester moieties are either located at the crystal/amorphous interface or in the amorphous regions, depending on the length of the short-chain diacid.

1.5 References

(1) Kubik, S. *Angew. Chem. Int. Ed.* **2002**, *41*, 2721.

(2) Mandelkern, L.; Peacock, A. J. In *Stud. Phys. Theor. Chem.*; Lacher, R. C., Ed.; Elsevier Science B. V.: Amsterdam, 1988; Vol. 54, pp 201-227.

(3) Strobl, G. R. *Eur. Phys. J. E* **2000**, *3*, 165.

(4) Lotz, B. *Eur. Phys. J. E* **2000**, *3*, 185.

(5) Muthukumar, M. *Eur. Phys. J. E* **2000**, *3*, 199.

(6) Young, R. J.; Lovell, P. A. *Introduction to Polymers*; 2nd ed.; Chapman & Hill: London, 1991.

(7) Mandelkern, L.; Price, J. M.; Gopalan, M.; Fatou, J. G. *J. Polym. Sci., A-2* **1966**, *4*, 385.

(8) Voigt-Martin, I. G.; Mandelkern, L. *J. Polym. Sci., Polym. Phys. Ed.* **1984**, *22*, 1901.

(9) Voigt-Martin, I. G.; Alamo, R. G.; Mandelkern, L. *J. Polym. Sci., Polym. Phys. Ed.* **1986**, *24*, 1283.

(10) Stack, G. M.; Mandelkern, L.; Voigt-Martin, I. G. *Polym. Bull.* **1982**, *8*, 421.

(11) Axelson, D. E.; Mandelkern, L.; Popli, R.; Mathieu, P. *J. Polym. Sci., Polym. Phys. Ed.* **1983**, *21*, 2319-2335.

(12) Alamo, R. G.; Domszy, R. C.; Mandelkern, L. *J. Phys. Chem.* **1984**, *88*, 6587.

(13) Keller, A. *Philos. Mag.* **1957**, *2*, 1171.

(14) Fischer, E. W. *Z. Naturforsch.* **1957**, *12a*, 753.

(15) Till, P. H. *J. Polym. Sci.* **1957**, *24*, 301.

(16) Hoffman, J. D.; Lauritzen, J. I. *J. Res. Nat. Bur. Stand. Sect. A. Phys. Chem.* **1961**, *65A*, 297.

(17) Flory, P. J. *J. Am. Chem. Soc.* **1962**, *84*, 2857.

(18) Glotin, M.; Mandelkern, L. *Macromolecules* **1981**, *14*, 1394.

(19) Hoffman, J. D.; Davis, G. T.; Lauritzen, J. I. In *Treatise on Solid State Chemistry*; Hannay, N. B., Ed.; Plenum: New York, 1976; Vol. 3.

(20) Hoffman, J. D. *Polymer* **1982**, *23*, 656.

(21) Hoffman, J. D. *Polymer* **1983**, *24*, 3.

(22) Hoffman, J. D. *SPE Transactions* **1964**, 315.

(23) Prasad, A. In *Polymer Data Handbook*; Oxford University: Oxford, 1999, p 518.

(24) Doak, K. W.; Schrage, A. In *Crystalline Olefin Polymers Part 1*; Raff, R. A. V., Doak, K. W., Eds.; Interscience: New York, 1965.

(25) Mandelkern, L.; Alamo, R. G. In *Polymer Data Handbook*; Oxford University: Oxford, 1999, p 493.

(26) Prasad, A. In *Polymer Data Handbook*; Oxford University: Oxford, 1999, p 508.

(27) Breslow, D. S.; Newburg, N. R. *J. Am. Chem. Soc.* **1957**, *79*, 5072.

(28) Spaleck, W. *Organometallics* **1994**, *13*, 954.

(29) Soga, K. *Macromol. Symp.* **1996**, *101*, 281.

(30) Prasad, A. In *Polymer Data Handbook*; Oxford University: Oxford, 1999, p 529.

(31) Alamo, R. G.; Mandelkern, L. *Macromolecules* **1989**, 22, 1273.

(32) Alamo, R. G.; VanderHart, D. L.; Nyden, M. R.; Mandelkern, L. *Macromolecules* **2000**, *33*, 6094-6105.

(33) Alamo, R. G.; Viers, B. D.; Mandelkern, L. *Macromolecules* **1995**, *28*, 3205-3213.

(34) Alamo, R. G.; Viers, B. D.; Mandelkern, L. *Macromolecules* **1993**, *26*, 5740-5747.

(35) Failla, M. D.; Lucas, J. C.; Mandelkern, L. *Macromolecules* **1994**, *27*, 1334-1337.

(36) Graham, J. T.; Alamo, R. G.; Mandelkern, L. *J. Poly. Sci., Polym. Phys. Ed.* **1997**, *35*, 213-223.

(37) Hagemann, H.; Snyder, R. G.; Peacock, A. J.; Mandelkern, L. *Macromolecules* **1989**, *22*, 3600.

(38) Isasi, J. R.; Haigh, J. A.; Graham, J. T.; Mandelkern, L.; Alamo, R. G. *Polymer* **2000**, *41*, 8813-8823.

(39) Lu, L.; Alamo, R. G.; Mandelkern, L. *Macromolecules* **1994**, *27*, 6571-6576.

(40) Crist, B.; Howard, P. R. *Macromolecules* **1999**, *32*, 3057.

(41) Janimak, J. J.; Stevens, G. C. *Polymer* **2000**, *41*, 4233.

(42) Vanden Eyde, S.; Mathot, V. B. F.; Koch, M. H. J.; Reynaers, H. *Polymer* **2000**, *41*, 4889.

(43) Baker, A. M. E.; Windle, A. H. *Polymer* **2001**, *42*, 651.

(44) Baker, A. M. E.; Windle, A. H. *Polymer* **2001**, *42*, 667.

(45) Baker, A. M. E.; Windle, A. H. *Polymer* **2001**, *42*, 681.

(46) Kumar, S. K.; Yoon, D. Y.; Dill, K. A. *Macromolecules* **1989**, *22*, 3458.

(47) Shimizu, Y.; Harashina, Y.; Sugiura, Y.; Matsuo, M. *Macromolecules* **1995**, *28*, 6889.

(48) Eckman, R. R.; Henrichs, P. M.; Peacock, A. J. *Macromolecules* **1997**, *30*, 2474-2481.

(49) Mowery, D. M.; Schmidt-Rohr, K. *Polymeric Materials: Science & Engineering* **2001**, *85*, 35.

(50) Mandelkern, L. *Chemtracts (Macromol. Chem.)* **1992**, *3*, 347.

(51) Carothers, W. H.; Arvin, J. A. *J. Am. Chem. Soc.* **1929**, *51*, 2560.

(52) Fuller, C. S.; Erickson, C. L. *J. Am. Chem. Soc.* **1937**, *59*, 344-351.

(53) Fuller, C. S.; Frosch, C. J. *J. Am. Chem. Soc.* **1939**, *61*, 2575.

(54) Fuller, C. S. *Chem. Rev.* **1940**, *26*, 143-167.

(55) Fuller, C. S.; Frosch, C. J.; Pape, N. R. *J. Am. Chem. Soc.* **1942**, *64*, 154-160.

(56) Ueda, A. S.; Chatani, Y.; Tadokoro, H. *Polym. J.* **1971**, *2*, 387.

(57) Kanamoto, T.; Tanaka, K. *J. Polym. Sci.: Part A-2* **1971**, *9*, 2043.

(58) Kanamoto, T. *J. Polym. Sci., Polym. Phys. Ed.* **1974**, *12*, 2535.

(59) Ito, M.; Serizawa, H.; Tanaka, K. *Polym. J.* **1978**, *10*, 215.

(60) Minke, R.; Blackwell, J. *J. Macromol. Sci., Phys.* **1979**, *B16*, 407-417.

(61) Keith, H. D. *Macromolecules* **1982**, *14*, 114.

(62) Jourdan, N.; Deguire, S.; Brisse, F. *Macromolecules* **1995**, *28*, 8086-8091.

(63) Yoo, E. S.; Im, S. S.; Ihn, K. J. *Bull. Korean Chem. Soc.* **1997**, *18*, 350.

(64) Miyata, T.; Masuko, T. *Polymer* **1998**, *39*, 1399-1404.

(65) Armelin, E.; Casas, M. T.; Puiggali, J. *Polymer* **2001**, *42*, 5695-5699.

(66) Aylwin, P. A.; Boyd, R. H. *Polymer* **1984**, *25*, 323-329.

(67) Turner-Jones, A.; Bunn, C. W. *Acta Crystallogr.* **1962**, *15*, 105.

(68) Liau, W.-B.; Boyd, R. H. *Macromolecules* **1990**, *23*, 1531-1539.

(69) Krejchi, M. T.; Atkins, E. D. T.; Waddon, A. J.; Fournier, M. J.; Mason, T. L.; Tirrell, D. A. *Science* **1994**, *265*, 1427.

(70) Lokey, R. S.; L., I. B. *Nature* **1995**, *375*, 303.

(71) Irwin, R. S. *Macromolecules* **1993**, *26*, 7125-7133.

(72) Iwata, M. *Jpn. J. Appl. Phys.* **2001**, *40*, 1352.

(73) Zhang, X.; Li, Z.; Lu, Z.; Sun, C. *Macromolecules* **2002**, *35*, 106.

(74) Wagener, K. B.; Boncella, J. M.; MNel, J. G. *Macromolecules* **1991**, *24*, 2649.

(75) Wagener, K. B.; Valenti, D.; Hahn, S. F. *Macromolecules* **1997**, *30*, 6688.

(76) Smith, J. A.; Brezezinska, K. R.; Valenti, D.; Wagener, K. B. *Macromolecules* **2000**, *33*, 3781.

(77) Schall, J. D. Ph.D., University of Massachusetts, 2001.

(78) McKiernan, R. L. Ph. D., University of Massachusetts, 2002.

(79) Le Fevere de Ten Hove, C. Ph. D., Université Catholique de Louvain, 2001.

(80) Schmidt-Rohr, K. *Macromolecules* **1996**, *29*, 3975-3981.

(81) Clauss, J.; Schmidt-Rohr, K.; Spiess, H. W. *Acta Polymer.* **1993**, *44*, 1-17.

(82) Hu, W.-G.; Schmidt-Rohr, K. *Polymer* **2000**, *41*, 2979-2987.

CHAPTER 2

SYNTHESIS AND CHARACTERIZATION OF DIOL AND DIACID MONOMERS

2.1 Introduction

In order to synthesize polyethylene-like polymers carrying "defects" at regular distances along the backbone, monomers with a polyethylene-like structure and two functional ends for introduction of this irregularity were needed. In this study, polyesters consisting of long-chain aliphatic α,ω-diols and short-chain diacids were chosen as model compounds that mimic polyethylene. The structural irregularity was introduced by diacids, which provide a wide variety of functionalities and side groups. The diols can be viewed as telechelic, perfectly monodisperse polyethylene oligomers. The diacids introduce irregularity into the polyethylene-like backbone and can be used to probe local structure and dynamics of the "defects" *via* solid-state NMR through ^{13}C-labeling in their carbonyl functionalities.

It is of crucial importance to consider a valid starting point for choosing an appropriate diol length that can potentially lead to a stable crystal. It was assumed that a diol length of at least 20 methylene units is required, as eicosane, a linear alkane containing 20 carbon atoms, is the first alkane to be a solid at room temperature.

Previous work performed in the Penelle group by Le Fevere de Ten Hove to synthesize long-chain aliphatic diols used a Wurtz coupling reaction between protected iodo-alcohols of varying length that had been first introduced by Rusanova and

coworkers.[1,2] In this study, this procedure was used to synthesize 1,22-docosanediol. The reaction sequence is given in Scheme 2.1.

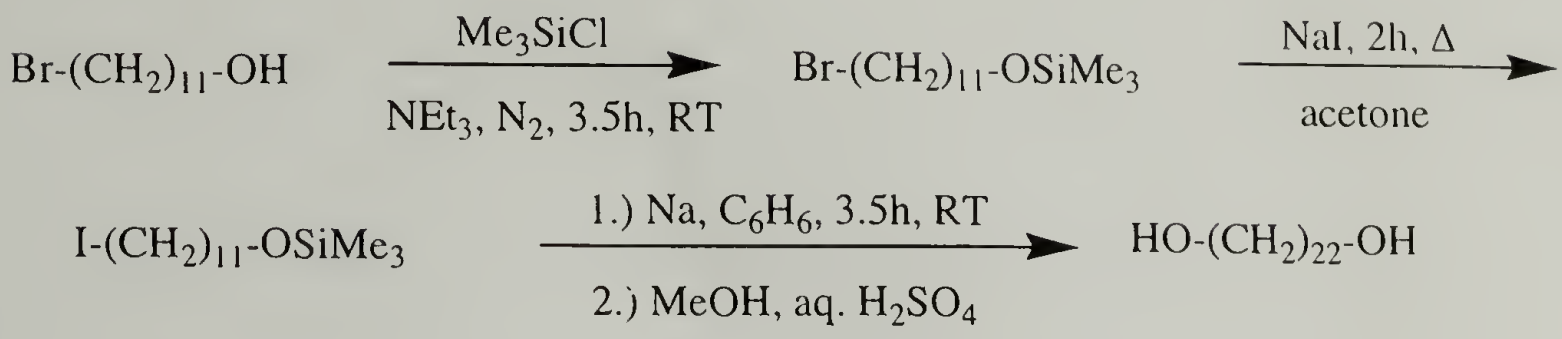

Scheme 2.1 Synthesis of 1,22-docosanediol.

However, subsequent synthesis of 1,44-tetratetracontanediol, as performed by Le Fevere de Ten Hove, was tedious and produced low yields due to purification difficulties. This procedure also precluded the assessment of a wider range of variable length diols.

As a result, an alternative route to 1,32-dotriacontanediol and 1,46-hexatetracontanediol was employed. First introduced by Hünig and Buysch, it relies on repeated enamine couplings to diacid chlorides of variable length, and the reaction sequence is shown in Scheme 2.2.[3-5] The lengths of both the enamine and the diacid chloride can be varied, allowing for the synthesis of long-chain aliphatic diols variable in length by increments of two methylene units.

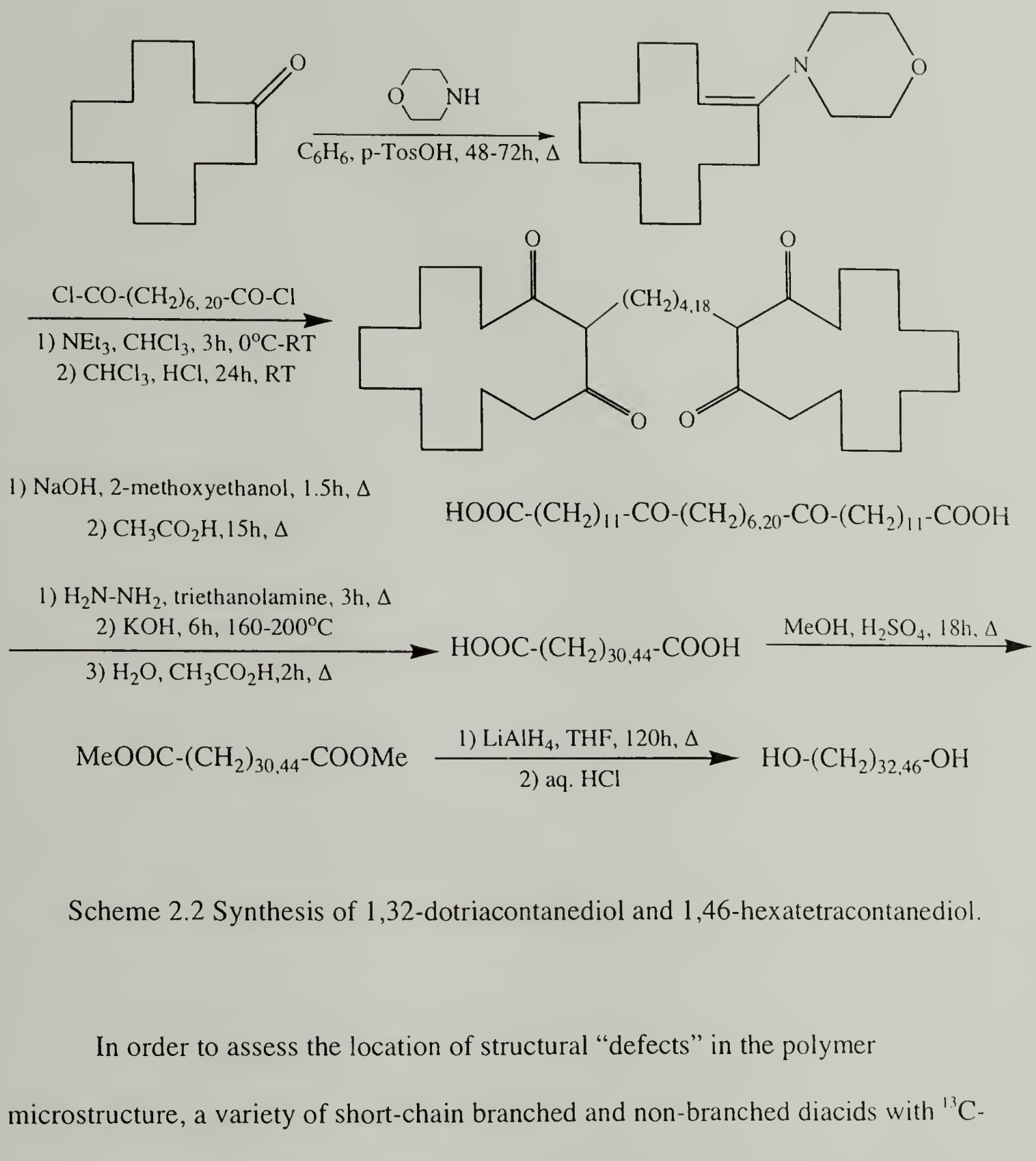

Scheme 2.2 Synthesis of 1,32-dotriacontanediol and 1,46-hexatetracontanediol.

In order to assess the location of structural "defects" in the polymer microstructure, a variety of short-chain branched and non-branched diacids with ^{13}C-labelled carbonyl segments were synthesized. Their structures are summarized in Scheme 2.3.

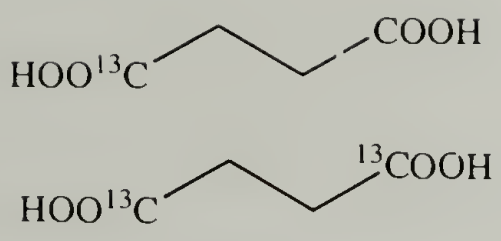

Succinic Acid

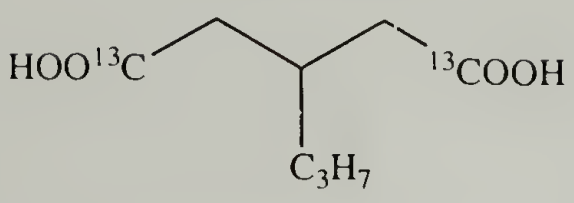

3-Propylglutaric Acid

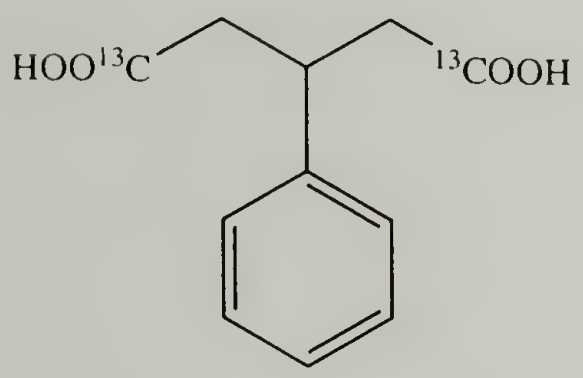

3-Phenylglutaric Acid

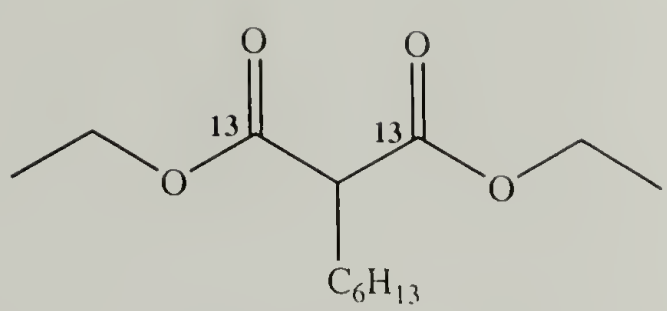

Diethyl hexylmalonate

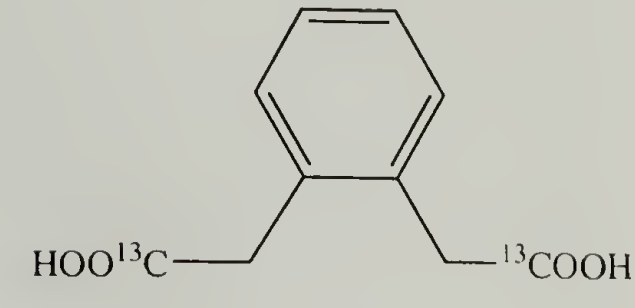

1,2-Phenylenediacetic acid

Scheme 2.3 Summary of ^{13}COO-labeled diacids and diesters.

The ^{13}C-labeling was performed in two different ways. In the case of diacids bearing two or more carbon atoms between carbonyl groups, the ^{13}C-labels were introduced by nucleophilic substitution of an appropriate bromide, chloride, or p-toluenesulfonate with ^{13}C-labeled potassium cyanide, followed by hydrolysis of the formed nitriles.[6-12] This reaction pathway is shown in Scheme 2.4 on the example of succinic acid.

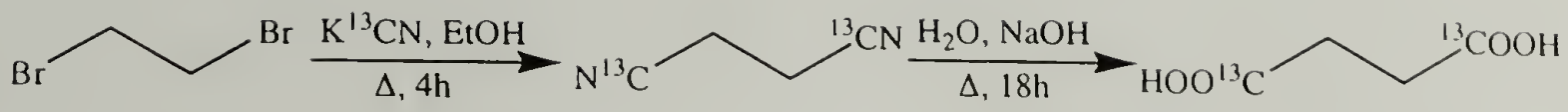

Scheme 2.4 ^{13}COO-labeling of short-chain diacids through nucleophilic substitution with $K^{13}CN$ and hydrolysis of formed nitrile.

In the case of the hexyl-branched malonate, a nucleophilic substitution of deprotonated 1,3C-^{13}C-labeled diethyl malonate with hexylbromide yielded mono-substituted diethyl malonates.[13,14] This reaction is depicted in Scheme 2.5.

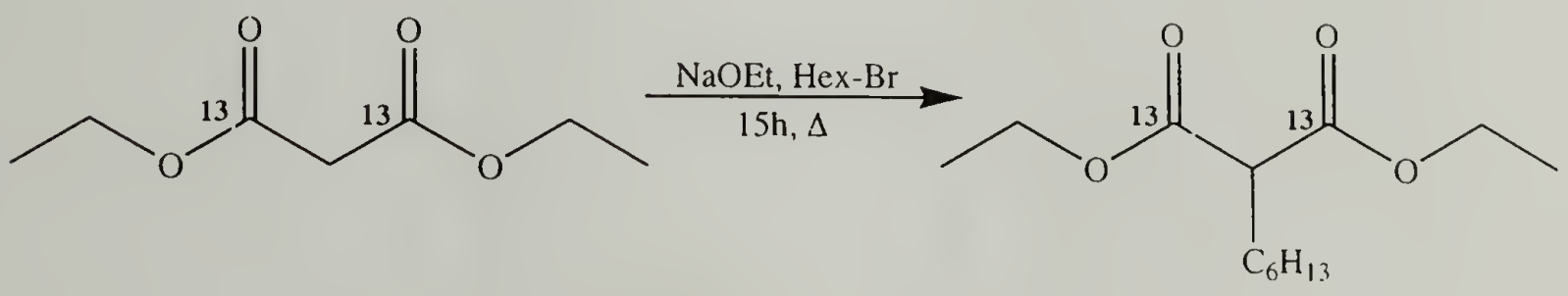

Scheme 2.5 Synthesis of ^{13}COO-labeled diethyl hexylmalonate.

2.2 Experimental

2.2.1 Characterization

Solution ^{1}H- and ^{13}C-nuclear magnetic resonance (NMR) spectra at room temperature were obtained with a Bruker DPX 300 MHz spectrometer in either $CDCl_3$, d_6-DMSO, or d_4-MeOH. Solution ^{1}H- and ^{13}C-NMR spectra at elevated temperatures were obtained in either $CDCl_3$ or d_6-DMSO with a Bruker Avance 600 MHz spectrometer. Infrared (IR) spectra were recorded with a Bio-Rad FTS 175C infrared spectrometer, using either 16 or 64 scans, and are reported after background subtraction.

Melting points were determined using a Perkin Elmer Pyris DSC flushed with helium at a scan rate of 10 $K \cdot min^{-1}$, and are reported as the onset of melting for the second run. The first heating and cooling was performed to erase former thermal histories and to provide all the samples with the same crystallization conditions. Calibration of the temperature scale and melting enthalpy was performed with indium and eicosane.

2.2.2 Materials and Equipment Required for the Synthesis

All reagents used in the synthesis of long-chain diols 1,22-docosanediol, 1,32-dotriacontanediol, and 1,46-hexatetracontanediol were obtained from commercial sources such as Aldrich and VWR, and were used without further purification. Unlabeled 1,2-phenylenediacetic acid, phenyl diethylmalonate and 3-phenylglutaric acid were obtained from Aldrich. $K^{13}CN$ used in the synthesis of doubly ^{13}C-labeled diacids and diethyl 1,3-$^{13}C_2$-malonate were obtained from Cambridge Isotope Laboratories. Triethylamine was dried over calcium hydride and distilled prior to use. Chloroform was dried over phosphorous pentoxide and distilled prior to use. The Wurtz coupling reaction as performed using a 20 kHz, 600 Watt Sonics & Materials Inc. VCX ultrasonicator at an amplitude of 30 %.

2.2.3 Synthesis of α,ω-Long Chain Aliphatic Diols

2.2.3.1 Synthesis of 1,22-Docosanediol

11-Bromo-1-(trimethylsilyloxy)undecane (1). In a two neck round bottom flask equipped with a pressure equalizing addition funnel and a condenser topped with a

nitrogen filled balloon, 53.9 g (0.21 mol) of 11-bromo-1-undecanol was dissolved in 200 mL of triethylamine dried previously over CaH_2, followed by purging the reaction mixture with nitrogen. Under stirring, 30 mL (0.23 mol) of trimethylchlorosilane were added dropwise. After complete addition, the mixture was allowed to react for an additional 3.5 hours at room temperature. Light petroleum ether was added, the mixture filtered, and the residue washed with additional petroleum ether. The petroleum ether was then evaporated from the filtrate to yield 65 g (94 %) of the protected bromoalcohol. ^{1}H-NMR (300 MHz, $CDCl_3$) δ 3.56 (t, J = 7.4 Hz, 2H, C$\underline{H}_2$-OTMS), 3.39 (t, J = 7.6 Hz, 2H, C$\underline{H}_2$-Br), 1.84 (p, J = 7.8 Hz, 2H, C$\underline{H}_2$-CH_2-OTMS), 1.51 (p, J = 7.0 Hz, 2H, C$\underline{H}_2$-CH_2-Br), 1.45-1.10 (m, 14H, -(C$\underline{H}_2$)$_7$-), 0.10 (s, 9H, O-Si(C$\underline{H}_3$)$_3$).

11-Iodo-1-(trimethylsilyloxy)undecane (2). 43.0 g (0.13 mol) of 11-bromo-1-(trimethylsilyloxy)undecane (**1**) and 32.0 g (0.21 mol) of sodium iodide in 175 mL dry acetone were refluxed for 2 hours. After evaporation of the acetone, light petroleum ether was added, the mixture filtered, and the solid washed with more light petroleum ether. Evaporation of the petroleum ether yielded 42.8 g (95 %) of 11-iodo-1-(trimethylsilyloxy)undecane as a slightly yellow oil. ^{1}H-NMR (300 MHz, $CDCl_3$) δ 3.55 (t, 2H, C$\underline{H}_2$-OTMS), 3.16 (t, 2H, C$\underline{H}_2$-I), 1.80 (p, 2H, C$\underline{H}_2$-CH_2-OTMS), 1.48 (p, 2H, C$\underline{H}_2$-CH_2-I), 1.40-1.10 (m, 14H, -(C$\underline{H}_2$)$_7$-), 0.10 (s, 9H, O-Si(C$\underline{H}_3$)$_3$).

1,22-Docosanediol (3). Sodium (1.2 g, 0.052 mol) was added to 30 mL of dry benzene in an argon-purged four-necked, double-jacketed glass vessel. The mixture was sonicated at 30 % amplitude for 30 minutes to remove residual water and to clean the surface of the metal. To the grey solution 11.0 g (0.029 mol) of 11-iodo-1-(trimethylsilyloxy)undecane (**2**) was added, changing the color of the solution to deep

blue. The reaction mixture was then sonicated at an amplitude of 30 % for an additional 3.5 hours while cold water was circulated through the outer vessel in order to cool the reaction mixture. After cooling to room temperature, small amounts of methanol, followed by water, and finally aqueous sulfuric acid were added to the reaction mixture to destroy the remaining sodium metal. The precipitated white product was filtered and washed with water. After recrystallization from methanol, 2.89 g (56 %) of pure 1,22-docosanediol were obtained; m.p. 105°C. ^{1}H-NMR (300 MHz, $CDCl_3$) δ 3.55 (t, 4H, $C\underline{H}_2$-OH), 1.80 (p, 4H, $C\underline{H}_2$-CH_2-OH), 1.40-1.10 (m, 36H, -$(C\underline{H}_2)_{18}$-). IR (KBr pellet): 3321 cm^{-1} (OH stretch), 2919 cm^{-1} (asymmetric CH stretch), 2850 cm^{-1} (symmetric CH stretch), 1473 and 1463 cm^{-1} (CH_2 bend), 1062 cm^{-1} (C-O stretch), 731 cm^{-1} (in-phase CH_2 rock), 720 cm^{-1} (out-of-phase CH_2 rock).

2.2.3.2 Synthesis of 1,32-Ditriacontanediol

1-Morpholino-1-cyclododecene (4). In a two necked flask equipped with a Dean-Stark trap, a mixture of 58 g (0.66 mol) of morpholine, 61 g (0.33 mol) of cyclododecanone, 150 mL of dry benzene and a few milligrams of p-toluenesulfonic acid as the catalyst were refluxed under inert atmosphere until no more water was collected (48-72 hours). Benzene and excess morpholine were distilled off and the remaining brown oil was fractionally distilled under vacuum (mechanical pump). Caution is required as distilled cyclododecanone, boiling at 90-110°C, may crystallize in the cooler. The desired enamine was obtained as a clear liquid with a boiling point of 125-130°C, in a yield of 66 g (78 %). ^{1}H-NMR (300 MHz, $CDCl_3$) δ 4.47 (t, 1H, C$\underline{H}$=CR), 3.64 (t, 4H,

$C\underline{H}_2$-O), 2.64 (t, 4H, $C\underline{H}_2$-N), 2.24 (t, m, 4H, $C\underline{H}_2$-CH=CR), 1.6-1.2 (m, 20H. (CH_2-$C\underline{H}_2$-CH_2).

1,4-Bis-(2,14-dioxo-cyclotetradecyl)butane (5). To an ice cooled mixture of 45.5 g (0.16 mol) of 1-morpholino-1-cyclododecene (**4**) and 25 mL (0.175 mol) of triethylamine in 25 mL of dry chloroform, a solution of 13.4 g (0.063 mol) of suberoyl chloride in 25mL of dry chloroform was added over the course of 15 minutes while maintaining the temperature below 5°C. The mixture was allowed to stir at room temperature for three hours. Upon addition of 300 mL of chloroform and 300 mL of 2.5 M HCl, the reaction mixture was hydrolized for 24 hours. The organic layer was collected, the water phase extracted twice with chloroform, and the organic phases combined. After removal of the chloroform, the crude product was heated in methanol. The hot solution was filtered, the solid washed with a little methanol and dried in vacuum. (**5**) was obtained as 20.3 g (64 %) of a white powder; m.p. 182°C. ^{1}H-NMR (300 MHz, $CDCl_3$) δ 3.58 (t, J = 8.0 Hz, 2H, $C\underline{H}$-$(C=O)_2$), 2.50-2.34 (m, 8H, $C\underline{H}_2$-(C=O)), 1.79-1.53 (m, 12H, $C\underline{H}_2$-CHR-(C=O)), 1.42-1.18 (m, 32H, CH_2-$C\underline{H}_2$-CH_2). IR (KBr pellet): 2940 cm^{-1} (cyclic, asymmetric CH stretch), 2923 cm^{-1} (acyclic, asymmetric CH stretch), 2862 cm^{-1} (cyclic, symmetric CH stretch), 1694 cm^{-1} (C=O stretch), 1463 cm^{-1} (CH_2 bend), 1024 cm^{-1} (C-O stretch), 725 cm^{-1} (out-of-phase CH_2 rock).

13,20-Dioxodotriacontanedioic acid (6). Hot solutions of 4.4 g (0.11 mol) of sodium hydroxide in 90 mL of 2-methoxyethanol and 9.42 g (0.02 mol) of 1,4-bis(2,14-dioxo-cyclotetradecyl)butane (**5**) in 50 mL of methoxyethanol were combined and refluxed for 1-1.5 hours. The obtained precipitate was filtered, washed with ethanol, and dried. The disodium salt obtained in this reaction was pure enough to be used in the

following Wolff-Kishner reduction. The reaction yielded 10.02 g (89 %) of slightly pink disodium salt. Pure dioxodiacid was obtained by hydrolysis of the disodium salt with acetic acid. ^{1}H-NMR (300 MHz, d_6-DMSO) δ 2.35 (t, J = 8.1 Hz, 8H, C$\underline{H}_2$-C=O), 2.16 (t, J = 8.1 Hz, 4H, C$\underline{H}_2$-COOH), 1.41 (m, 12H, C$\underline{H}_2$-CH_2-(C=O)), 1.30-1.17 (m, 32H, CH_2-C$\underline{H}_2$-CH_2).

1,32-Dotriacontanedioic acid (7). In a three-necked round-bottom flask equipped with a reflux condenser and an inner thermometer, 10.02 g (0.018 mol) of 13,20-dioxodotriacontanedioic acid disodium salt were dissolved in 55 mL of triethanolamine by heating the reaction mixture. 37 mL of hydrazine hydrate (85 %) were added, and the mixture refluxed at an oil bath temperature of 170°C for 3 hours. After cooling to 140°C, the hot solution of 9.63 g (0.17 mol) of potassium hydroxide dissolved in 50 mL of triethanolamine was added. The flask was left open to remove the excess hydrazine and water, while carefully heated to an inner temperature of 190-200°C over the course of one hour. The decomposition of the formed hydrazone, accompanied by foaming, started at an inner temperature of about 160°C. As soon as the inner temperature had reached 190-200°C, the flask was closed and the reaction mixture kept at this temperature for an additional 6 hours. Upon cooling, the dipotassium salt precipitated. Adding water to the triethanolamine mixture and slightly heating it enabled filtration. To obtain the free diacid, the dipotassium salt was refluxed in acetic acid for two hours, filtered after cooling to room temperature, and washed with acetone followed by drying in vacuum. This yielded 6.31 g (70 %) of 1,32-dotriacontanedioic acid as colorless crystals; m.p. 126°C. ^{1}H-NMR (300 MHz, d_6-DMSO) δ 2.35 (t, J = 8.1 Hz, 8H,

$C\underline{H}_2$-C=O), 2.16 (t, J = 8.1 Hz, 4H, $C\underline{H}_2$-COOH), 1.41 (m, 12H, $C\underline{H}_2$-CH_2-(C=O)), 1.30-1.17 (m, 32H, CH_2-$C\underline{H}_2$-CH_2).

Dimethyl 1,32-dotriacontanoate (8). In a round bottom flask, 10.11 g (0.02 mol) of 1,32-dotriacontanedioic acid (**7**), 150 mL of methanol, and a few drops of concentrated sulfuric acid were refluxed overnight. After cooling to room temperature, the diester was filtered off, washed with water, and dried in vacuum to yield 10.5 g (98 %) of pure dimethyl 1,32-dotriacontanoate; m.p.: 88°C. ^{1}H-NMR (300 MHz, $CDCl_3$) δ 3.68 (s, 6H, -COOC$\underline{H}_3$), 2.30 (t, J = 8.3 Hz, 4H, $C\underline{H}_2$-$COOCH_3$), 1.62 (p, J = 8.2 Hz, 4H, $C\underline{H}_2$-CH_2-$COOCH_3$), 1.32-1.18 (m, 52H, CH_2-$C\underline{H}_2$-CH_2).

1,32-Dotriacontanediol (9). To a suspension of 4 g (0.1 mol) of lithium aluminum hydride in 200 mL of dry THF, 10.5 g (0.02 mol) of dimethyl 1,32-dotriacontanoate (**8**) were added in small portions. The reaction mixture was then refluxed for three days. After cooling to room temperature, the excess lithium aluminum hydride was destroyed by careful addition of water, followed by sulfuric acid, to dissolve the formed lithium and aluminum salts. The 1,32-dotriacontanediol was filtered off and recrystallized from benzene to yield the pure diol; m.p.: 111°C. ^{1}H-NMR (300 MHz, $CDCl_3$) δ 3.64 (t, J = 6.6 Hz, 4H, $C\underline{H}_2$-OH), 1.58 (p, J = 6.9 Hz, 4H, $C\underline{H}_2$-CH_2-OH), 1.37-1.23 (m, 56H, CH_2-$C\underline{H}_2$-CH_2). IR (KBr pellet): 3323 cm^{-1} (OH stretch), 2919 cm^{-1} (asymmetric CH stretch), 2850 cm^{-1} (symmetric CH stretch), 1473 and 1463 cm^{-1} (CH_2 bend), 1063 cm^{-1} (C-O stretch), 731 cm^{-1} (in-phase CH_2 rock), 720 cm^{-1} (out-of-phase CH_2 rock).

2.2.3.3 Synthesis of 1,46-Hexatetracontanediol

1-Morpholino-1-cyclohexene (10). In a two-necked flask equipped with a Dean-Stark trap, a mixture of 44 g (0.5 mol) of morpholine, 48 g (0.49 mol) of cyclohexanone, 100 mL of dry benzene and a few milligrams of p-toluenesulfonic acid as the catalyst was refluxed under inert atmosphere for 4 hours until no more water was collected. Benzene and excess morpholine were removed by distillation and the remaining brown oil was fractionally distilled under vacuum (mechanical pump). The desired 1-morpholino-1-cyclohexene was obtained as a clear liquid at a boiling point of 85-90°C in a yield of 58 g (71 %). ^{1}H-NMR (300 MHz, $CDCl_3$) δ 4.69 (t, J = 4.0 Hz, 1H, C<u>H</u>=CR), 3.66 (t, J = 5.2 Hz, 4H, C<u>H</u>$_2$-O), 2.66 (t, J = 5.3 Hz, 4H, C<u>H</u>$_2$-N), 2.19 (m, 2H, C<u>H</u>$_2$-C(=CR)N), 1.97 (t, 2H, C<u>H</u>$_2$-CH=CR), 1.72-1.57 (m, 4H. (CH_2-C<u>H</u>$_2$-CH_2).

2,2'-Sebacoyldicyclohexanone (11). A mixture of 58.0 g (0.35 mol) of 1-morpholino-1-cyclohexene **(10)** and 35 mL of triethylamine in 170 mL of dry chloroform was heated to 35°C. 41.64 g (0.17 mol) of sebacoyl chloride in 70 mL of dry chloroform were added to the mixture over the course of 0.5 hours. The solution was then stirred for an additional 3 hours at 35°C during which it turned yellow, then dark orange. 200 mL of 20 % hydrochloric acid was then added and the reaction mixture refluxed for 5.5 hours. The organic layer was separated, and the water layer was extracted twice with chloroform. The combined organic phases were evaporated to yield the desired product as a viscous, yellow oil in a yield of approximately 64 g (103 %). The product was used without further characterization or purification.

7,16-Dioxodocosanedioic acid disodium salt (12). A mixture of 41.6 g (1.04 mol) of sodium hydroxide in 480 mL of ethanol was heated until all sodium hydroxide

was dissolved. The solution was cooled down to room temperature and 64 g of 2,2'-sebacoyldicylcohexanone (**11**) in 100 mL of ethanol were added. The reaction mixture was then refluxed for 1.5 hours, during which the solution turned red and a white precipitate formed. After cooling to room temperature, the mixture was filtered, the product washed with more ethanol, and then dried in vacuum to yield 80 g (105 %) of a slightly pink, crude 7,16-dioxodocosanedioic acid disodium salt. ^{1}H-NMR (300 MHz, $CDCl_3$) δ 2.38 (m, 12H, C$\underline{H}_2$-CO and C$\underline{H}_2$-COONa), 1.61 (m, 12H, C$\underline{H}_2$-CH_2-CO and C$\underline{H}_2$-CH_2-COONa), 1.28 (m, 12H, -(CH_2)-).

1,22-Docosanedioic acid (13). In a round bottom flask, 32.7 g (0.07 mol) of crude 7,16-dioxo-docosanedioic acid disodium salt (**12**) were dissolved in 130 mL of hot triethanolamine (inner temperature >100°C). To this hot solution, 80 mL of hydrazine hydrate (82 %) were added, and the reaction mixture was refluxed for 4 hours. 22 g (0.39 mol) of potassium hydroxide were dissolved in 55 mL of triethanolamine and added to the hydrazone solution. The open reaction vessel was carefully heated to an inner temperature of 195-205°C (oil bath at 230°C). After the excess hydrazine and water had completely been removed and the inner temperature had risen to 195-205°C, the vessel was closed and the solution allowed to react for an additional 6 hours. After cooling to room temperature, the solidified mixture was diluted with water, filtered, and washed with additional water. The obtained dipotassium salt was acidified with dilute hydrochloric acid to yield 18.5 g (68 %) of 1,22-docosanedioic acid. ^{1}H-NMR (300 MHz, d_4-MeOH) δ 2.28 (t, J = 7.3Hz, 4H, C$\underline{H}_2$-COOH), 1.60 (p, J = 7.0Hz, 4H, C$\underline{H}_2$-CH_2-COOH), 1.29 (m, 32H, -(CH_2)-).

1,22-Docosanediacid dichloride (14). To a suspension of 18.5 g (0.05 mol) of 1,22-docosanedioic acid (**13**) in 100 mL of benzene, 18 g (0.15 mol) of thionyl chloride were added and the mixture slowly heated to 60°C. The mixture was kept at 60°C for an additional 1.5 hours. After cooling to room temperature, the benzene and excess thionyl chloride were removed by distillation. The diacid chloride was obtained as a viscous brown oil, which was immediately used in the following enamine coupling reaction. The yield was estimated at 96 %.

1,18-Bis(2,14-dioxocyclotetradecyl)octadecane (15). To an ice-cooled mixture of 36.0 g (0.13 mol) of 1-morpholino-1-cyclododecene (**4**) and 20 mL (0.14mol) of triethylamine in 20mL of dry chloroform, a solution of 1,22-docosanedioic diacid dichloride (**14**) in 50 mL of dry chloroform was added over the course of 30 minutes, while the inner temperature was maintained below 5°C. The mixture was stirred at room temperature for five hours. Upon addition of 200 mL of chloroform and 200 mL of 2.5 M HCl, the reaction mixture was hydrolized at room temperature for 24 hours. The organic layer was separated, the water phase extracted twice with chloroform, and the organic phases combined. After removal of the chloroform in vacuum, the product was recrystallized from ethyl acetate to yield 22.6 g (67 %) of the tetraketone as a white solid. ^{1}H-NMR (300 MHz, $CDCl_3$) δ 3.60 (t, J = 7.3 Hz, 2H, C<u>H</u>-$(C=O)_2$), 2.51-2.34 (m, 8H, C<u>H_2</u>-(C=O)), 1.79-1.53 (m, 12H, C<u>H_2</u>-CHR-(C=O)), 1.42-1.18 (m, 32H, CH_2-C<u>H_2</u>-CH_2).

13,34-Dioxohexatetracontanedioic acid disodium salt (16). Hot solutions of 17.5 g (0.025 mol) of 1,18-bis(2,14-dioxocyclotetradecyl)octadecane (**15**) in 125 mL of 2-methoxyethanol and 6 g (0.15 mol) of sodium hydroxide in 75 mL of 2-methoxyethanol were combined and refluxed for 2 hours. The precipitated disodium salt

was filtered, washed with ethanol, and dried in vacuum. The crude 13,34-dioxo-hexatetracontanedioic acid disodium salt was obtained as 22.67 g (116 %) of an off-white solid.

1,46-Hexatetracontanedioic acid (17). In a three-necked round-bottom flask equipped with a reflux condenser and an inner thermometer, 22.67 g (0.03 mol) of 13,34-dioxohexatetracontanedioic acid disodium salt (**16**) was dissolved in 100 mL of hot triethanolamine. 60 mL of hydrazine monohydrate were added, and the mixture heated at an oil bath temperature of 140°C for 3 hours. A hot solution of 16.8 g (0.3 mol) of potassium hydroxide dissolved in 90 mL of triethanolamine was then added. To remove the excess hydrazine and water, the flask was left open and carefully heated to an inner temperature of 200°C over the course of one hour. The decomposition of the formed hydrazone (foaming) began at an inner temperature of about 160°C. As soon as the inner temperature had reached 200°C (oil bath at 220-230°C), the flask was closed, and the reaction mixture was allowed to react for an additional 7 hours. Upon cooling, the diacid precipitated. Adding water to the triethanolamine mixture and slightly heating it enabled filtration. To obtain the free diacid, the dipotassium salt was refluxed in acetic acid for a few hours, filtered after cooling to room temperature, and washed with acetone followed by drying in vacuum. This yielded 11.0 g (62 %) of 1,32-dotriacontanedioic acid as colorless crystals; m.p. 109°C. ^{1}H-NMR (600 MHz, d_6-DMSO, 100°C) δ 2.18 (t, 4H, C$\underline{H}_2$-COOH), 1.52 (m, 12H, C$\underline{H}_2$-CH_2-COOH), 1.33-1.23 (m, 80H, CH_2-C$\underline{H}_2$-CH_2). IR (KBr pellet): 3069 cm^{-1} (OH stretch), 2917 cm^{-1} (asymmetric CH stretch), 2850 cm^{-1} (symmetric CH stretch), 1644 cm^{-1} (C=O stretch), 1475 and 1471 cm^{-1} (CH_2 bend),

1056 cm^{-1} (C-O stretch), 730 cm^{-1} (in-phase CH_2 rock), 725 and 723 cm^{-1} (out-of-phase CH_2 rock).

Dimethyl 1,46-hexatetracontanoate (18). In a round bottom flask, 11.0 g (0.016 mol) of 1,46-hexatetracontanedioic acid (**17**), 150 mL of methanol and a few drops of concentrated sulfuric acid were refluxed overnight. The precipitated diester was filtered off, washed with water, and dried in vacuum to yield 9.93 g (87 %) of dimethyl 1,46-hexatetracontanoate. ^{1}H-NMR (300 MHz, $CDCl_3$) δ 3.67 (s, 6H, $COOC\underline{H}_3$), 2.30 (t, J = 7.5 Hz, 4H, $C\underline{H}_2$-COOMe), 1.59 (p, J = 7.7 Hz, 4H, $C\underline{H}_2$-CH_2-COOMe), 1.35-1.15 (m, 80H, CH_2-$C\underline{H}_2$-CH_2).

1,46-Hexatetracontanediol (19). To a suspension of 5 g (0.125 mol) of lithium aluminum hydride in 150 mL of dry THF, 9.93 g (0.014 mol) of dimethyl 1,46-hexatetracontanoate (**18**) were added in small portions. After complete addition, the reaction mixture was refluxed for seven days. After cooling to room temperature, the excess lithium aluminum hydride was destroyed by careful addition of water, followed by dilute sulfuric acid to dissolve the formed lithium and aluminum salts. The 1,46-hexatetracontanediol was filtered off and recrystallized from benzene to yield the pure diol; m.p.: 109°C ^{1}H-NMR (500 MHz, d_6-DMSO) δ 3.49 (t, J = 6.5 Hz, 4H, $C\underline{H}_2$-OH), 1.53 (p, J = 6.7 Hz, 4H, $C\underline{H}_2$-CH_2-OH), 1.42-1.25 (m, 84H, CH_2-$C\underline{H}_2$-CH_2). ^{12}C-NMR (150 MHz, C_6D_6) δ 61.83 (OCH_2), 33.43 ($OCH_2\underline{C}H_2$), 29.83, 29.67, 26.36 (-(CH_2)-). IR (KBr pellet): 3325 cm^{-1} (OH stretch), 2919 cm^{-1} (asymmetric CH stretch), 2850 cm^{-1} (symmetric CH stretch), 1473 and 1463 cm^{-1} (CH_2 bend), 1057 cm^{-1} (C-O stretch), 730 cm^{-1} (in-phase CH_2 rock), 719 cm^{-1} (out-of-phase CH_2 rock).

2.2.4 Synthesis of ^{13}C-Labeled Short-Chain Diacids

2.2.4.1 Synthesis of ^{13}C-Labeled Non-Branched Diacids

2.2.4.1.1 Synthesis of Succinic Acid

1-^{13}C-labeled succinic acid (20). To a solution of 0.44 g (0.0067 mol) of ^{13}C-labeled potassium cyanide in 3 mL of dimethyl sulfoxide, 0.96 g (0.0067 mol) of 3-bromopropionitrile was added. The reaction mixture was stirred at 80°C overnight. After cooling to room temperature, 10 mL of a 1 M sodium hydroxide solution was added, and the mixture refluxed overnight. After cooling to room temperature, the solution was acidified to a pH of 1 with concentrated hydrochloric acid, yielding the desired product as a white precipitate. ^{1}H-NMR (300 MHz, $CDCl_3$) δ 2.40 (s, 4H, C$\underline{H}_2$-^{13}COOH). ^{13}C-NMR (75 MHz, $CDCl_3$) δ 177.41 ($^{13}\underline{C}$OOH).

1,4C-$^{13}C_2$-labeled succinic acid (21). In a two-necked round bottom flask equipped with reflux condenser and additional funnel, a solution of 1.5 g (0.008 mol) of 1,2-dibromoethane in 3 mL of ethanol was heated. To the hot mixture, 1 g (0.016 mol) of ^{13}C-labeled potassium cyanide, dissolved in a minimal amount of water, was added dropwise. After refluxing for several hours, the mixture was cooled to room temperature and 10 ml of a 1 M sodium hydroxide solution was added. The mixture was then refluxed overnight. The desired product was obtained as a white precipitate after acidifying the reaction mixture with hydrochloric acid. ^{1}H-NMR (300 MHz, $CDCl_3$) δ 2.42 (s, 4H, C$\underline{H}_2$-^{13}COOH). ^{13}C-NMR (75 MHz, $CDCl_3$) δ 177.55 ($^{13}\underline{C}$OOH).

2.2.4.2 Synthesis of ^{13}C-Labeled Branched Diacids

2.2.4.2.1 Synthesis of Branched Glutaric Acids

2-Propylpropane-1,3-diol (22). To a suspension of 7.6 g (0.2 mol) of lithium aluminum hydride in 100 mL of diethylether, a solution of 20.22 g (0.1 mol) of diethyl propylmalonate in 100 mL of diethylether was added dropwise at a rate that maintained a slight reflux. After complete addition, the mixture was refluxed overnight. After cooling to room temperature, the unreacted lithium aluminum hydride was destroyed by careful addition of water followed by dilute hydrochloric acid. The 2-propylpropane-1,3-diol was extracted with ether to yield 12 g (102 %) of product after solvent evaporation. ^{1}H-NMR (300 MHz, $CDCl_3$) δ 3.74 (m, 4H, C<u>H</u>$_2$-OH), 1.79 (m, 1H, -C<u>H</u>-), 1.26 (m, 4H, CH-(C<u>H</u>$_2$)$_2$-CH$_3$), 0.93 (m, 3H, -C<u>H</u>$_3$).

2-Propylpropane-1,3-diol ditosylate (23). To an ice-cooled solution of 12 g (0.1 mol) of 2-propylpropane-1,3-diol (**22**) in 30 mL of dry pyridine, a solution of 40 g (0.22 mol) of p-toluenesulfonyl chloride in 50 mL of dry pyridine was added dropwise. The slightly pink solution was placed in the refrigerator for 48 hours. The precipitated product was filtered and recrystallized from methanol to yield 7.8 g (19 %) of ditosylate as white crystals. ^{1}H-NMR (300 MHz, $CDCl_3$) δ 7.73 (d, J = 7.0 Hz, 4H, aromatic C<u>H</u>), 7.37 (d, J = 7.7 Hz, 4H, aromatic C<u>H</u>), 3.94 (m, 4H, C<u>H</u>$_2$-O), 2.46 (s, 6H, -SO$_2$-C$_6$H$_4$-C<u>H</u>$_3$), 1.97 (p, 1H, -C<u>H</u>-), 1.20 (m, 4H, CH-(C<u>H</u>$_2$)$_2$-CH$_3$), 0.80 (t, 3H, CH$_2$-C<u>H</u>$_3$).

1,5-^{13}C$_2$-3-Propylglutaric acid (24). To a solution of 0.788 g (0.002 mol) of 2-propylpropane-1,3-diol ditosylate (**23**) in 3 mL of dry ethanol, a solution of 0.264 g (0.004 mol) of ^{13}C-labeled potassium cyanide dissolved in dry ethanol was added, and the mixture refluxed overnight. After removal of the ethanol, 10 mL of dilute sodium

hydroxide solution were added, and the mixture was again refluxed overnight. After cooling the solution to room temperature and acidifying with concentrated hydrochloric acid, the acid was extracted with diethyl ether to yield 0.137g (42%) of the desired product after solvent removal. ^{1}H-NMR (300 MHz, $CDCl_3$) δ 11.71 (s, 2H, COO<u>H</u>), 2.49 (m, 4H, C<u>H</u>$_2$-COOH), 2.17 (m, 1H, CH_2-C<u>H</u>-CH_2), 1.36 (m, 4H, -CH-$(CH_2)_2$), 0.92 (t, J = 6.1 Hz, 3H, -$(CH_2)_2$-C<u>H</u>$_3$). ^{13}C-NMR (75 MHz, $CDCl_3$) δ 180.14 (^{13}<u>C</u>OOH).

2-Phenylpropane-1,3-diol (25). To a suspension of 3.8 g (0.1 mol) of lithium aluminum hydride in 100 mL of diethyl ether, a solution of 23.6 g (0.1 mol) of diethyl phenylmalonate in 100 mL of diethylether was added dropwise while maintaining the temperature at a slight reflux. After complete addition and refluxing overnight, unreacted lithium aluminum hydride was destroyed by careful addition of water, followed by aqueous hydrochloric acid. The 2-phenylpropane-1,3-diol was extracted with ether to yield the desired product after solvent evaporation. ^{1}H-NMR (300 MHz, $CDCl_3$) δ 7.35-7.23 (m, 5H, aromatic C<u>H</u>), 3.99 (m, 4H, C<u>H</u>$_2$-O), 3.12 (t, 1H, -C<u>H</u>-), 1.93 (s, 2H, O<u>H</u>).

2-phenylpropane-1,3-diol ditosylate (26). To an ice-cooled solution of 21.5 g (0.14 mol) of 2-phenylpropane-1,3-diol (**25**) in 40 mL of dry pyridine, a solution of 56.25 g (0.30 mol) of p-toluenesulfonyl chloride in 55 mL of dry pyridine was added dropwise. The solution was placed in the refrigerator for 48 hours. The precipitated product was then filtered to yield the ditosylate as white crystals. ^{1}H-NMR (300 MHz, $CDCl_3$) δ 7.67-6.98 (m, 13H, aromatic C<u>H</u>), 4.18 (d, J = 6.3 Hz, 4H, C<u>H</u>$_2$-O), 3.25 (p, J = 6.3 Hz, 1H, -C<u>H</u>-), 2.44 (s, 6H, -C_6H_4-C<u>H</u>$_3$).

1,5C-$^{13}C_2$-3-Phenylglutaric acid (27). To a solution of 0.460 g (0.001 mol) of 2-phenylpropane-1,3-diol ditosylate (**26**) in 3mL of dry ethanol, a solution of 0.132 g (0.002 mol) ^{13}C-labeled potassium cyanide dissolved in 5 mL of dry ethanol was added. After refluxing the reaction mixture overnight, the ethanol was evaporated. To the obtained dinitrile, 10 mL of dilute sodium hydroxide solution was added, and the mixture was refluxed overnight. After cooling to room temperature, the reaction mixture was acidified with concentrated hydrochloric acid, and the acid was extracted with diethyl ether. After solvent removal, the desired product was obtained in a yield of 0.07 g (33 %). ^{1}H-NMR (300 MHz, $CDCl_3$) δ 7.51-7.38 (m, 5H, aromatic C<u>H</u>), 2.74 (m, 1H, -C<u>H</u>-), 2.60 (m, 4H, -C<u>H</u>$_2$-). ^{13}C-NMR (75 MHz, $CDCl_3$) δ 178.10 (^{13}<u>C</u>OOH).

2.2.4.2.2 Synthesis of 1,2-Phenylenediacetic Acid

$^{13}C_2$-1,2-Phenylenediacetic acid (28). To a solution of 1.02 g (0.0039 mol) of α,α'-dibromo-o-xylene in 5 mL of acetone, a solution of 0.52 g (0.0079 mol) of ^{13}C-labeled potassium cyanide dissolved in 5 ml of acetone was added. After refluxing the reaction mixture overnight, the acetone was removed. To the formed dinitrile, 10 mL of concentrated hydrochloric acid were added, and the mixture refluxed for five hours. After cooling, the acid was extracted with diethyl ether, and after solvent removal, the desired product was obtained in a yield of 0.231 g (31 %). ^{1}H-NMR (300 MHz, $CDCl_3$) δ 7.32-7.20 (m, 4H, aromatic C<u>H</u>), 3.71 (d, J = 7.9 Hz, 4H, -C<u>H</u>$_2$-). ^{13}C-NMR (75 MHz, $CDCl_3$) δ 178.39 (^{13}<u>C</u>OOH).

2.2.4.2.3 Synthesis of Branched Malonic Acid Diethylester

Diethyl 1,3-$^{13}C_2$-hexylmalonate (29). To 0.075 g (0.003 mol) of freshly cut sodium, 2 mL of absolute ethanol were added dropwise, maintaining the mixture at a slight reflux. After all the sodium was consumed, 0.5 g (0.003 mol) diethyl malonate and 0.51 g (0.003 mol) of 1-bromohexane were added. After 5 minutes, the solution became turbid, and the formation of a white precipitate of sodium bromide was observed. The reaction mixture was refluxed overnight. After cooling to room temperature, just enough water to dissolve the sodium bromide was added, and the aqueous phase extracted with ether. After removal of the ether, the obtained raw product was distilled using a Kugelrohr apparatus to yield 0.250 g (33 %) of pure diethyl 1,3-$^{13}C_2$-hexylmalonate. ^{1}H-NMR (300 MHz, $CDCl_3$) δ 4.13 (dq, 4H, O-C$\underline{H}_2$), 3.26 (t, 1H, CO-C$\underline{H}$-CO), 1.84 (m, 2H, CH-C$\underline{H}_2$-CH_2), 1.19 (m, 14H, -$(CH_2)_4$, ester C$\underline{H}_3$), 0.82 (t, 3H, -$(CH_2)_5$-C$\underline{H}_3$. ^{13}C-NMR (75 MHz, $CDCl_3$) δ 170.04 ($^{13}\underline{C}$OOEt).

2.3 Results and Discussion

2.3.1 General Synthetic Routes to the Long-Chain Aliphatic Diols

In Nature, long-chain linear aliphatic α,ω-diols can be found in wood, cork, and waxes. They can be extracted from these sources,[15] but complete removal of contaminating homologues having almost identical lengths is difficult. Since our project requires perfectly regular placement of defects along the polymer backbone, impurities with slightly different lengths are unacceptable. As a result, the long-chain aliphatic α,ω-diols used in this study were synthesized, and not extracted from natural materials.

Over the past decade, a wide variety of reactions potentially applicable for the synthesis of long-chain aliphatic diols have been described in the literature. [16] These reactions are very limited, however, and only work efficiently for aliphatic α,ω-diols with methylene segments smaller than 20 due to low solubilities and yields. To produce longer chains efficiently, difunctional starting materials can be coupled to produce the longer diols. A variety of electrolysis coupling reactions have been employed for the synthesis of long-chain diols.[17-21] Schlosser and coworkers devised a synthetic scheme based on Grignard couplings to synthesize difunctional hydrocarbon chains, with the potential for long-chain diol synthesis.[22] Dicarboxylic acids with methylene segment lengths of 48 and 192 units, which can be reduced to diols, have been synthesized by Brooke et al.[23] As a major goal in this study was to probe a variety of long-chain diols and to determine the minimum length of diol segment needed to achieve polyethylene-like crystallization, a versatile synthetic approach with easily variable diol segment lengths was needed. Both Rusanova and coworkers and Duhamel and coworkers used the Wurtz coupling to synthesize 1,22- and 1,24-diols, a reaction sequence that was employed in this project.[1,24] Over the course of a decade, Hünig and coworkers published a series of papers describing the syntheses of long-chain dicarboxylic acids, by coupling enamines derived from various size cyclic ketones and morpholine with diacid chlorides.[3,4,25-27] These coupling reactions allow for a variation in diacid length of 2 methylene units at a time, therefore providing the versatility needed here.

These enamine coupling reactions are described in detail below. The variations in length of starting materials and the relative ease of repetition of the reaction sequence,

yielding longer diols, provide a versatile approach for the synthesis of a variety of long-chain diols.

2.3.2 Synthetic Routes to Long-Chain Aliphatic Diols Used in this Study

The first long-chain diol synthesized in this study was 1,22-docosanediol. One potential synthetic route to 1,22-docosanediol is the reduction of the commercially available 1,22-docosanedioic acid. However, this acid is only 94% pure, being contaminated by a variety of slightly longer or shorter diacids. This type of impurity will prevent a perfectly regular spacing between structural elements to be obtained in the targeted polyesters. Consequently, 1,22-docosanediol was synthesized by a procedure first introduced by Rusanova, and later optimized by Le Fevere de Ten Hove.[1,2] The reaction sequence is shown in Scheme 2.6 and yields 1,22-docosanediol in three steps, starting from commercially available 11-bromo-1-undecanol. The hydroxyl functionality is protected with trimethylsilyl chloride in a yield of 94 %. This is followed by exchange of the bromide with an iodide in a yield of 95 % *via* the Finkelstein reaction. The formed iodide has increased reactivity in the subsequent Wurtz coupling, performed under sonication. After acidic work-up, the 1,22-docosanediol is obtained in a yield of 56 %, which results in an overall yield of 50 %.

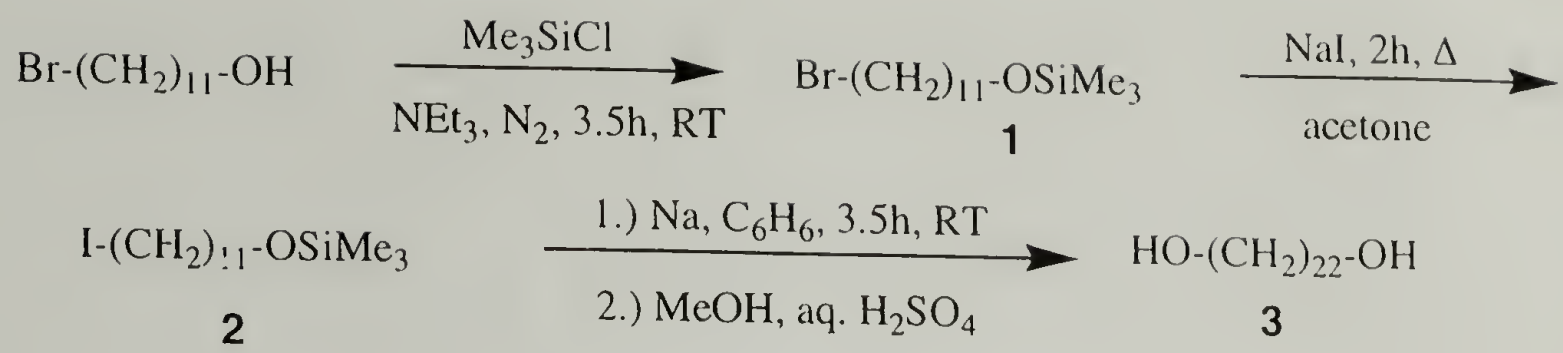

Scheme 2.6 Synthesis of 1,22-docosanediol.

Side-products that are identified by solution ^{1}H-NMR are 10-undecen-1-ol and 1-undecanol potentially formed in a radical reaction by disproportionation. These unwanted side products are removed through recrystallization of 1,22-docosanediol from methanol, yielding the pure diol.

As mentioned before, Le Fevere de Ten Hove subsequently synthesized 1,44-tetratetracontanediol from 1,22-docosanediol by monobromination of the diol, followed by the same reaction sequence as described above for the synthesis of 1,22-docosanediol. Due to low yields and difficulties in separating unreacted 1,22-docosanediol from the mono- and dibrominated product, this synthetic route was not repeated. Instead, the procedure first introduced by Hünig and Buysch was used.[3,4]

This procedure is based on the coupling of two equivalents of a cyclic enamine, obtained by reaction of a cyclic ketones of variable length with morpholine, and a diacid chloride of variable length. Reaction of the diacid chloride with triethylamine formed a diketene in situ. This diketene then reacted with the enamine in a [2+2] cycloaddition to yield a cyclic tetraketone after hydrolysis. Subsequently, the tetraketone was ring-opened under basic conditions to yield a diketodiacid containing terminal acid groups as well as two ketone groups. The final α,ω-diacid was obtained after reduction of these ketones by

a Wolff-Kishner reduction with hydrazine. Esterification to a methyl ester facilitates the subsequent reduction with lithium aluminum hydride to yield the desired α,ω-diol.

To synthesize 1,32-dotriacontanediol, two equivalents of 1-morpholino-1-cyclododecene, obtained by reaction of morpholine with cyclododecane in 78 % yield, were reacted with suberoyl chloride to form a cyclic tetraketone, 1,4-bis(2,14-dioxocyclotetradecyl)butane, in 64 % yield. Ring-opening of the tetraketone with sodium hydroxide in methoxyethanol produced 13,20-dioxodotriacontanedioic acid in 89 % yield. A Wolff-Kishner reduction of the ketone groups with hydrazine hydrate, and subsequent reaction of the formed hydrazones with potassium hydroxide in triethanolamine, resulted in a yield of 70 % of 1,32-dotriacontanedioic acid. The diacid was esterified in methanol and reduced with lithium aluminum hydride over several days to yield 1,32-dotriacontanediol after acidic workup. The reaction sequence is depicted in Scheme 2.7.

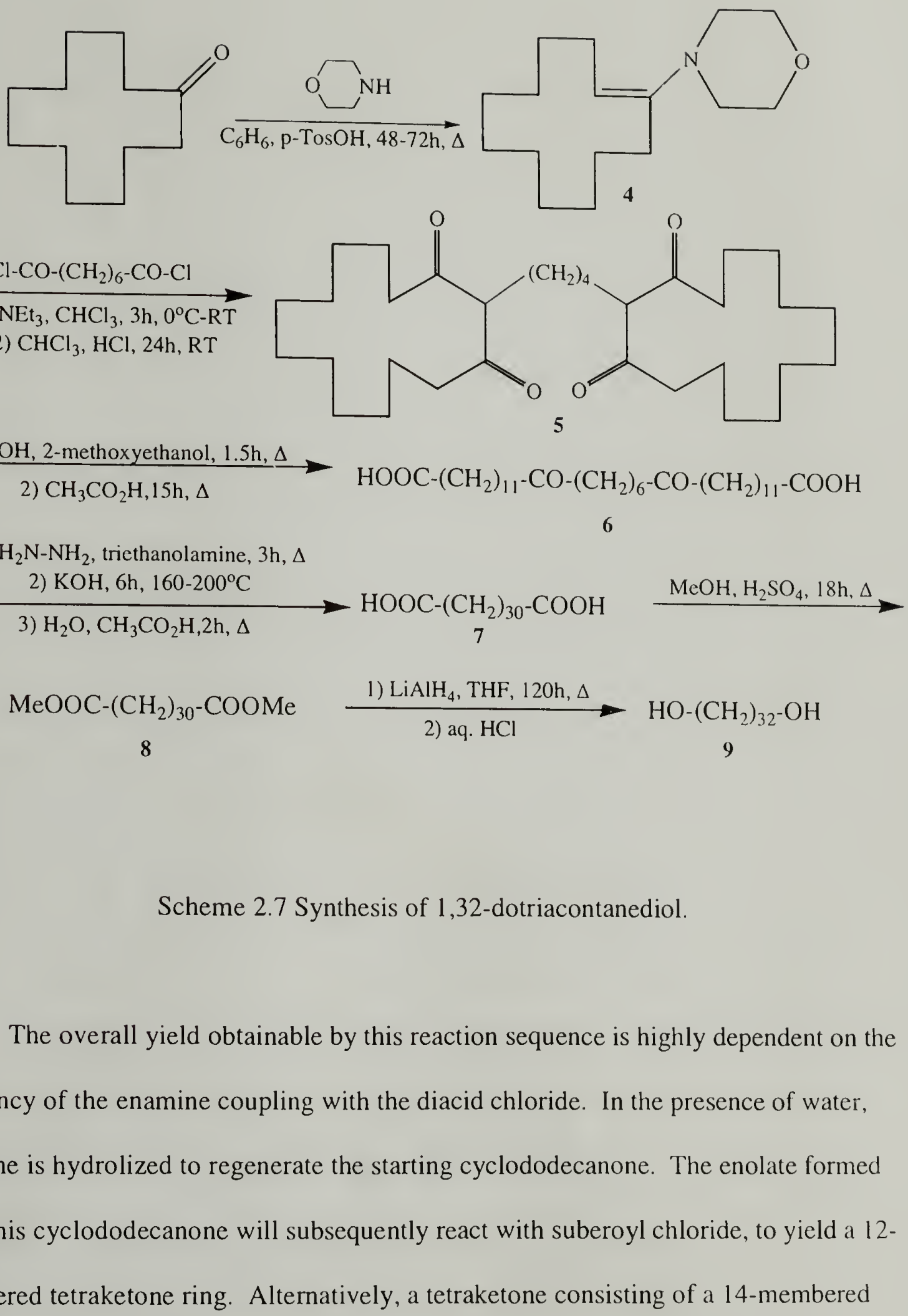

Scheme 2.7 Synthesis of 1,32-dotriacontanediol.

The overall yield obtainable by this reaction sequence is highly dependent on the efficiency of the enamine coupling with the diacid chloride. In the presence of water, enamine is hydrolized to regenerate the starting cyclododecanone. The enolate formed from this cyclododecanone will subsequently react with suberoyl chloride, to yield a 12-membered tetraketone ring. Alternatively, a tetraketone consisting of a 14-membered ring from reaction of the ketene with the enamine on one side, and a 12-membered ring arising from the reaction of the ketene with cyclododecanone enolate on the other side,

can be formed. Both of these side products can be observed by ^{1}H-solution NMR for each of the enamine coupling reactions examined. Although these side-products are structural isomers of the desired tetraketone, their subsequent ring-opening reaction will result in regeneration of the cyclododecanone. The different solubilities of product and side-products in methanol allow the product mixture to be purified by heating in methanol, followed by hot filtration. The side products dissolve in methanol, while the desired tetraketone does not. The desired tetraketone is obtained in its pure form upon filtration. A yield of 64 % was obtained here, a significant improvement compared to the yield of 55 % reported by Hünig and Buysch.[3]

In order to obtain even longer diols, 1,22-docosanedioic acid is synthesized as a precursor to 1,46-hexatetracontanediol. It can indeed be converted to a diacid chloride, and then used in a subsequent enamine coupling.[4] The reaction sequence to synthesize 1,22-docosanedioic acid, shown in Scheme 2.8, is similar to the one employed for the synthesis of 1,32-docosanedioic acid.

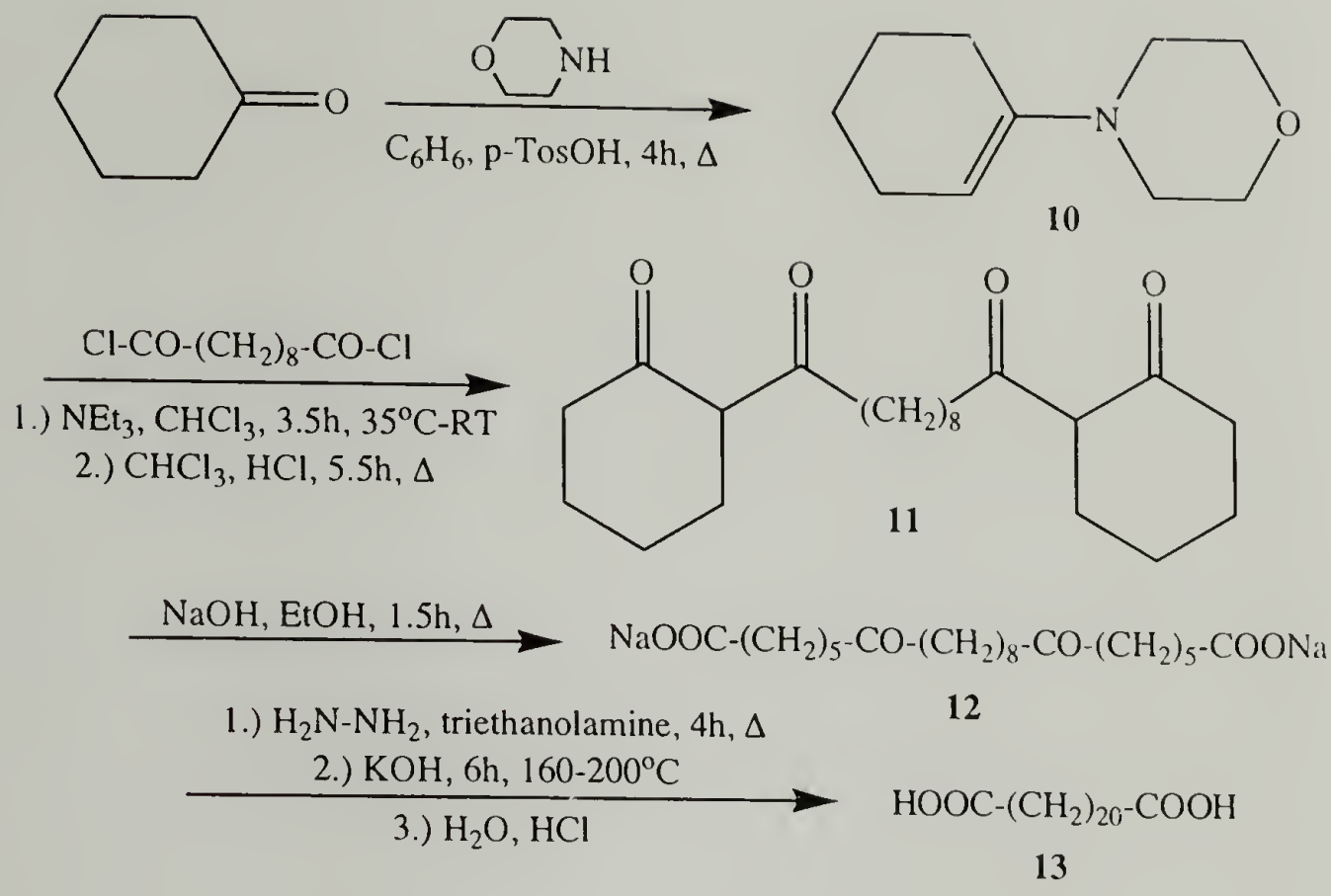

Scheme 2.8 Synthesis of 1,22-docosanedioic acid.

The reaction of cyclohexanone with morpholine yields 71 % of 1-morpholino-1-cyclohexene **10** after distillation. Two equivalents of this enamine are coupled with sebacoyl chloride in triethanolamine to yield 2,2'-sebacoyldicyclohexanone **11** in quantitative yield. **11** is then ring-opened under basic conditions to yield a crude 7,16-dioxo-1,32-docosanedioic acid **12** in a quantitative yield. A Wolff-Kishner reduction eliminates the ketones in **12** to produce pure 1,22-docosanedioic acid **13** in 68 % yield, uncontaminated by longer or shorter homologues. Starting from commercially available 1-morpholino-1-cyclohexene **10** , the 1,22-docosanedioic acid **13** is synthesized in an overall yield of 71 %.

Transformation to the diacid chloride **14** with thionyl chloride and subsequent enamine coupling with two equivalents of 1-morpholino-1-cyclododecene **4**, yields the

tetraketone **15** containing 46 carbon atoms. The reaction sequence to 1,46-hexatetracontanediol **19**, is summarized in Scheme 2.9 and is similar to the procedure employed previously for the 1,32-dotriacontanediol **9**.

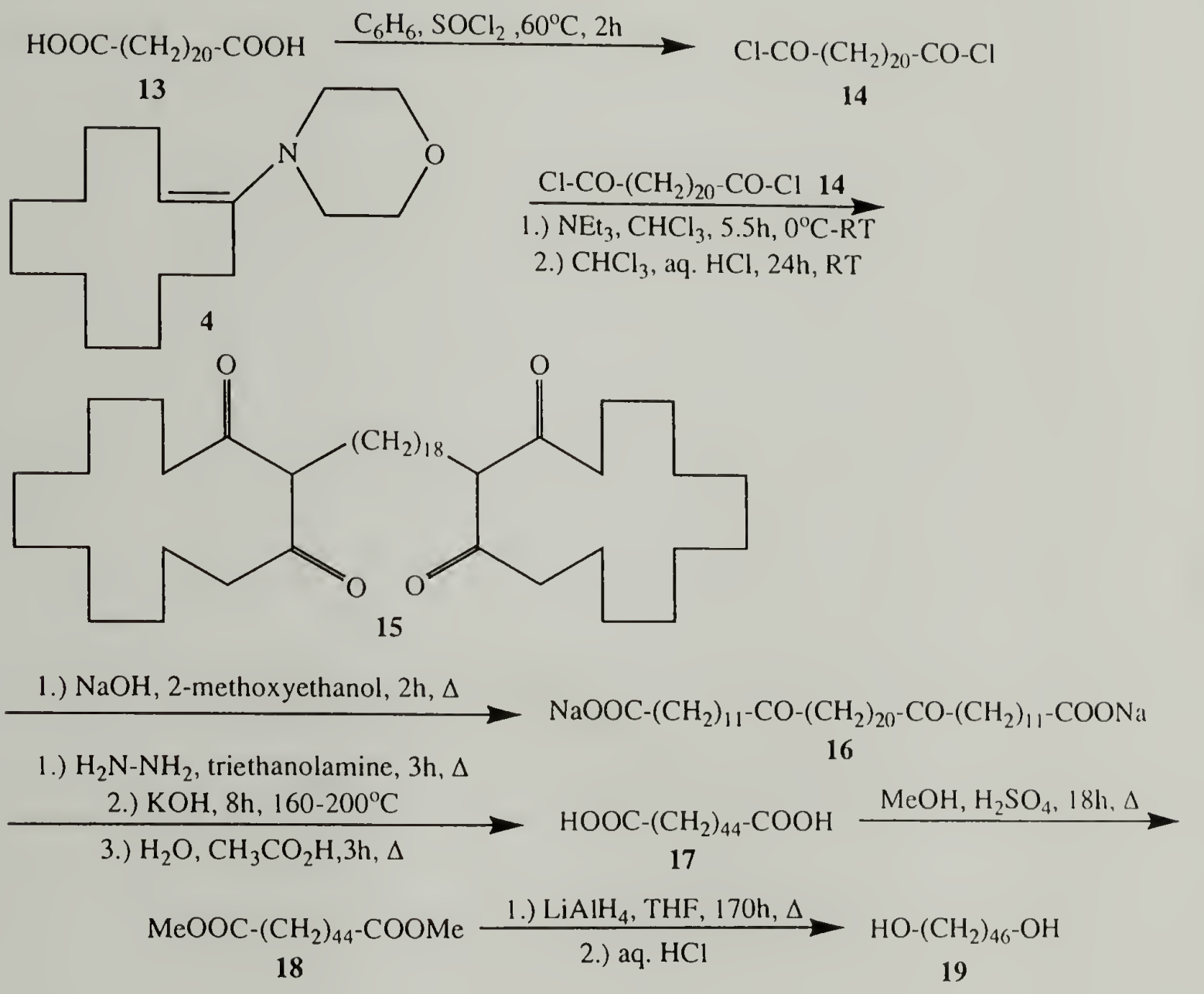

Scheme 2.9 Synthesis of 1,46-hexatetracontanediol.

The enamine coupling produces the tetraketone **15** in 67% yield after recrystallization. Subsequent ring-opening under basic conditions affords a quantitative yield of **16**, followed by a yield of 62 % for the Wolff-Kishner reduction. The synthesized long-chain diacid **17** is converted to the dimethylester **18** in a yield of 87 %.

This facilitates the reduction of the carbonyl to hydroxyl functionalities with lithium aluminum hydride, yielding the desired 1,46-hexatetracontanediol **19**. Formation of the tetraketone and separation from the side-products are crucial for a satisfactory overall yield. The overall route is achieved in 67 %, compared to a yield of 46 % reported by Hünig and Buysch.[3]

Synthesis of 1,56-hexapentacontanediol utilizing the previously synthesized 1,32-dotriacontanedioic acid could not be performed in satisfactory yields. This is attributed to low solubility and difficulties in the crucial purification of the tetraketone formed by the enamine coupling.

2.3.3 Synthetic Routes to ^{13}C-labeled Short-Chain Diacids Used in this Study

In order to enable or in certain cases facilitate solid-state NMR characterization, it is desirable to introduce ^{13}C-labels into the short-chain diacids used in subsequent polymerizations. Two major considerations in the design of the following labeling reactions are the ease of synthesis and purification of the products. Of special importance is the availability of clean and complete separation from side products. The third, equally important, consideration is the cost of the labeled material to be used in the synthesis. For example, reasonably inexpensive ^{13}C-labeled potassium cyanide, which can be used in a variety of nucleophilic substitution reactions, is a good starting material for labeling reactions.

Reaching this goal is not always possible though. For example, the synthesis of hexyl-branched malonate had to be performed using the significantly more expensive ^{13}C-labeled diethyl malonate. The use of higher cost starting material is necessary in this case

as there are no other synthetic routes to substituted malonates that start from more reasonably priced labeled precursors.

The first targeted diacid, succinic acid, was synthesized in both its mono- and doubly-labeled versions by nucleophilic substitution with ^{13}C-labeled potassium cyanide of bromoproprionitrile and 1,2-dibromoethane, respectively as is shown in Scheme 2.10.

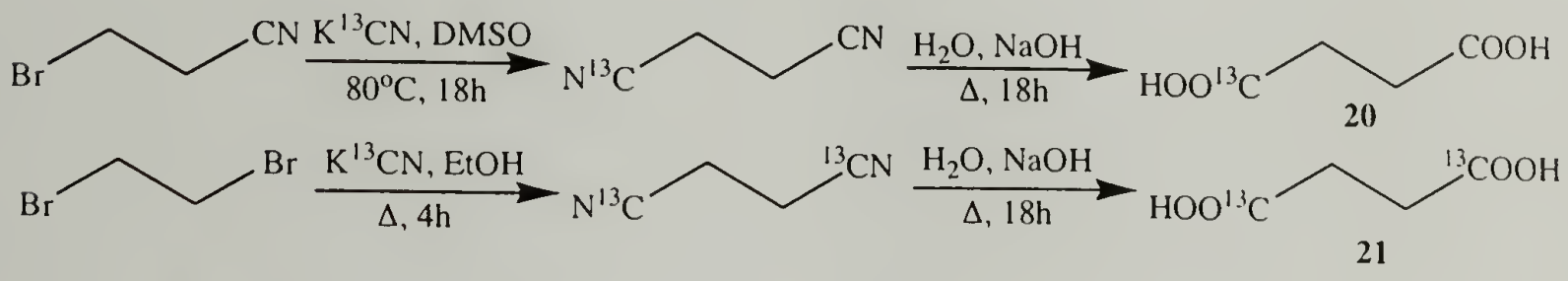

Scheme 2.10 Synthesis of ^{13}C-labeled succinic acid.

In order to include branches into the polyester backbone, diacids bearing branches of varying length were also synthesized. Le Fevere de Ten Hove had shown that inclusion of 3-propylglutaric acid into a sufficiently long (44 methylene units) polymer backbone yields control over lamellar thickness. Therefore, ^{13}C-labeled 3-propylglutaric and 3-phenylglutaric acid were synthesized according to the reaction sequence shown in Scheme 2.11. First, propyl- and phenyl-branched diethylmalonate were reduced to the branched propanediols **22** and **25** by reaction with lithium aluminum hydride. The hydroxyl functionalities were subsequently reacted with p-toluenesulfonyl chloride, introducing tosylates as good leaving groups. Subsequent nucleophilic substitution with ^{13}C-labeled potassium cyanide yielded dinitriles. The dinitriles were then hydrolized under basic conditions to yield ^{13}C-labeled branched glutaric acids **24** and **27**.

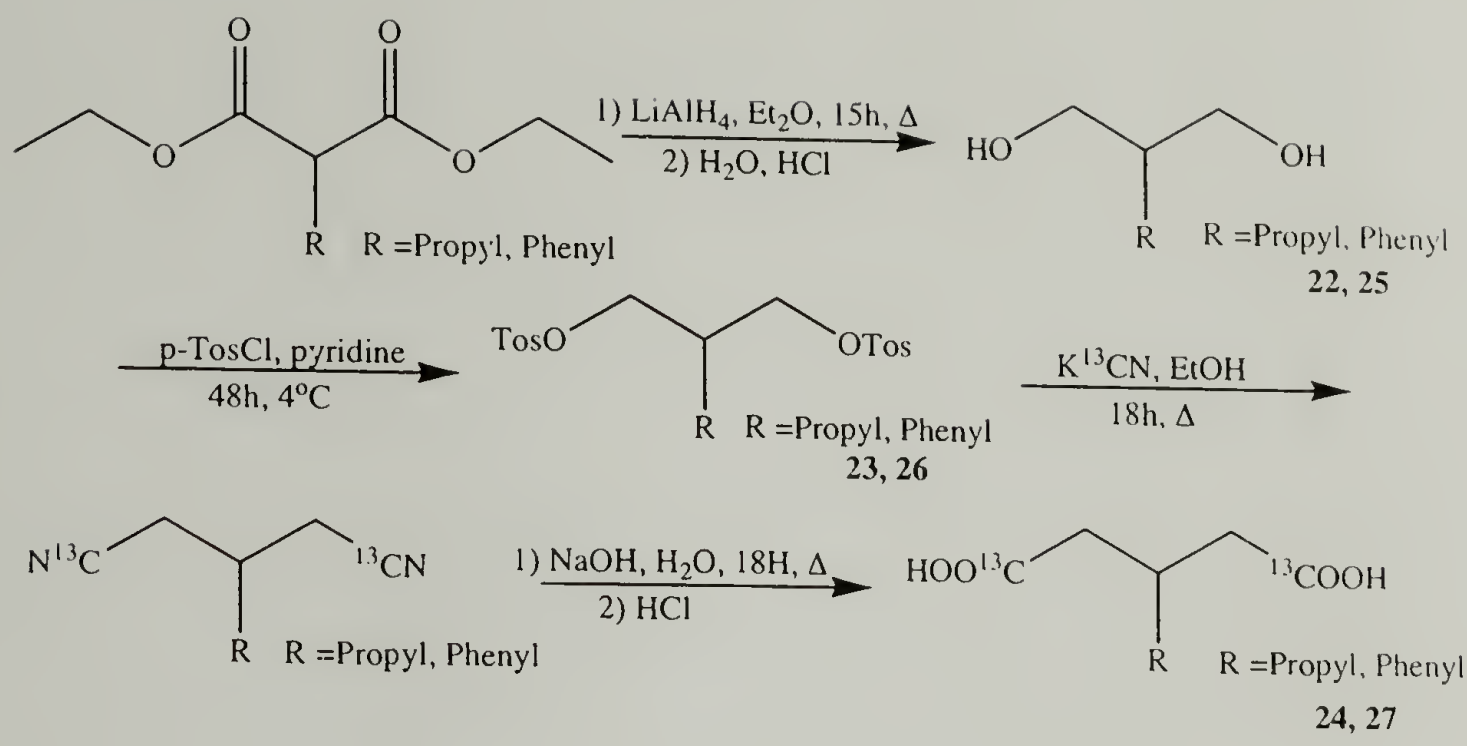

Scheme 2.11 Synthesis of branched glutaric acids.

The substitution of ditosylates by potassium cyanide was hindered by the relatively large side groups on the vicinal position (propyl or phenyl), which limit access to the reaction side. Therefore, the substitution reaction was allowed to proceed overnight in order to ensure the complete substitution of tosylate groups by cyanides.

In order to introduce a cis-bond into the diacid unit, ^{13}C-labeled 1,2-phenylenediacetic acid was synthesized from α,α'-dibromo-o-xylene by nucleophilic substitution with ^{13}C-labeled potassium cyanide in acetone, followed by hydrolysis of the dinitrile, in an overall yield of 31 %. The reaction is shown in Scheme 2.12.

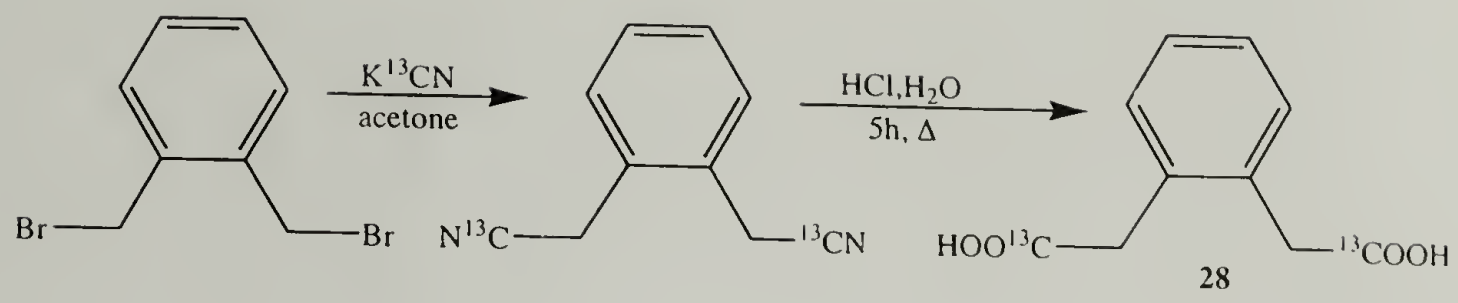

28

Scheme 2.12 Synthesis of 1,2-phenylenediacetic acid.

The last diacid monomer synthesized in this study was diethyl hexylmalonate. Starting from ^{13}C-labeled diethyl malonate, the hexyl branch is introduced *via* deprotonation of diethylmalonate with freshly prepared sodium ethoxide, followed by nucleophilic substitution of 1-bromohexane with the formed malonate anion. The product **29** is obtained in 33% yield after purification by Kugelrohr distillation. The reaction sequence is shown in Scheme 2.13.

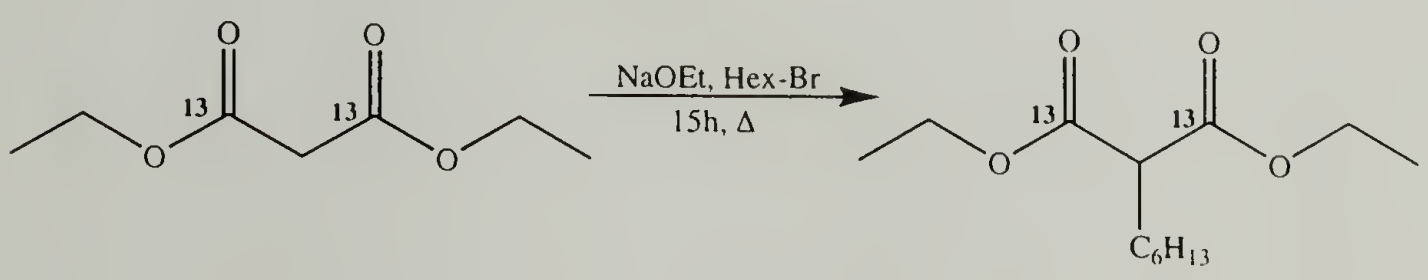

29

Scheme 2.13 Synthesis of 1,3-^{13}C-diethyl hexylmalonate.

2.3.4 Characterization of Monomers

2.3.4.1 Spectroscopic Characterization

The obtained long-chain diols were characterized by ^{1}H-NMR and IR spectroscopy in order to determine their purity and suitability as monomers in

polyesterification reactions. In the case of the 1,22-docosanediol synthesized by Wurtz coupling the reaction course can be monitored by shifts in the ^{1}H-NMR resonances (α-CH_2 next to Br, I, OH). Side products such as 1-undecanol and 10-undecen-1-ol are also easily detectable by ^{1}H-NMR, and disappear after recrystallization of the 1,22-docosanediol in methanol, yielding a pure product.

The purification of the intermediates used in the synthesis of longer diols is more difficult. The Wolff-Kishner reduction of dioxo diacids does not always proceed to full conversion, leaving residual ketone functionalities on some by-products. These ketones are not tolerated in subsequent steps of the reaction scheme, as the reduction of esters to hydroxyl groups with lithium aluminum hydride will also reduce ketones. This would introduce hydroxyl functionalities not only at the ends of the diols, but also internally, resulting in crosslinking in subsequent polyesterifications. As a result, great care has to be taken to ensure complete reduction of the ketones before the terminal ester functionalities are reduced.

Due to the low concentration of methylene groups adjacent to the ketone functionalities, unreduced ketones cannot always be detected by ^{1}H-NMR. On the other hand, IR proved to be a very effective tool to confirm the absence of internal ketones after full conversion, since the carbonyl group is very IR-active. In some instances, repeated Wolff-Kishner reduction had to be performed to ensure complete reduction of internal ketone functionalities, as monitored by IR.

Another yield-limiting step is the actual reduction of diesters to diols. Due to the low solubility of both, reagents and products, the reactions had to be carried out for several days. On several occasions it was found that even after these long reaction times,

unreduced ester functionalities were still present. This required a repetition of the reduction procedure, which inevitably results in some loss of product.

The monomer purity was confirmed by ^{1}H-NMR and IR. The diols exhibit Davydov splittings typically observed for orthorhombically packed n-paraffins, but no residual carbonyl group signals.[28] These splittings in the CH_2 bending (1460 and 1470 cm^{-1}) and rocking (720 and 730 cm^{-1}) have also been previously observed for 1,22-docosanediol and 1,44-tetratetracontanediol, providing strong evidence of orthorhombic packing of the long-chain diols synthesized here.[2] The IR spectrum of 1,32-dotriacontanediol is shown in Figure 2.1 as an example of the long-chain diols' Davydov splittings observed for all samples.

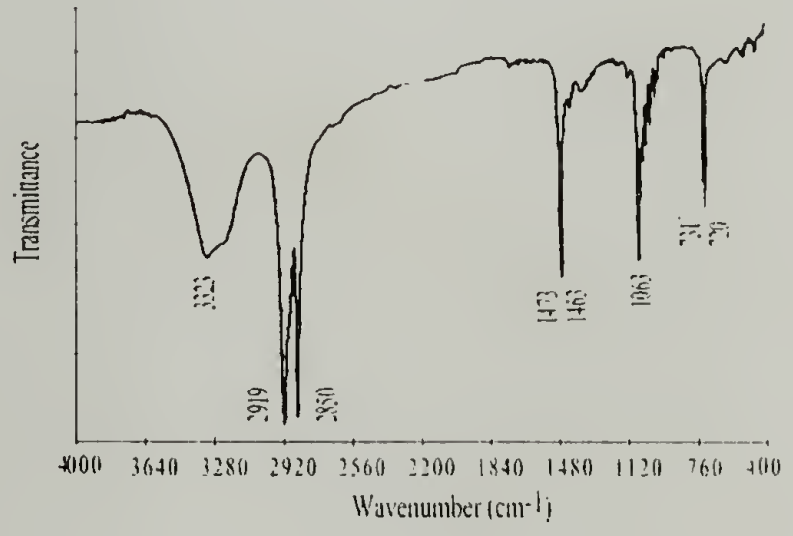

Figure 2.1 IR spectrum of 1,32-dotriacontanediol.

The purity of the labeled short-chain diacids synthesized in this study was determined by ^{1}H- and ^{13}C-NMR spectra. The labeled carbonyl group can be clearly observed by ^{13}C-NMR after only a few scans. The formation of nitriles, as well as the protonation of sodium salts after hydrolysis of nitriles, is easily monitored due to the

significant amplification of ^{13}C-NMR signals resulting from the almost quantitative labeling.

2.3.4.2 Thermal Properties

Long-chain diols have been shown previously to exhibit not only a melting endotherm, but also an additional endotherm attributed to a solid-solid phase transition.[2,29,30] This solid-solid transition has been classified as a rotator phase, with the higher temperature solid adopting a smectic G liquid crystalline structure.[30] In Figure 2.2, a typical DSC thermogram (second heating curve) is shown for the case of 1,32-dotriacontanediol, exemplifying the thermal behavior exhibited by this and other long-chain diols.

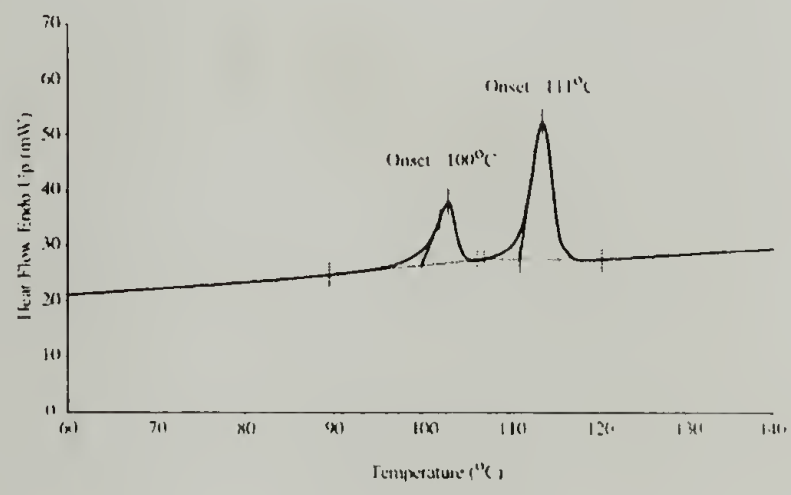

Figure 2.2 DSC thermogram of 1,32-dotriacontanediol.

The transition temperatures obtained for 1,22-docosanediol of 96°C for the solid-solid phase transition and 105°C for the melting temperature are in good agreement with the values of 97°C and 106°C obtained by Ogawa.[29] This observation confirms the high

purity of the monomer. Similarly, 1,32-dotriacontanediol exhibits transitions at 100°C and 111°C, which are close to the values observed by McKiernan.[31] The long-chain diol 1,46-hexatetracontanediol has transitions at 89°C and 109°C, which are both eight degrees lower than the transitions observed by McKiernan.[31] It is possible that a slight amount of residual ketone functionalities caused the lowering of transitions as compared to the results obtained by McKiernan, but the exact reasons for these lower transition temperatures were not further investigated here. As spectroscopic characterizations indicated sufficient purity of the 1,46-hexatetracontanediol, it was used in subsequent polymerizations.

2.4 Conclusions

A series of long-chain aliphatic diols was synthesized in high purity as shown by ^{1}H-NMR, IR, and DSC measurements. 1,22-docosanediol was obtained in an overall yield of 50 % using Wurtz coupling. To synthesize 1,32-dotriacontanediol and 1,46-hexatetracontanediol, a number of enamine couplings were performed. Due to repeated reductions of diesters to diols, calculating an overall yield was not possible. However, the actual enamine couplings were achieved in yields significantly higher than those reported in the literature, demonstrating the feasibility of this approach to the synthesis of long-chain diols. However, attempts to synthesize 1,56-hexapentacontanediol from 1-morpholino-1-cyclododecene and 1,32-dotriacontanedioic acid were unsuccessful. Nevertheless, the synthetic route utilizing repeated enamine couplings is promising. The diols synthesized here all possessed solid-solid phase transitions attributed to a rotator phase. Although an increase in the methylene segment lengths does lead to difficulties in

work-ups and purification due to low solubilities, overall it is preferable to the Wurtz coupling procedure previously employed by Le Fevere de Ten Hove.

A variety of short-chain ^{13}COO-labeled diacids were synthesized by nucleophilic substitution. Although yields of these labeling reactions are fairly low (30-40 %), the ease of substitution, ready availability of starting materials, and the use of relatively inexpensive ^{13}C-labeled potassium cyanide makes this a feasible route to ^{13}COO-labeled diacids. In the case of hexyl-branched malonate, more expensive ^{13}COO-labeled diethyl malonate had to be used, but again, ease of reaction and the enabling of sophisticated NMR experiments through ^{13}C-enrichment justify the added expense. Finally, purity of labeled diacids was ensured by ^{1}H- and ^{13}C-NMR.

2.5 References

(1) Rusanova, E. E.; Sebyakin, Y. L.; Volkova, L. V.; Evstigneeva, R. P. *Zh. Org. Khim.* **1984**, *20*, 279-282.

(2) Le Fevere de Ten Hove, C. Ph. D., Université Catholique de Louvain, 2001.

(3) Hünig, S.; Buysch, H. *Chem. Ber.* **1967**, *100*, 4010.

(4) Hünig, S.; Lücke, E.; Brenninger, W. *Org. Synth. Coll. Vol.* **1973**, *5*, 533-539.

(5) Ehrenstein, M.; Dellsperger, S.; Kocher, C.; Stutzmann, N.; Weder, C.; Smith, P. *Polymer* **2000**, *41*, 3531-3539.

(6) Brown, R. D.; Godfrey, P. D.; Elmes, P. S.; Rodler, M.; Tack, L. M. *J. Am. Chem. Soc.* **1985**, *107*, 4112-4115.

(7) Holmes, D. L.; Lightner, D. A. *Tetrahedron* **1996**, *52*, 5319-5338.

(8) Mowry, D. T. *Chem. Rev.* **1948**, *42*, 189-284.

(9) Friedman, L.; Shechter, H. *J. Org. Chem.* **1960**, *25*, 877.

(10) Kobler, H. *Liebigs Ann. Chem.* **1978**, 1946-1962.

(11) Hadjoudis, E.; Pulima, I. *Mol. Cryst. Liq. Cryst.* **1986**, *137*, 29-36.

(12) von Braun, J.; Kruber; Danziger *Chem. Ber.* **1916**, *49*, 2647.

(13) Becker, H. G. O. *Organikum*; 19 ed.; Barth Verlagsgesellschaft mbH: Leipzig, 1993.

(14) Petragnani, N.; Yonashiro, M. *Synthesis* **1982**, 521-578.

(15) *Dictionary of Natural Products*; 1st ed.; Chapman & Hill: London, 1994.

(16) Patwardhan, S. A. *Org. Prep. Proced. Int.* **1994**, *26*, 645-670.

(17) Murray, K. E.; Schoenfeld, R. *Aust. J. Chem.* **1955**, *8*, 432.

(18) Saotome, K.; Komoto, H.; Yamazaki, T. *Bull. Chem. Soc. Japan* **1966**, *39*, 480.

(19) Signer, R.; Sprecher, P. *Helv. Chim. Acta* **1947**, *30*, 1001.

(20) Musgrave, O. C.; Stark, J.; Spring, F. S. *J. Chem. Soc.* **1952**, 4393.

(21) Adams, K. R.; Beonnett, R. *Phytochemistry* **1971**, *10*, 1885.

(22) Schlosser, M.; Bossert, H. *Tetrahedron* **1991**, *47*, 6287-6292.

(23) Brooke, G. M.; Burnett, S.; Mohammed, S.; Proctor, D.; Whiting, M. C. *J. Chem. Soc.-Perkin Trans. 1* **1996**, 1635-1645.

(24) Duhamel, L. *Ann. Chim. (Paris)* **1963**, *8*, 315.

(25) Hünig, S.; Lücke, E. *Chem. Ber.* **1959**, *92*, 652.

(26) Hünig, S.; Lendle, W. *Chem. Ber.* **1960**, *93*, 913.

(27) Hünig, S.; Hoch, H. *Tetrahedron Lett.* **1966**, *42*, 5215-5220.

(28) Lee, K.-S.; Wegner, G.; Hsu, S. L. *Polymer* **1987**, *28*, 889.

(29) Ogawa, Y.; Nakamura, N. *Bull. Chem. Soc. Jpn.* **1999**, *72*, 943-946.

(30) Kobayashi, H.; Nakamura, N. *Cryst. Res. Technol.* **1995**, *30*, 495-500.

(31) McKiernan, R. L. Ph. D., University of Massachusetts, 2002.

CHAPTER 3

SYNTHESIS OF POLYETHYLENE-LIKE POLYESTERS DERIVED FROM α,ω-LONG-CHAIN DIOLS

3.1 Introduction

In the mid to late 19th century, Berzelius and others first synthesized polyesters.[1,2] However, the first systematic study of polyesters had to wait until the 1920s for Carothers and coworkers at DuPont.[3-5] They synthesized a series of linear aliphatic polyesters which ended up being of little commercial interest due to their low melting points. Fifteen years later, Whinfield synthesized poly(ethylene terephtalate) (PET), which gained wide use as fibers and films under the brand name "Terylene".[6] Since those pioneering days, a number of polyesters, aliphatic as well as aromatic, have become of significant commercial importance. More recently, biodegradable polyesters such as poly(ε-caprolactone) and poly(L-lactide) have gained wide interest because of their potential use as hydrophobic drug carriers.[7,8] Additionally, hyperbranched polyesters synthesized from multifunctional monomers have been exploited to produce nanoscopically tailored materials with novel mechanical and rheological properties.[9]

As mentioned previously in chapter 1, the goal of this study is to identify, synthesize, and thoroughly characterize model polymers with perfectly regularly-located structural "defects", in contrast to randomly-located branches in some polyethylenes. Polyesters were selected for this investigation due to their ease of synthesis and the wide variety of potential structural defects that can be incorporated by an appropriate choice of monomers. These model polyesters will allow to study the influence of the "defects" on

the obtained polymer morphology. This, in turn, is expected to enable a better understanding of the connection between chemical structure and crystalline microstructure in synthetic semi-crystalline polymers. Copolymerization of diols of varying length with branched and non-branched diacids bearing ^{13}C-labels will generate a large variety of systems that can be studied by X-ray scattering and solid-state NMR.

Previous studies in the Penelle group have shown structural control over lamellar thicknesses of polyethylene-like polyesters through copolymerization of a branched diacid with a sufficiently long aliphatic linear diol.[10] As a result, a primary objective was to establish the scope of this approach, and to determine the minimum length required for the aliphatic spacer to control the crystal thickness.

The structure of all the polyesters targeted in this study is summarized in Scheme 3.1, along with the abbreviation that will be used later in this document.

Polyester	n	R	Abbreviation
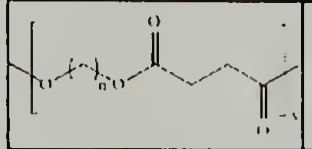	22; 32/12	n.a.	22.4 32/12.4
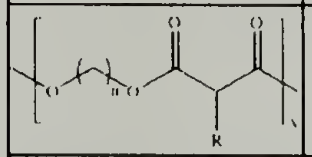	22; 32; 44	H, Ph, Hex	22.3-6;22.3-ph 32.3;32.3-6, 32.3-ph 44.3
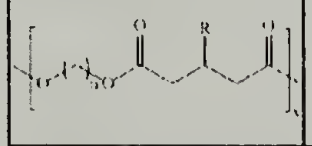	22: 32; 46	Ph, Prop	22.5-ph 32.5-3, 32.5-ph 46.5-3, 46.5-ph
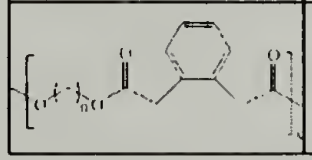	22: 32; 46	n.a.	22.phac 32.phac 46.phac

Scheme 3.1 Structures and abbreviations of polyesters synthesized in this study.

3.2 Experimental

3.2.1 Spectroscopic Characterization

Solution ^{1}H- and ^{13}C-nuclear magnetic resonance (NMR) spectra at room temperature were obtained with a Bruker DPX 300 MHz spectrometer $CDCl_3$. Solution ^{1}H- and ^{13}C-NMR spectra at elevated temperatures were obtained with a Bruker Avance 600 MHz spectrometer in either $CDCl_3$ or d_6-DMSO. Infrared (IR) spectra were recorded with a Bio-Rad FTS 175C infrared spectrometer, using either 16 or 64 scans, and are reported after background subtraction.

3.2.2 Molecular Weight Characterization

Molecular weights and weight distributions were obtained by gel permeation chromatography relative to polystyrene standards using a system equipped with Polymer Laboratories PL mixed bead gel columns, a HP series 1500 HPLC pump with chloroform as the mobile phase, and a HP 1047A Refractive Index detector. An elution rate of 1 ml min^{-1} was used.

3.2.3 Polymer Synthesis

Unlabeled diacids were obtained from commercial sources, and used as received without further purification. All solid monomers, diols and diacids, were dried in vacuum overnight prior to polymerization. The polymerization tubes used in the synthesis of the polyesters were also dried at least overnight prior to reaction.

Synthesis of polyesters containing a diacid unit consisting of more than three carbon atoms in length was achieved by direct polycondensation of equimolar amounts of

the long-chain diols and short-chain diacids. It was performed under inert atmosphere (purging of reaction vessel with nitrogen), and used p-toluenesulfonic acid as the catalyst at 120°C. A typical reaction procedure is given below:

In a polymerization tube, 0.10 g (0.083 mmol) of 1,4-$^{13}C_2$-labeled succinic acid, 0.285 g (0.083 mmol) of 1,22-docosanediol, and a few milligrams of p-toluenesulfonic acid were melted in an oil bath preheated at 120°C. The vessel was then purged with nitrogen for 5 minutes, and let to react overnight. Vacuum was applied over an additional night to remove water formed during the polymerization and to drive the polymerization to completion. After cooling to room temperature, the polyester was dissolved in chloroform, precipitated into methanol, filtered, and dried in vacuum to yield 0.25 g (68%) of polyester.

For the polymerization of malonates, transesterification of diethyl malonates rather than direct polycondensation was performed. Titanium isopropoxide, acting as a Lewis acid, was used as the catalyst.[11,12] A typical polymerization reaction was performed as follows:

In a polymerization tube, 0.123 g (0.50 mmol, 0.13 mL) of diethyl 1,3-$^{13}C_2$-hexylmalonate and 0.241 g (0.50 mmol) of 1,32-dotriacontanediol were melted in an oil bath preheated to 120°C. After complete melting of the diol, a few drops of titanium isopropoxide were added, upon which bubbles of evaporating ethanol became visible. After purging the vessel with nitrogen for a few minutes, the reaction was allowed to continue overnight under atmospheric pressure to form oligomers. Vacuum was then applied for an additional 15 hours to remove the formed ethanol and to drive the polymerization to completion. After cooling to room temperature, the polyester was

dissolved in chloroform, precipitated into methanol, filtered, and dried in vacuum to yield 0.25g (72%) of polyester.

All polyesters are designated in this document by a first number referring to the number of methylene units in the diol segment, followed by a specific abbreviation for the diacid segment based on the number of carbon atoms as well as the nature of the branch in the diacid unit. The following polyesters were synthesized and characterized by solution ^{1}H- and ^{13}C-NMR (with the exception of 46,5-3, 46,5-ph, and 46,phac due to low solubility), and by IR spectroscopy.

Poly(docosanediol-alt-succinic acid) (22,4). ^{1}H-NMR (300 MHz, $CDCl_3$) δ 4.08 (4H, t, J = 6.8 Hz, $C\underline{H}_2$-OOC), 2.62 (s, 4H, OOC-$C\underline{H}_2$- $C\underline{H}_2$-COO), 1.62 (p, 4H J = 6.4 Hz, $C\underline{H}_2$-CH_2-OOC), 1.30-1.20 (m, 36H, -($C\underline{H}_2$)-). ^{13}C-NMR (75 MHz, $CDCl_3$) δ 172.87 (COO), 63.26 (OCH_2), 29.83, 29,76, 29.58, 25.88 (-(CH_2)-). IR (KBr pellet): 2914 cm^{-1} (asymmetric CH stretch), 2850 cm^{-1} (symmetric CH stretch), 1716 cm^{-1} (C=O stretch), 1480 and 1475 cm^{-1} (CH_2 bend), 1161 cm^{-1} (C-O stretch), 723 and 719 cm^{-1} (CH_2 rock).

Poly(dodecanol/dotriacontanediol-alt-succinic acid) (32/12,4). ^{1}H-NMR (300 MHz, $CDCl_3$) δ 4.08 (4H, t, J = 6.5 Hz, $C\underline{H}_2$-OOC), 2.62 (s, 4H, OOC-$C\underline{H}_2$- $C\underline{H}_2$-COO), 1.62 (p, 4H, $C\underline{H}_2$-CH_2-OOC), 1.40-0.92 (m, 36H, -($C\underline{H}_2$)-). ^{13}C-NMR (75 MHz, $CDCl_3$) δ 172.57 (COO), 65.07 (OCH_2), 29.87, 29,70, 29.42, 29.34, 28.74, 26.04 (-(CH_2)-). IR (KBr pellet): 2920 cm^{-1} (asymmetric CH stretch), 2852 cm^{-1} (symmetric CH stretch), 1732 cm^{-1} (C=O stretch), 1472 and 1465 cm^{-1} (CH_2 bend), 1148cm^{-1} (C-O stretch), 731 and 720 cm^{-1} (CH_2 rock).

Poly(dotriacontanediol-alt-malonic acid) (32,3). ^{1}H-NMR (300 MHz, $CDCl_3$) δ 4.19 (t, 4H, O-C$\underline{H}_2$), 3.36 (s, 2H, OOC-C$\underline{H}_2$-COO), 1.64 (m, 4H, C$\underline{H}_2$-CH$_2$-O), 1.38-1.06 (m, 56H, -(C$\underline{H}_2$)-). ^{13}C-NMR (75 MHz, $CDCl_3$) δ 172.89 (COO), 65.23 (OCH_2), 29.89 (-(CH_2)-). IR (KBr pellet): 2921 cm^{-1} (asymmetric CH stretch), 2851 cm^{-1} (symmetric CH stretch), 1732 cm^{-1} (C=O stretch), 1475 and 1467 cm^{-1} (CH_2 bend), 1161cm^{-1} (C-O stretch), 725 and 719 cm^{-1} (CH_2 rock).

Poly(docosanediol-alt-hexylmalonic acid) (22,3-6). ^{1}H-NMR (300 MHz, $CDCl_3$) δ 4.12 (4H, t, J = 6.4 Hz, C$\underline{H}_2$-OOC), 3.32 (s, 1H, J = 7.5 Hz, OOC-C$\underline{H}$R-COO), 1.88 (m, 2H, CH-C$\underline{H}_2$), 1.60 (m, 6H, C$\underline{H}_2$-CH$_2$-OOC, CH-CH$_2$-C$\underline{H}_2$), 1.40-1.15 (m, 42H, -(C$\underline{H}_2$)-), 0.86 (t, 3H, J = 6.8 Hz, -C$\underline{H}_3$). ^{13}C-NMR (75 MHz, $CDCl_3$) δ 170.10 (COO), 65.81 (OCH_2), 52.54 (CO-CH-CO), 31.94, 30.16, 30.03, 29.97, 29.65, 29.30, 29.18, 28.92, 27.71, 26.24, 22.94 (-(CH_2)-), 14.44 (-CH_3), IR (KBr pellet): 2918 cm^{-1} (asymmetric CH stretch), 2852 cm^{-1} (symmetric CH stretch), 1732 cm^{-1} (C=O stretch), 1467 cm^{-1} (CH_2 bend), 1152 cm^{-1} (C-O stretch), 719 cm^{-1} (CH_2 rock).

Poly(dotriacontanediol-alt-hexylmalonic acid) (32,3-6). ^{1}H-NMR (300 MHz, $CDCl_3$) δ 4.11 (4H, t, J = 6.0 Hz, C$\underline{H}_2$-OOC), 3.31 (s, 1H, J = 7.5 Hz, OOC-C$\underline{H}$R-COO), 1.87 (m, 2H, CH-C$\underline{H}_2$), 1.60 (m, 6H, C$\underline{H}_2$-CH$_2$-OOC, CH-CH$_2$-C$\underline{H}_2$), 1.45-1.05 (m, 64H, -(C$\underline{H}_2$)-), 0.85 (t, 3H, J = 6.2 Hz, -C$\underline{H}_3$). ^{13}C-NMR (75 MHz, $CDCl_3$) δ 169.86 (COO), 65.56 (OCH_2), 52.27 (CO-CH-CO), 31.70, 29.91, 29.78, 29.42, 29.07, 28.93, 28.68, 26.00, 22.71 (-(CH_2)-), 14.21 (-CH_3), IR (KBr pellet): 2921 cm^{-1} (asymmetric CH stretch), 2851 cm^{-1} (symmetric CH stretch), 1694 cm^{-1} (C=O stretch), 1473 and 1465 cm^{-1} (CH_2 bend), 1123 cm^{-1} (C-O stretch), 725 and 719 cm^{-1} (CH_2 rock).

Poly(docosanediol-alt-phenylmalonic acid) (22,3-ph). ^{1}H-NMR (300 MHz, $CDCl_3$) δ 7.39 (m, 5H, aromatic CH), 4.61 (s, 1H, OOC-C<u>H</u>R-COO), 4.14 (4H, t, J = 5.5 Hz, C<u>H</u>$_2$-OOC), 1.59 (m, 4H, C<u>H</u>$_2$-CH$_2$-OOC), 1.40-1.10 (m, 36H, -(C<u>H</u>$_2$)-). ^{13}C-NMR (75 MHz, $CDCl_3$) δ 168.63 (COO), 133.30, 129.69, 128.94, 128.55 (aromatic C) 66.32 (OCH_2), 58.47 (CO-<u>C</u>H-CO), 30.15, 30.00, 29.93, 29.59, 28.84, 26.15 (-(CH_2)-). IR (KBr pellet): 2919 cm^{-1} (asymmetric CH stretch), 2851 cm^{-1} (symmetric CH stretch), 1735 cm^{-1} (C=O stretch), 1468 and 1456 cm^{-1} (CH_2 bend), 1144 cm^{-1} (C-O stretch), 723 and 710 cm^{-1} (CH_2 rock), 695 cm^{-1} (aromatic CH bend).

Poly(dotriacontanediol-alt-phenylmalonic acid) (32,3-ph). ^{1}H-NMR (300 MHz, $CDCl_3$) δ 7.40 (m, 5H, aromatic CH), 4.61 (s, 1H, OOC-C<u>H</u>R-COO), 4.15 (m, 4H, C<u>H</u>$_2$-OOC), 1.59 (m, 4H, C<u>H</u>$_2$-CH$_2$-OOC), 1.40-1.10 (m, 56H, -(C<u>H</u>$_2$)-). ^{13}C-NMR (75 MHz, $CDCl_3$) δ 168.39 (COO), 129.44, 128.69, 128.31 (aromatic C) 66.08 (OCH_2), 58.21 (CO-<u>C</u>H-CO), 28.89, 29.75, 29.68, 29.34, 28.59, 25.90 (-(CH_2)-). IR (KBr pellet): 2919 cm^{-1} (asymmetric CH stretch), 2851 cm^{-1} (symmetric CH stretch), 1735 cm^{-1} (C=O stretch), 1473 and 1465 cm^{-1} (CH_2 bend), 1144 cm^{-1} (C-O stretch), 729 and 720 cm^{-1} (CH_2 rock) 694 cm^{-1} (aromatic CH bend).

Poly(docosanediol-alt-3-phenylglutaric acid) (22,5-ph). ^{1}H-NMR (300 MHz, $CDCl_3$) δ 7.28-7.20 (m, 5H, aromatic CH), 3.96 (t, 4H, J = 6.7 Hz, C<u>H</u>$_2$-OOC), 3.64 (p, 1H, J = 7.2 Hz, C<u>H</u>Ph), 2.67 (m, 4H, C<u>H</u>$_2$-COO), 1.49 (p, 4H, J = 6.6 Hz, C<u>H</u>$_2$-CH$_2$-OOC), 1.39-1.05 (m, 36H, -(C<u>H</u>$_2$)-). ^{13}C-NMR (75 MHz, $CDCl_3$) δ 172.11 (COO), 142.90, 128.92, 127.68, 127.31 (aromatic C) 65.06 (COO<u>C</u>H$_2$), 41.18 (OOC-<u>C</u>H$_2$), 38.87 (<u>C</u>HPh), 30.16, 30.03, 29.93, 29.65, 28.93, 26.24 (-(CH_2)-). IR (KBr pellet): 2914 cm^{-1} (asymmetric CH stretch), 2850 cm^{-1} (symmetric CH stretch), 1717 cm^{-1} (C=O stretch),

1477 and 1473 cm^{-1} (CH_2 bend), 1163 cm^{-1} (C-O stretch), 720 and 715 cm^{-1} (CH_2 rock) 750 and 695 cm^{-1} (aromatic CH bend).

Poly(dotriacontanediol-alt-3-phenylglutaric acid) (32,5-ph). ^{1}H-NMR (600 MHz, $CDCl_3$) δ 7.28-7.21 (m, 5H, aromatic CH), 3.98 (t, 4H, J = 6.7 Hz, $C\underline{H}_2$-OOC), 3.64 (p, 1H, C<u>H</u>Ph), 2.67 (dq, 4H, $C\underline{H}_2$-COO), 1.51 (p, 4H, J = 6.9 Hz, $C\underline{H}_2$-CH_2-OOC), 1.35-1.15 (m, 56H, -($C\underline{H}_2$)-). ^{13}C-NMR (150 MHz, $CDCl_3$) δ 171.34 (COO), 128.31, 127.13, 126.67 (aromatic C) 64.41 (COO<u>C</u>H_2), 40.67 (OOC-<u>C</u>H_2), 38.44 (<u>C</u>HPh), 29.51, 29.46, 29.39, 29.31, 29.04, 28.46, 25.70 (-(CH_2)-). IR (KBr pellet): 2917 cm^{-1} (asymmetric CH stretch), 2850 cm^{-1} (symmetric CH stretch), 1736 cm^{-1} (C=O stretch), 1476 cm^{-1} (CH_2 bend), 1150 cm^{-1} (C-O stretch), 721 cm^{-1} (CH_2 rock) 761 and 702 cm^{-1} (aromatic CH bend).

Poly(hexatetracontanediol-alt-3-phenylglutaric acid) (46,5-ph). ^{1}H-NMR (600 MHz, $CDCl_3$) δ 7.30-7.15 (m, 5H, aromatic CH), 3.98 (t, 4H, J = 6.8 Hz, $C\underline{H}_2$-OOC), 3.64 (p, 1H, J = 7.1 Hz, C<u>H</u>Ph), 2.67 (dq, 4H, $C\underline{H}_2$-COO), 1.53-1.42 (m, 4H, $C\underline{H}_2$-CH_2-OOC), 1.36-1.22 (m, 84H, -($C\underline{H}_2$)-). IR (KBr pellet): 2925 cm^{-1} (asymmetric CH stretch), 2847 cm^{-1} (symmetric CH stretch), 1739 cm^{-1} (C=O stretch), 1467 cm^{-1} (CH_2 bend), 1173 cm^{-1} (C-O stretch), 723 cm^{-1} (CH_2 rock) 761 and 698 cm^{-1} (aromatic CH bend).

Poly(dotriacontanediol-alt-3-propylglutaric acid) (32,5-3). ^{1}H-NMR (600 MHz, $CDCl_3$) δ 4.07 (t, 4H, J = 6.8 Hz, $C\underline{H}_2$-OOC), 2.35 (s, 4H, $C\underline{H}_2$-COO), 1.63 (p, 1H, J = 7.0 Hz, CH_2-C<u>H</u>Prop-CH_2), 1.38-1.22 (m, 64H, -($C\underline{H}_2$)-), 0.92 (t, 3H, J = 7.1 Hz, $C\underline{H}_3$). ^{13}C-NMR (150 MHz, $CDCl_3$) δ 172.33 (COO), 64.27 (COO<u>C</u>H_2), 38.60 (OOC-<u>C</u>H_2), 36.18 (<u>C</u>HProp), 31.91, 29.52, 29.49, 29.40, 29.34, 29.08, 28.58, 25.81, 19.59 (-(CH_2)-), 13.79 (CH_3). IR (KBr pellet): 2920 cm^{-1} (asymmetric CH stretch), 2850 cm^{-1}

(symmetric CH stretch), 1694 cm^{-1} (C=O stretch), 1472 cm^{-1} (CH_2 bend), 1126 cm^{-1} (C-O stretch), 721 cm^{-1} (CH_2 rock).

Poly(hexatetracontanediol-alt-3-propylglutaric acid) (46,5-3). ^{1}H-NMR (600 MHz, $CDCl_3$) δ 4.07 (t, 4H, J = 6.8 Hz, C$\underline{H}_2$-OOC), 2.35 (s, 4H, C$\underline{H}_2$-COO), 1.63 (p, 1H, J = 7.0 Hz, CH_2-C$\underline{H}$Prop-CH_2), 1.38-1.22 (m, 64H, -(C$\underline{H}_2$)-), 0.92 (t, 3H, J = 7.1 Hz, C$\underline{H}_3$). ^{13}C-NMR (150 MHz, $CDCl_3$) δ 172.33 (COO), 64.27 (COO$\underline{C}H_2$), 38.60 (OOC-$\underline{C}H_2$), 36.18 ($\underline{C}$HProp), 31.91, 29.52, 29.49, 29.40, 29.34, 29.08, 28.58, 25.81, 19.59 (-(CH_2)-), 13.79 (CH_3). IR (KBr pellet): 2922 cm^{-1} (asymmetric CH stretch), 2849 cm^{-1} (symmetric CH stretch), 1694 cm^{-1} (C=O stretch), 1473 and 1463 cm^{-1} (CH_2 bend), 1165 cm^{-1} (C-O stretch), 731 and 719 cm^{-1} (CH_2 rock).

Poly(docosanediol-alt-1,2-phenylenediacetic acid) (22,phac). ^{1}H-NMR (300 MHz, $CDCl_3$) δ 7.40-7.10 (m, 5H, aromatic CH), 4.20 (t, 4H, C$\underline{H}_2$-OOC), 3.61 (s, 1H, CO-C$\underline{H}_2$Ph), 1.59 (m, 4H, C$\underline{H}_2$-CH_2-OOC), 1.40-1.15 (m, 36H, -(C$\underline{H}_2$)-). ^{13}C-NMR (75 MHz, $CDCl_3$) δ 171.80 (COO), 133.73, 131.16, 127.96 (aromatic C) 65.50 (COO$\underline{C}H_2$), 39.39 (OOC-$\underline{C}H_2$-Ph), 30.16, 30.10, 30.00, 29.95, 29.63, 28.95, 26.23 (-(CH_2)-). IR (KBr pellet): 2914 cm^{-1} (asymmetric CH stretch), 2850 cm^{-1} (symmetric CH stretch), 1716 cm^{-1} (C=O stretch), 1480 cm^{-1} (CH_2 bend), 1160 cm^{-1} (C-O stretch), 750 cm^{-1} (aromatic CH bend), 719 cm^{-1} (CH_2 rock).

Poly(dotriacontanediol-alt-1,2-phenylenediacetic acid) (32,phac). ^{1}H-NMR (600 MHz, $CDCl_3$) δ 7.26-7.09 (m, 4H, aromatic CH), 4.07 (t, 4H, C$\underline{H}_2$-OOC), 3.71 (s, 1H, CO-C$\underline{H}_2$Ph), 1.59 (m, 4H, C$\underline{H}_2$-CH_2-OOC), 1.38-1.18 (m, 56H, -(C$\underline{H}_2$)-). ^{13}C-NMR (75 MHz, $CDCl_3$) δ 171.55 (COO), 133.72, 131.16, 127.97 (aromatic C) 65.51 (COO$\underline{C}H_2$), 39.39 (OOC-$\underline{C}H_2$-Ph), 30.15, 29.95, 29.63, 28.95, 26.24 (-(CH_2)-). IR (KBr

pellet): 2917 cm^{-1} (asymmetric CH stretch), 2850 cm^{-1} (symmetric CH stretch), 1736 cm^{-1} (C=O stretch), 1476 cm^{-1} (CH_2 bend), 1148 cm^{-1} (C-O stretch), 750 cm^{-1} (aromatic CH bend), 723 cm^{-1} (CH_2 rock).

Poly(hexatetracontanediol-alt-1,2-phenylenediacetic acid) (46,phac). ^{1}H-NMR (600 MHz, $CDCl_3$) δ 7.27-7.08 (m, 4H, aromatic CH), 4.08 (t, 4H, J = 6.8 Hz, $C\underline{H}_2$-OOC), 3.71 (s, 1H, CO-$C\underline{H}_2$Ph), 1.60 (m, 4H, J = 6.6 Hz, $C\underline{H}_2$-CH_2-OOC), 1.35-1.15 (m, 84H, -($C\underline{H}_2$)-). IR (KBr pellet): 2922 cm^{-1} (asymmetric CH stretch), 2846 cm^{-1} (symmetric CH stretch), 1737 cm^{-1} (C=O stretch), 1472 cm^{-1} (CH_2 bend), 1155 cm^{-1} (C-O stretch), 765 cm^{-1} (aromatic CH bend), 726 cm^{-1} (CH_2 rock).

3.3 Results and Discussion

3.3.1 Synthetic Routes to Polyesters Investigated in this Study

Two different synthetic routes to the aliphatic polyesters shown in Scheme 3.1 were used. In the case of diacids with more than three carbon atoms, direct polycondensation of equimolar amounts of diol and diacid under p-toluenesulfonic acid catalysis was performed. After reaching the oligomeric state, vacuum was applied to drive the reaction to completion through removal of the water formed during the polycondensation and to obtain high molecular weight polyesters. Typical isolated polymer yields ranged between 60-70%. The polyesters were purified by dissolution in chloroform followed by precipitation into methanol.

In the case of polyesters incorporating a malonate unit, a direct polycondensation of malonic acid with diols was not possible as malonic acid decarboxylates at the high temperatures required for the polymerizations. Instead, polyesters were synthesized by

transesterification of branched and non-branched diethyl malonates with long-chain diols catalyzed by titanium isopropoxide acting as a Lewis acid. Again, the polymerizations were allowed to proceed under atmospheric pressure to reach an oligomeric state. Vacuum was then applied to remove the formed ethanol and to drive the polymerization to completion. The two reaction pathways are shown in Scheme 3.2.

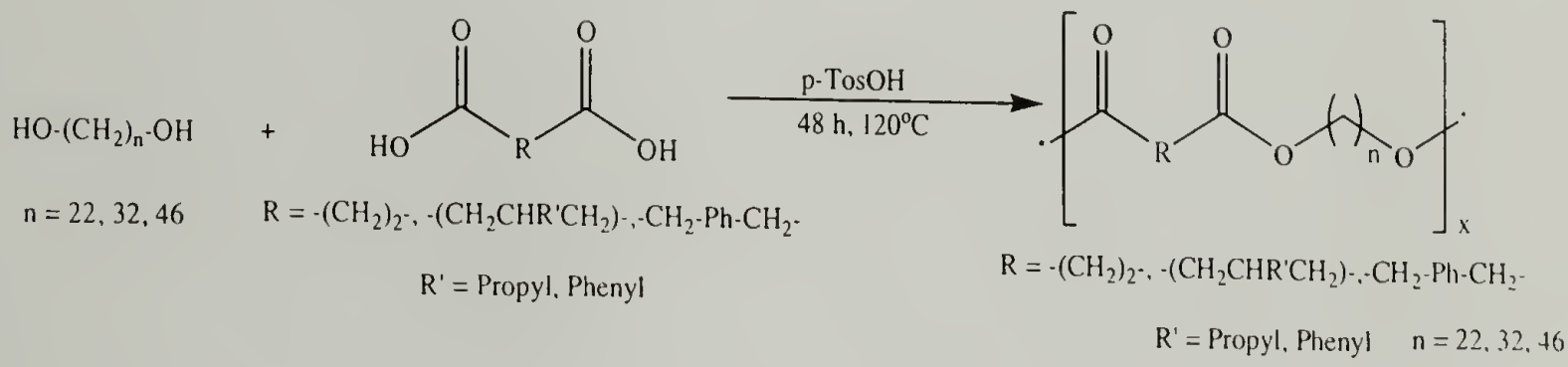

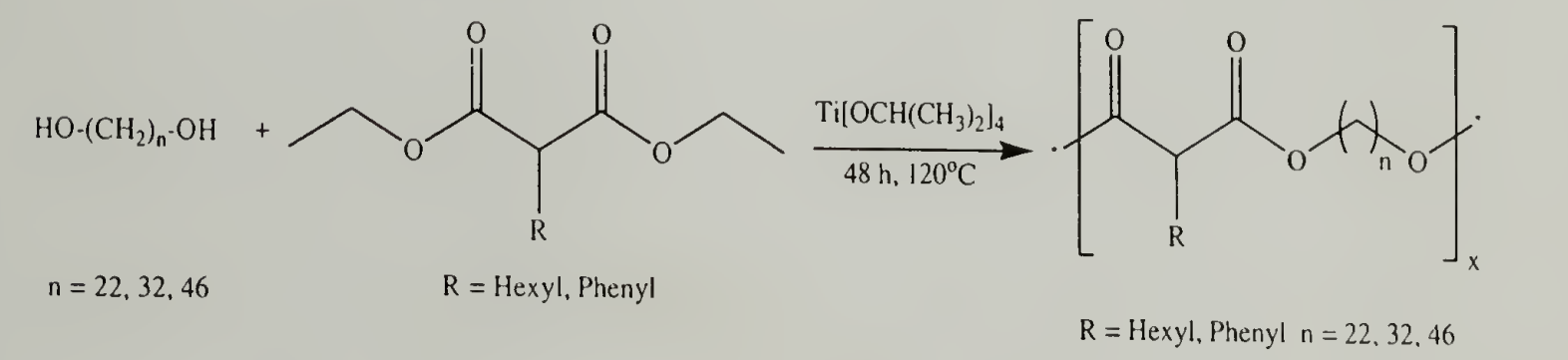

Scheme 3.2 Polyesterification of long-chain diols and short-chain diacids and diesters.

In both polyesterification reactions, condensation was observed at the top of the polymerization tube shortly after mixing the monomers. In the case of direct polyesterification, water was formed; in the case of transesterification, ethanol condensed.

All polyesters were white powders after precipitation into methanol and drying in vacuum, but adopted an off-white brownish color after extended storage. They were all soluble in chloroform, although an increase in diol segment length from 22 to 46 yielded

polymers that required heating in order to fully dissolve in chloroform. Methanol was a non-solvent for all polyesters, and was used to precipitate the polyesters after dissolution in chloroform. DMSO at elevated temperatures was found to be a good solvent for polyesters derived from 1,46-hexatetracontanediol. ^{1}H- and ^{13}C-NMR spectra showed only the expected peaks, with low molecular weight polymers showing traces of CH_2-OH and CH_2-COOH end groups in the ^{1}H-NMR spectra.

IR spectra were recorded for all polyesters to confirm the desired structure and to investigate the packing in the polymer crystal lattice. It was found that non-branched aliphatic polyesters exhibited Davydov splittings at 720 and 730 cm^{-1} (CH_2 rocking) and 1460 and 1470 cm^{-1} (CH_2 bending). This observation is typical of orthorhombic dense packing in polyethylene as well as of long-chain n-paraffins.[13] Branched polyesters, however, showed a different behavior in the IR spectra. The occurrence of Davydov splittings was not only dependent on diol segment length, but also on the nature of the defect. Polyesters derived from 1,22-docosanediol generally did not show Davydov splittings, independent of the nature of the diacid unit. Increasing the diol segment length to 32 and even 46 methylene units still did not yield Davydov splittings in polyesters incorporating 3-phenylglutaric acid as well as 1,2-phenylenediacetic acid. However, increasing the methylene segment lengths by using 1,32-dotriacontanediol as well as 1,46-hexatetracontanediol showed recovery of Davydov splittings for polyesters incorporating branched malonates as well as 3-propylglutaric acid.

3.3.2 Characterization of Polymers

3.3.2.1 Molecular Weight Distributions

All polyesters in this study were synthesized by polycondensation of a long-chain diol and either a short-chain diacid or diester. This polyesterification, like many step growth polymerizations, is an equilibrium reaction. Shifting the equilibrium to produce the product becomes increasingly more difficult with increasing conversion due to an increase in viscosity. As the reaction proceeds, increased viscosity makes removal of small molecule condensate more difficult. In order to obtain high molecular weight polymers, it is of crucial importance to remove the condensate and to drive the reaction to completion, because high molecular weight is only obtained at very high conversion. It is also of great importance to use equimolar amounts of monomers when using difunctional monomers, as an excess in either monomer will lead to a premature termination of polymerization after one component is completely consumed.[14] Using equimolar amounts of monomers and complete removal of small molecule condensates produces a polymer with high molecular weight and a molecular weight distribution approaching two. The ratio of weight average molecular weight to number average weight is usually equal to 1+p, where p is conversion.[14]

The weight average molecular weights and polydispersity indices obtained for polyesters synthesized in this study are given in Table 3.1.

Table 3.1 Molecular weight characterization of synthesized polyesters.

Polyester	$M_w \cdot 10^{-3}$	PDI
ul-22,4	18.8	2.43*
ml-22,4	8.6	3.19*
dl-22,4	21.1	2.54*
ul-32/12,4	21.3	3.02*
ml-32/12,4	23.0	4.29*
ul-32,3	12.0	2.30*
dl-44,3[a]	21.1	2.50
ul-22,3-6	16.8	1.95
ul-32,3-6	6.1	1.76
dl-32,3-6	6.5	2.77*
ul-22,3-ph	8.1	1.66
ul-32,3-ph	5.4	2.01
ul-22,5-ph	31.3	2.08
ul-32,5-ph	25.0	2.00
dl-32,5-ph	16.5	2.79*
ul-46,5-ph	n. a.	n. a.
ul-32,5-3	24.5	2.47*
dl-32,5-3	28.4	1.95
dl-46,5-3	n. a.	n. a.
ul-22,phac	8.1	2.13*
ul-32,phac	16.5	2.65*
dl-32,phac	20.1	1.81
ul-46,phac	n. a.	n. a.

[a] sample synthesized by Le Fevere de Ten Hove
* unexpected higher PDI due to hydrolysis in the solid state

Molecular weights obtained for the polyesters synthesized here range from 5 to 30 $\cdot 10^3$ g/mol. As discussed above, lower molecular weights obtained for some of the polymers can be attributed to an imbalance in amount of monomers, which did not permit full conversion. A number of polyesters, marked in the above table by an asterisk, showed unexpected polydispersity indices above two. These higher values are most likely the result of ester hydrolysis in the solid state. Although polymer purity and approximate molecular weight were checked by ^{1}H-NMR immediately after polymerization, the unavailability of a GPC instrument with chloroform as the mobile

phase at the time of the polymer synthesis prevented determination of molecular weight distributions immediately after polymerization. In cases applicable (polyester soluble in THF), a GPC trace with THF as the mobile phase was obtained, showing PDIs of slightly below 2. As soon as a GPC with chloroform as the mobile phase became available, molecular weight characterization was performed for those polyesters now showing a PDI of 2 or higher. However, extended storage, even after precautions to ensure stability during storage had been taken, had led to some degradation. It is reasonable to expect that the higher PDIs observed after storage result from slow hydrolysis in the solid state during the storage period, leading to a broadening of the initially obtained, lower molecular weight distribution. This observation, however, does not indicate problems with the synthesis, and in applicable cases it was shown that molecular weight distributions obtained immediately after polymerization indeed showed expected PDIs of about 2.

3.4 Conclusions

A series of branched and non-branched polyesters were synthesized by melt polycondensation of long-chain aliphatic α,ω-diols and short-chain aliphatic and aromatic diacids. A progressive increase in the diol segment length from 22 to 46 methylene units leads to a variety of polymers with varying defect density.

Spectroscopic characterization by ^{1}H- and ^{13}C-NMR, as well as by IR, confirmed the expected polymer structure. In the IR spectra, a dependence of Davydov splitting on diol lengths as well as on the nature of the defect was observed. While non-branched defects showed splittings independent of diol length, branched systems showed Davydov

splittings only for polyesters of 32 or more methylene units in the diol segment. In polymers derived from 1,32-dotriacontanediol and 1,46-hexatetracontanediol, incorporation of aromatic defects, either as side chains or incorporated into the polymer backbone, also resulted in a loss of Davydov splittings.

Molecular weight characterization by GPC produced a range of molecular weights, with a lower value of 5-30 $\cdot 10^3$ g/mol. The polydispersity indices of polyesters characterized shortly after polymerization had the expected values of 2 or slightly below. After storage for a long period of time, the polyesters exhibited broader molecular weight distributions, resulting from hydrolysis.

3.5 References

(1) Berzelius, J. *Rapp. Ann.* **1847**, 26.

(2) Kraut, K. *Liebigs Ann. Chem.* **1869**, *150*, 1.

(3) Carothers, W. H.; Arvin, J. A. *J. Am. Chem. Soc.* **1929**, *51*, 2560.

(4) Carothers, W. H. *J. Am. Chem. Soc.* **1930**, *52*, 711.

(5) Carothers, W. H. *J. Am. Chem. Soc.* **1932**, *54*, 1559.

(6) Whinfield, J. R. *Nature (London)* **1946**, *158*, 930.

(7) Hakkarainen, M. In *Degradable Aliphatic Polyesters*, 2002; Vol. 157, pp 113-138.

(8) Soo, P. L.; Luo, L. B.; Maysinger, D.; Eisenberg, A. *Langmuir* **2002**, *18*, 9996-10004.

(9) Trollsås, M.; Hedrick, J.; Mecerreyes, D.; Jérôme, R.; Dubois, P. *J. Polym. Sci., Polym. Chem. Ed.* **1998**, *36*, 3187-3192.

(10) Le Fevere de Ten Hove, C. Ph. D., Université Catholique de Louvain, 2001.

(11) Reck, B ; Ringsdorf, H. *Makromol. Chem., Rapid Commun.* **1985**, *6*, 291.

(12) Kapitza, H.; Zentel, R. *Macromol. Chem. Phys.* **1988**, *189*, 1793.

(13) Lee, K.-S.; Wegner, G.; Hsu, S. L. *Polymer* **1987**, *28*, 889.

(14) Odian, G. *Principles of Polymerization*; 3rd ed.; John Wiley: New York, 1991.

CHAPTER 4

MORPHOLOGICAL CHARACTERIZATION OF POLYETHYLENE-LIKE POLYESTERS DERIVED FROM α,ω-LONG-CHAIN DIOLS

4.1 Introduction

Since the first aliphatic polyesters were synthesized by Carothers and coworkers in the late 1920s[1], multiple studies on their crystal structures have been performed.[2-8] Extensive X-ray studies found that aliphatic short-chain polyesters (consisting of diols and diacids of 2-10 methylene units) adopt either orthorhombic or monoclinic unit cells, while also exhibiting c-axis cell dimensions that are significantly shortened from the values expected on the basis of a planar zig-zag conformation.[9,10] The deviation of the chain conformation from the all-trans planar zig-zag form when the two ester groups are closely located along the backbone was explained by the incorporation of specific torsion angles, namely two *gauche* bonds of opposite sign separated by one or more trans bonds. These structural irregularities produce stable kinked structures, which can pack more efficiently than can planar forms and minimize dipole-dipole interactions. However, when the short-chain polyester is lengthened to 6-10 methylene units, packing in the planar form is less perturbed, and the energy penalty for kink formation becomes more pronounced.[9] This favors packing in an all-trans planar zigzag form.[6] It must be mentioned that a few of the pertinent X-ray studies were performed at temperatures close to the melting temperature of the polyesters, decreasing the accuracy of the measurement and casting some doubt on the complete validity of some molecular models proposed in the literature for these polymers.

As has been described previously, the introduction of ester moieties into a polyethylene-like polymer backbone influences the resulting crystal structure. [11] In this chapter, similarities and deviations between polyethylene and model polyethylene-like polyesters in terms of decomposition temperatures, melting behavior, and crystal structure are described. The model systems contain long aliphatic segments mimicking polyethylene, but also incorporate ester moieties bearing branches of varying sizes. This comparison will allow us to determine the minimum length of the aliphatic segment necessary for obtaining a polyethylene-like crystallization in an orthorhombic unit cell. The influence of regularly spaced, as opposed to randomly distributed, branches on crystallization will also be determined.

4.2 Experimental

4.2.1 Thermal Properties

Decomposition temperatures were determined with a TA Instruments TGA 2950 under nitrogen at a heating rate of 10 $K \cdot min^{-1}$, and are reported as 2% weight loss. Melting points were determined using a Perkin Elmer Pyris DSC flushed with helium at a scan rate of 10 $K \cdot min^{-1}$ and are reported as the onset of melting for the second run. The first run was performed to erase former thermal histories and provide all samples with the same crystallization conditions. Calibration of the temperature scale and heat exchange was performed with indium and eicosane.

4.2.2 X-Ray Scattering

Powder wide-angle X-ray scattering (WAXS) diffraction patterns were obtained with a Ni-filtered CuK_α radiation source at a wavelength of 1.54 Å and an evacuated Statton camera.

4.3 Results and Discussion

4.3.1 Thermal Properties

Decomposition temperatures of the synthesized polyesters range from 160-330°C, as shown in Table 1. These temperatures refer to an initial weight loss of 2 % at a heating rate of 10 $K \cdot min^{-1}$ under nitrogen. They are lower than the decomposition temperature observed for high-density polyethylene because homolytic cleavage can occur at the weak ester linkages. The most common degradation reaction observed in aliphatic polyesters is the cleavage of the acyl-oxygen bond of the ester group, followed by the abstraction of a hydrogen atom from the α position of the methylene unit of the acid. This reaction leads to ketene and hydroxyl end-groups.[12] To a lesser degree, chain-scission leading to the formation of a carboxyl end-group and a vinyl end-group can be observed.[12] Decarboxylation can also occur, especially in the case of the malonates. This last feature explains the generally lower decomposition temperatures observed for polyesters derived from malonates.[13]

Table 4.1 Thermal properties of m,n-polyesters

Polyester	Decomposition Temperature[a] (°C)	Melting Temperature[b] (°C)
HDPE	370	Exp: 133-138 Theor: 145
22,4	327	92
32/12,4	242	87
32,3	161	70
44,3[c]	370	99
22,3-6	266	55
32,3-6	196	66
22,3-ph	215	52
32,3-ph	191	70
22,5-ph	315	43
32,5-ph	299	71
46,5-ph	295	82
32,5-3	329	72
46,5-3	260	93
22,phac	313	51
32,phac	288	77
46,phac	289	86

a) Reported as 2% weight loss at a heating rate of 10 $K \cdot min^{-1}$, nitrogen atmosphere.

b) Reported as onset of second heating run at a scan rate of 10 $K \cdot min^{-1}$.

c) Sample provided by Le Fevere de Ten Hove.

The melting temperatures observed for our polyesters (Table 4.1) are significantly lower than the melting point obtained for commercial high-density polyethylene. This is consistent with previous studies, and results from the presence of the ester moieties. However, increasing the length of the diol segment, making the polyesters gradually more polyethylene-like, increases the melting temperature as exemplified by the case of

polyesters derived from 3-phenylglutaric acid (22,5-ph; 32,5-ph; 46,5-ph). This overall trend of increasing more polyethylene-like melting behavior with an increase in diol segment length is summarized graphically in Figure 4.1. For the 3-phenylglutarates, the melting point increases from 43°C for the 22,5-ph to 71°C for 32,5-ph, and finally 82°C for 46,5-ph. This constitutes a 40°C increase in melting temperature resulting from an increase of 24 methylene units in the diol segment. A similar increase of 35°C is observed in the polyesters derived from 1,2-phenylenediacetic acid (22,phac; 32,phac; 46,phac) when the diol length is increased from 22 to 46 methylene units.

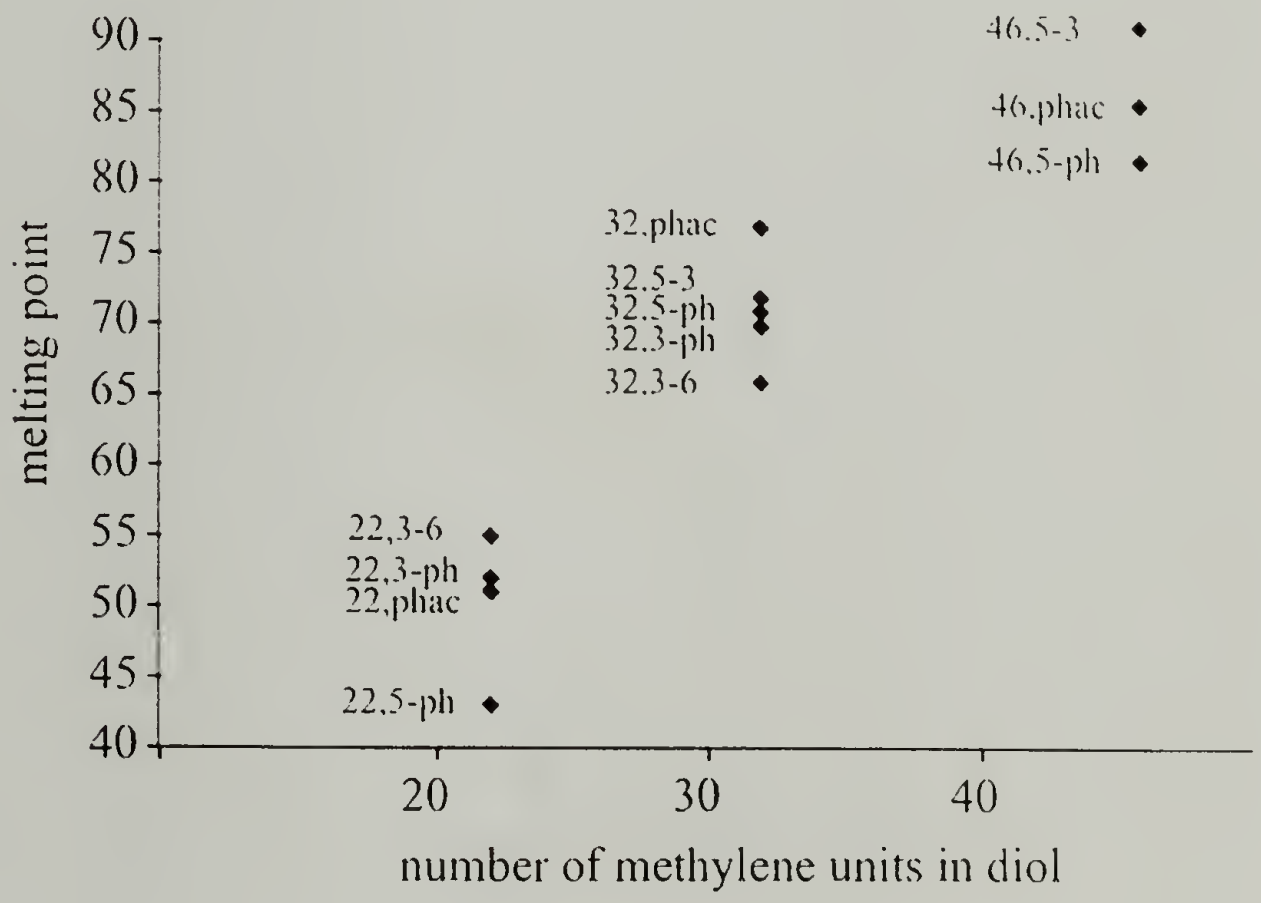

Figure 4.1. Melting behavior of polyesters: Dependence on diol segment length.

Another noteworthy observation is the existence of a melting endotherm for all polyesters synthesized during this study, indicating the presence of crystalline regions in

all samples. Even the placement of branches only separated by 26-28 methylene units along the backbone still allows for the formation of ordered crystalline structures.

4.3.2 Wide-Angle X-Ray Scattering

In order to determine the crystal structures of the polyesters synthesized in this study, and to compare them to polyethylene, wide-angle X-ray diffractograms were recorded.

As described earlier in chapter 1, high-density polyethylene crystallizes in an orthorhombic unit cell containing two chains, and is characterized by a "signature" WAXS pattern of sharp (110) and (200) reflections. Short-chain polyesters, on the other hand, crystallize in either a monoclinic structure with two chains per unit cell, or an orthorhombic structure with 4 chains per unit cell. The crystal structure depends on the length of the diol and diacid segments and on the amount of "gliding," or displacement of the repeat units, with respect to each other.[9]

The non-branched polyesters studied here (22,4, 32/12,4 and 32,3) produce WAXS diffractograms similar to those observed for HDPE. This indicates the formation of an orthorhombic crystal packing in a polyethylene-like structure, as shown in Figure 4.2.

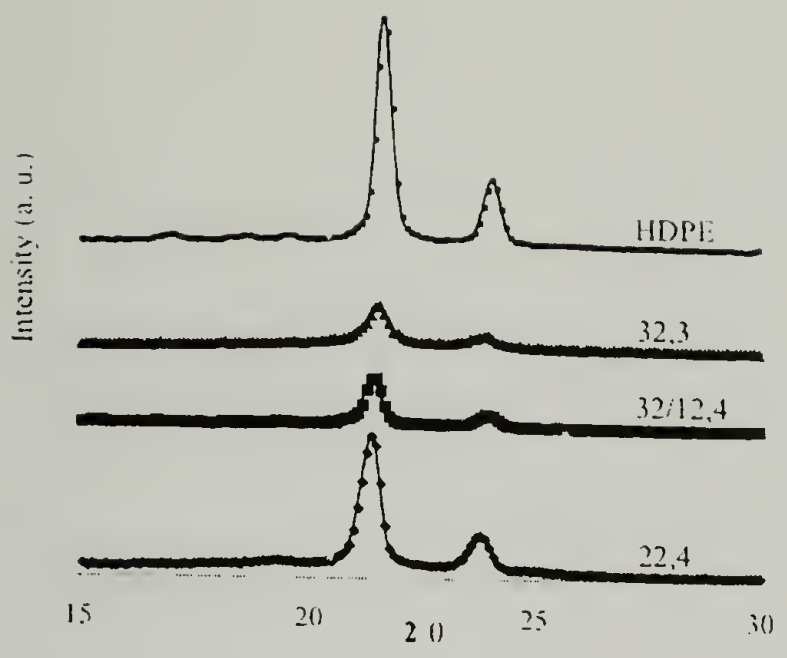

Figure 4.2. WAXS diffractograms of non-branched polyesters.

The orthorhombic packing is supported by the observation of Davydov splittings in the IR spectra for the CH_2 bending bands at 1470 and 1460 cm^{-1} and the CH_2 rocking bands at 730 and 720 cm^{-1} as reported in the previous chapter.[14]

A slightly different scattering behavior is observed for the branched polyesters. Although the 22,4 shows polyethylene-like scattering with sharp reflections, polyesters containing branched diacids separated by 22 methylene units stemming from the diol segment show a less distinct scattering pattern, indicative of very small or disordered crystals. A polyethylene-like scattering is recovered by increasing the diol segment length to 32 and ultimately 46 methylene units. This is manifested in sharp (110) and (200) reflections in the WAXS patterns at 21.7° and 24.8° for branched polyesters derived from 1,32-dotriacontanediol or 1,46-hexatetracontanediol. Figure 4.3 shows the WAXS patterns obtained for two series of polyesters with increasing diol length, where either 3-phenylglutaric acid or 1,2-phenylenediacetic acid provides the excluded branch as phenyl and 1,2-phenylene unit, respectively.

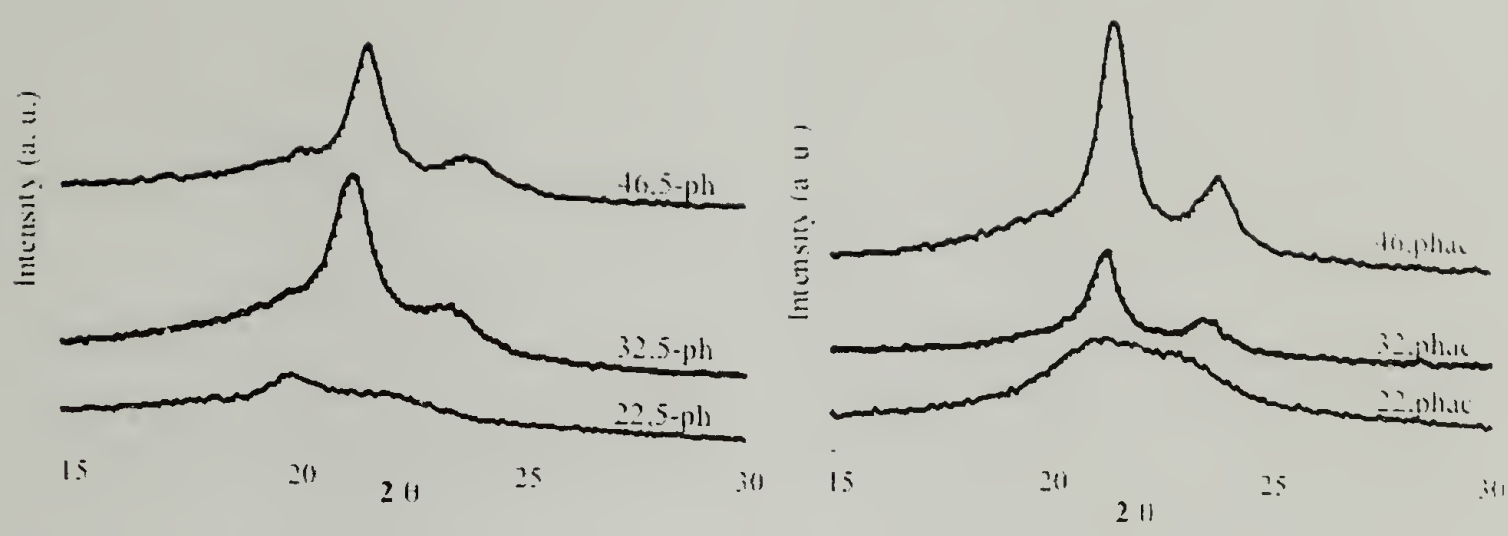

Figure 4.3. WAXS diffractograms of phenylglutarates and 1,2-phenylenediacetates.

The same trend is observed for 3-propylglutarates and branched malonates. While the polyesters derived from 1,22-docosanediol show a small or disordered crystal structure, polyesters derived from 1,32-dotriacontanediol and 1,46-hexatetracontanediol display a polyethylene-like scattering and orthorhombic chain packing. The WAXS patterns of 3-propylglutarates as well as of hexyl-and phenyl-branched malonates, are shown in Figure 4.4.

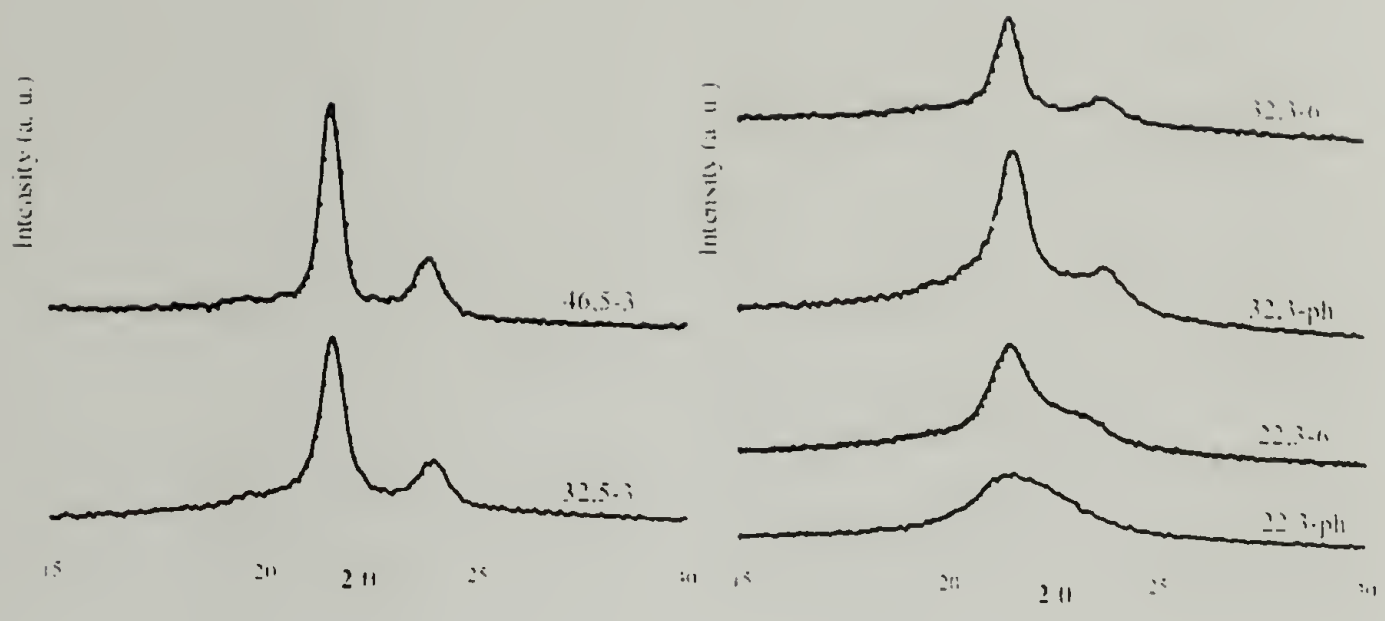

Figure 4.4. WAXS diffractograms of 3-propylglutarates and branched malonates.

The factor that predominantly influences the wide-angle X-ray scattering is the chemical structure, in particular the distance between diacid moieties. The molecular weight, although varying between 5-30·10^3 g/mol between samples, does not seem to exhibit a strong influence on crystal structure; however, this relationship was not further investigated. The reflections in the scattering patterns are sharper for samples annealed overnight at a 10°K undercooling, compared to samples precipitated after polymerization that were characterized without annealing.

4.4 Conclusions

The thermal properties and wide-angle X-ray scattering of long-chain aliphatic polyesters studied here show that they are largely comparable to linear polyethylene, although decomposition temperatures and melting points are both lower than for high-density polyethylene. The first feature is due to the presence of ester linkages along the backbone providing a weak point for homolytic cleavage. The lower melting points of

branched polyesters when compared to polyethylene can be explained by the formation of a single lamellar thickness of the length of the diol, giving rise to melting points comparable to linear alkanes of the same length. It is to be expected that longer spacers between diacid segments on the order of 100-150 methylene segments will yield melting points comparable to linear polyethylene.

The wide-angle X-ray scattering patterns show that polyesters derived from aliphatic diols of various lengths and non-branched aliphatic diacids exhibit polyethylene-like crystallization behavior. These polyesters have dense orthorhombic packing, independent of the diol length. In the case of polyesters derived from branched diacids, a more complex behavior is observed. Polyesters containing 22 methylene units as aliphatic spacers exhibit low melting points and small or disordered crystal structures, compatible with a liquid crystalline-like order. The increase in the aliphatic spacer length to 32, and ultimately to 46 methylene units, recovers polyethylene-like orthorhombic packing and results in higher melting points.

4.5 References

(1) Carothers, W. H.; Arvin, J. A. *J. Am. Chem. Soc.* **1929**, *51*, 2560.

(2) Fuller, C. S.; Erickson, C. L. *J. Am. Chem. Soc.* **1937**, *59*, 344-351.

(3) Fuller, C. S.; Frosch, C. J.; Pape, N. R. *J. Am. Chem. Soc.* **1942**, *64*, 154-160.

(4) Wilfong, R. E. *J. Polym. Sci.* **1961**, *54*, 385-410.

(5) Minke, R.; Blackwell, J. *J. Macromol. Sci., Phys.* **1979**, *B16*, 407-417.

(6) Liau, W.-B.; Boyd, R. H. *Macromolecules* **1990**, *23*, 1531-1539.

(7) Miyata, T.; Masuko, T. *Polymer* **1998**, *39*, 1399-1404.

(8) Armelin, E.; Casas, M. T.; Puiggali, J. *Polymer* **2001**, *42*, 5695-5699.

(9) Fuller, C. S. *Chem. Rev.* **1940**, *26*, 143-167.

(10) Turner-Jones, A.; Bunn, C. W. *Acta Crystallogr.* **1962**, *15*, 105.

(11) Le Fevere de Ten Hove, C. Ph. D., Université Catholique de Louvain, 2001.

(12) Luderwald, I. In *Developments in Polymer Degradation*; Grassie, N., Ed.; Applied Science: London, 1979; Vol. 2, p 77.

(13) Pilati, F. In *Comprehensive Polymer Science*; Pergamon: Oxford, 1989; Vol. 5, pp 275-317.

(14) Lee, K.-S.; Wegner, G.; Hsu, S. L. *Polymer* **1987**, *28*, 889.

CHAPTER 5

SOLID-STATE NMR CHARACTERIZATION OF NON-BRANCHED LONG-CHAIN POLYESTERS

5.1 Introduction

The structure, size, distribution, and regularity of structural "defects" in a semicrystalline polymer play a crucial role in many of the properties that are ultimately dependent on the specific morphologies obtained during crystallization. Control over polymer crystallization and morphology solely through van der Waals and steric interactions in polyethylene copolymers is limited, while the structure of polypeptides and polyamides can be tailored using directional interchain hydrogen-bonding.[1] Whether such a degree of control over polymer morphology can be attained using weaker Van der Waals forces remains an open issue. As a way to tackle this question, a structural model consisting in an aliphatic backbone mimicking polyethylene and containing structural "defects" at controlled distances will be examined. The structural "defects" will affect the lamellar thickness, crystallinity, chain dynamics, and ultimately strength, as do branches in LLDPE.

The use of polyesters as models for polyethylene and its crystallization requires a thorough understanding of the influence exercised by ester moieties incorporated at regular distances along the polymer backbone on the crystallization, microstructure, and final morphology. A large number of "defects", including non-crystallizable segments and branches of varying nature, are known to induce significant perturbations during the crystallization process. Whether the polyesters synthesized in this project can indeed

serve as viable models for polyethylene ultimately depends on the intrinsic perturbation derived from ester group incorporation, in particular at low dilution.

Polyethylene is known to crystallize in an orthorhombic, densely packed unit cell containing two chains per cell.[2] Short-chain polyesters, on the other hand, crystallize in either an orthorhombic or a monoclinic unit cell with lateral clustering of ester groups in layers.[3] It can also be expected that the fast polymer dynamics typical of polyethylene such as chain flips and chain diffusion[4] will be more difficult, or impossible, due to the anchoring effect related to the ester layers.

The goal of this chapter is to establish the influence of ester moieties placed regularly along the polymer backbone upon the polymer microstructure, and to verify the adequacy of long-chain aliphatic polyesters as valuable models to mimic polyethylene. This is accomplished through a model system, polyester 22,4, whose structure is shown in Scheme 5.1.

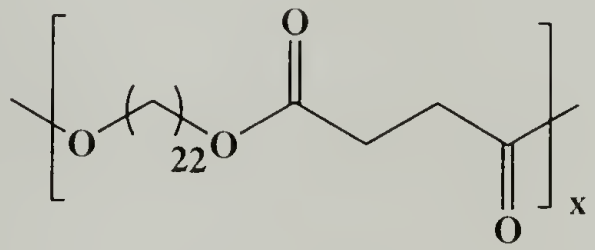

Scheme 5.1 Structure of model polyester 22,4.

^{13}C-labels in the ester units are placed along the backbone to enable sophisticated solid-state NMR experiments, that can elucidate how and to what extent ester groups influence crystallization, morphology, and dynamics of these otherwise polyethylene-like polymers. Solid-state NMR techniques as well as small angle X-ray scattering is

employed to probe structural features spanning the range of a few tenths of nanometers, when establishing local conformations, to a few nanometers, when determining the size of crystalline and amorphous regions.

5.2 Experimental

5.2.1 X-Ray Scattering

Small-angle X-ray scattering (SAXS) measurements were obtained with a Kratky camera (Anton-Paar KKK) using a Braun OED 50 M proportional position sensitive detector and Ni-filtered Cu K_α radiation. The data were smoothed, then desmeared using a variant of Glatter's algorithm. Parasitic scattering and background were subtracted, and a Lorentz correction was applied. Fourier transformation of the Lorentz-corrected desmeared experimental data multiplied by an apodization function yielded the corresponding correlation functions.

5.2.2 Solid-State NMR Parameters

Solid-state NMR experiments were conducted using either a Bruker DSX-300 or a Bruker DSX-400 spectrometer at a magnetic field of 7.0 or 9.4 T, respectively. Measurements under static as well as magic angle spinning (MAS) conditions were performed at ambient temperature. For all MAS experiments, 4-mm diameter zirconia rotors with Kel-F caps were used to hold the samples. For measurements on the Bruker DSX-300 spectrometer, a 5 kHz spinning speed and decoupling with two-pulse phase modulation[5] (TPPM) at $\gamma B_1/2\pi = 63$ kHz were utilized. Measurements on the Bruker DSX-400 were performed at a spinning speed of 6.5 kHz to avoid overlap of CH_2 peaks

with spinning side bands of the ester signals. For cross-polarization (CP) measurements, a ^{1}H 90° pulse length of 4 μs and a contact time of 1 ms were applied.

To determine crystallinity by direct polarization experiments (DP), ^{13}C magnetization was excited by a single 90° pulse. To obtain the fully relaxed polymer signal, a spectrum with a recycle delay of 3000 s and 24 scans was acquired. Signals for the non-crystalline all-trans and amorphous regions were obtained with recycle delays of 1 and 10 s, respectively. A total of 2048 scans was needed.

Proton spin diffusion measurements were carried out using the Goldman-Shen pulse sequence with ^{13}C detection. Lee-Goldburg cross polarization (LG CP) of 0.5 ms duration was used to prevent spin diffusion during CP. The crystalline signal will vanish after the dephasing time of ca. 15 μs, whereas most of the magnetization in the amorphous regions is retained and can undergo spin diffusion to the crystallites. In all MAS experiments, the chemical shift calibration is based on a chemical shift of 32.8 ppm for crystalline HDPE.

In the static measurements (without MAS), the sample was inserted as a cylindrical block of 4-mm diameter wrapped in Teflon tape into the 4.5-mm coil of a stationary Bruker double-resonance probe. The measurements were carried out at 298 K without sample rotation. The ^{1}H- and ^{13}C 90° pulse lengths ranged from 2.8-4.1 μs to 2.4-3.2 μs, respectively. In the DOQSY experiments, cross-polarization times ranged from 1 ms for ml-22,4 to 1.6 ms for the 100 % dl-22,4. For the doubly labeled polyesters, a recycle delay of 3 s, an acquisition time of 3.12 ms, and a dwell time of 3 μs were used. For the monolabeled polyester, a recycle delay of 2.5 s, an acquisition time of 1.78 ms, and a dwell time of 3.35 μs were used. The DQ excitation and reconversion delays (τ_{DQ} =

0.7 ms in the case of doubly labeled and τ_{DQ} = 1 ms for monolabeled polyester) each contained two cycles of the xy-16 pulse sequence with slightly different pulse spacings.

For the 2D HH/CSA experiment, LG CP with a contact time of 200 μs was used. Thirty-two slices with increments of 2 μs were acquired with 256 scans for each t_1 slice. To display dipolar modulation, the same experiment was rerun for 8 t_1 values with 1440 scans each.

The $T_{1\rho,H}$ relaxation time in the crystallites were measured at various temperatures with a pulse sequence consisting of a variable ^1H spin-lock, cross-polarization to ^{13}C, a 10 second phase-cycled z-filter to suppress signal from the non-crystalline regions, and ^1H-decoupled ^{13}C detection. The cross polarization time was 0.5 ms.

^{13}C spin-lattice relaxation times, $T_{1,C}$, were measured by the cross-polarization method developed by Torchia.[6] 90° Pulse lengths of 4 μs were used for both nuclei, ^{13}C and ^1H, with a cross-polarization time of 0.5 ms.

All PUREX spectra were recorded using 90° pulse lengths of 3.5 and 5 μs for ^{13}C and ^1H, respectively. The cross-polarization time was 1 ms.

The two-dimensional wideline separation (WISE) spectrum was recorded at a spinning frequency of 6.5 kHz with ^{13}C decoupling during evolution, 128 t_1 increments, a t_1 dwell time of 3 μs, and a Lee-Goldburg cross-polarization contact time of 0.5 ms.

5.3 Results and Discussion

5.3.1 X-Ray Scattering

The wide angle x-ray scattering (WAXS) of PE22,4, as shown in chapter 3, shows sharp and intense reflections indicative of an orthorhombic unit cell with either O⊥ or

O'⊥ crystal packing.[7] As only $(hk0)_s$ reflections are observed, it is not possible to decide from WAXS alone whether a O⊥ or O'⊥ crystal packing is adopted. Observation of the infrared Davydov splitting characteristic for orthorhombic crystals such as polyethylene or linear alkanes,[8] confirms the dense packing in either O⊥ or O'⊥ form.

As described in the literature[9], crystallization occurs with the diesters forming layers included into the crystalline regions, giving rise to intense (00l) reflections at low angles as observed by SAXS. The ester groups induce minimal perturbations in the crystal lattice, but odd-even effects related to the length of the diacid have to be expected. The SAXS diffractogram and calculated correlation function obtained for polyester 22,4 is shown in Figure 5.1.

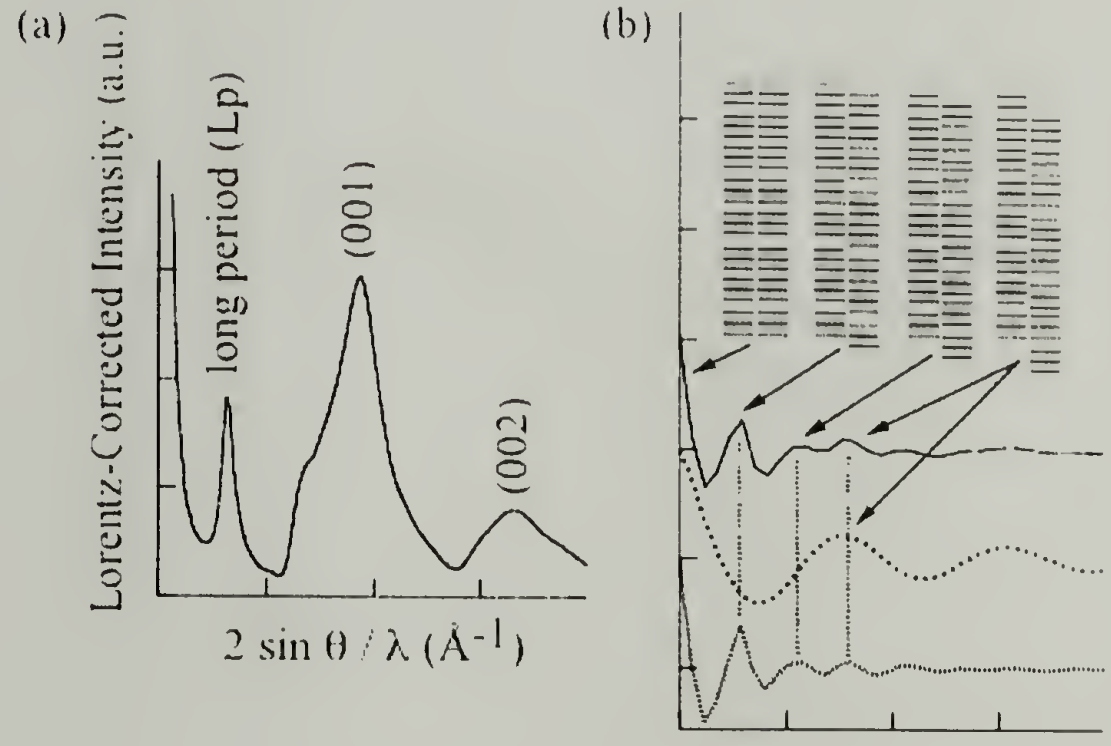

Figure 5.1 (a) Lorentz corrected SAXS diffractograms (b) normalized correlation functions computed from the complete SAXS data (top), low angle (L_p) peak (middle), and from (001) and (002) layer lines (bottom) for polyester 22,4.

The calculated extended length of one repeat unit of 22,4 is 33.6Å. From the (00l) reflection in the SAXS (Figure 5.1 (a)), an internal period of 26.7Å can be deduced, corresponding to a tilt angle of 37°. The long period as obtained from the SAXS correlation function is 76.8 Å with the polyester possessing a crystallinity of about 70%.

This crystal thickness can only be achieved by incorporation of ester groups deep into the crystal as each crystal consists of two repeat units. More conclusive evidence regarding this point can be gained by examination of the correlation functions. Correlations between diester planes appear prominently in the correlation function computed from the complete SAXS intensity data, and in the correlation function computed from the (00l) layer lines only. Three strong correlation peaks (excluding the one located at the origin, which results from self-correlation) can be detected in these curves. Because the thickness of amorphous interlayers is quite close to the distance between diester planes in the crystals, it is *a priori* difficult to separate the scattering into intra- and inter-crystallite contributions. However, the almost complete disappearance of correlation peaks for distances longer than the long period indicates that the correlation between the locations of diester planes in neighboring crystals is weak, except for distances strictly corresponding to the long period (i.e., when shifting brings two adjacent crystals into full coincidence). This intercrystalline correlation appears as the last marked peak in the complete $\gamma_1(r)$, for distances corresponding to the repeat period of the lamellar stacking, which can be obtained from the correlation function computed from the first SAXS peak only. Therefore, the peaks that are found in $\gamma_1(r)$ at distances shorter than the long period, must by necessity dominantly originate from correlation between diester planes in the same crystals. As there are three such peaks (counting now the self-

correlation peak centered at the origin), it becomes obvious that crystals include three diester planes as depicted schematically in Fig 5.1. Therefore, the crystal thickness must be close to twice the repeat period between diester planes, i.e., 53.5 Å, which would correspond to 70 % linear crystallinity, when divided by the long period.

The observed long period can be varied through thermal treatment, leading to lamellar thickening in discrete jumps as observed for a comparable polyester consisting of 22 methylene units in the diol segment and 3 methylene units stemming from glutaric acid.[10] An average crystal thickness derived from the related interface distribution functions has been observed to vary in sudden jumps with increasing crystallization temperature. These quantized crystal thicknesses are due to the necessity to intermolecularly pack the polar ester groups in close proximity, which requires a cooperative change when attempting to thicken the crystal.

It can be concluded that ester groups exert a measurable influence on the crystal structure as well as the crystal thickness and the chain tilt angle relative to the lamellar surface, while still allowing crystallization in a polyethylene-like crystal lattice.

5.3.2 Solid-State NMR

5.3.2.1 ^{1}H Wideline MAS Spectrum

In order to gain information on the mobility of polyester 22,4, a proton spectrum was recorded, which is depicted in Figure 5.2.

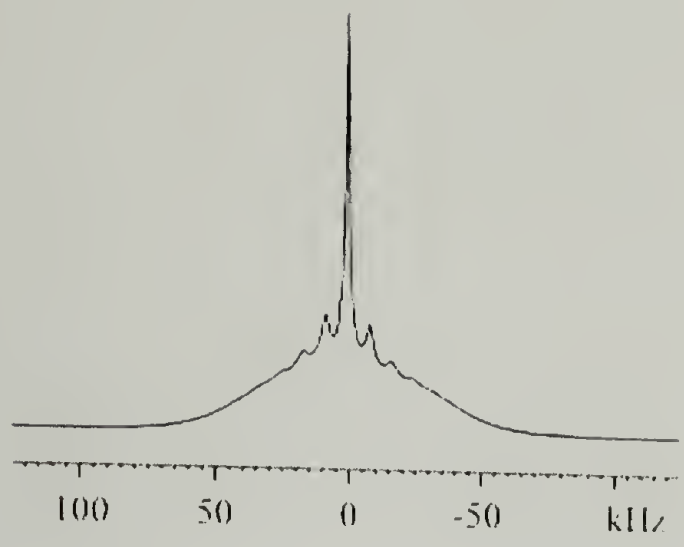

Figure 5.2 ^{1}H Wideline MAS NMR spectrum of polyester 22,4.

Two main features are clearly apparent: a broad peak due to the rigid crystalline region and a narrow signal due to mobile segments in the amorphous regions. This indicates a high crystallinity, but also the existence of a significant amount of mobile chains in the amorphous regions.

5.3.2.2 ^{13}C CP Spectra

The unfiltered and $T_{1,C}$-filtered ^{13}C-CP spectra of polyester 22,4 are shown in Figure 5.3.

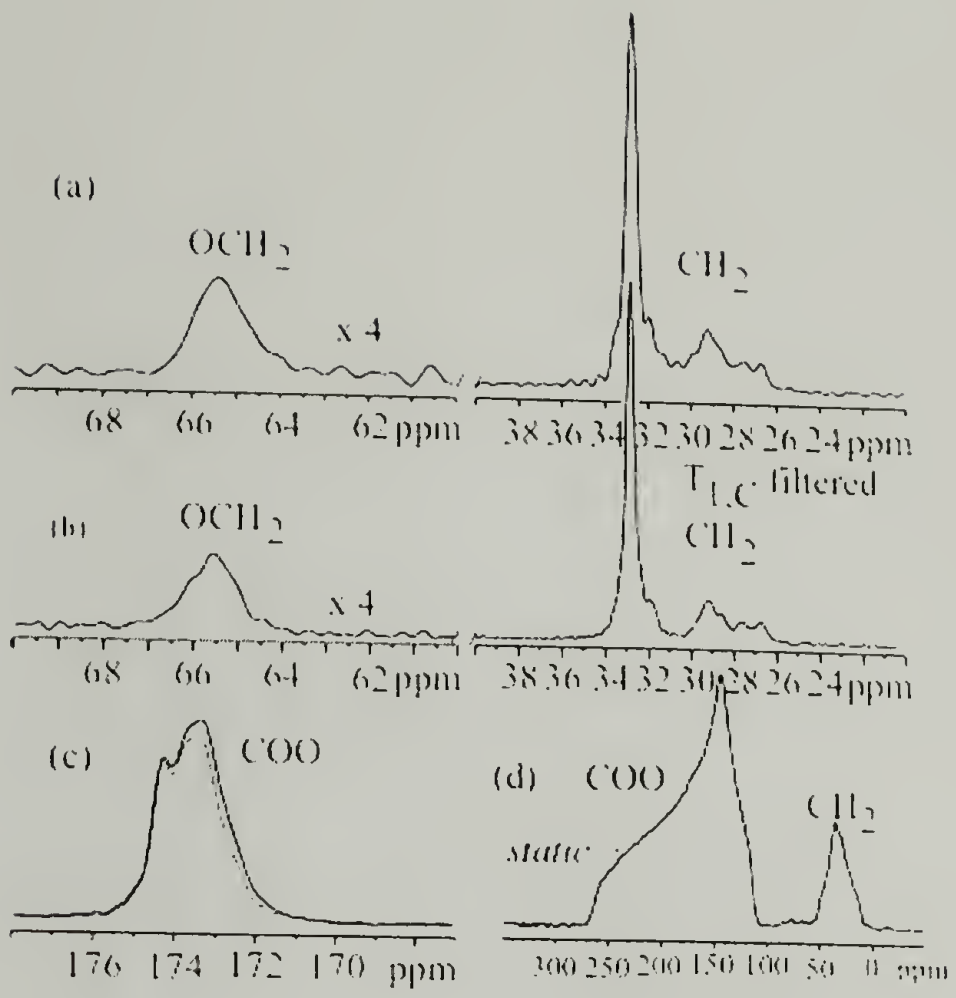

Figure 5.3 ^{13}C NMR spectra of doubly ^{13}COO-labeled polyester 22,4 (a) CP/MAS spectrum, CH_2 regions, (b) $T_{1,C}$-filtered, (c) COO regions, (d) static spectrum of ^{13}COO-labeled polyester 22,4, showing COO and $(CH_2)_n$ powder patterns.

The aliphatic region of the ^{13}C CP/MAS spectrum of polyester 22,4 as depicted in (a) is dominated by the crystalline $[-CH_2-]_n$ peak centered at 32.8 ppm. Nevertheless, significant signal intensity is observed between 30 and 25 ppm, where regular polyethylene shows no distinct bands. In ^{13}C NMR spectra (b), where the signals from the amorphous regions have been suppressed by $T_{1,C}$ filtering of ≥10 seconds as shown in the spectrum displayed in the middle of Figure 5.3, several relatively distinct bands are still observed in this spectral region. These are assigned to methylenes near the ester groups. Clearly, the two OCH_2 groups in each repeat unit are responsible for the peak

near 64 ppm. Chemical-shift simulations show that the other methylenes within three bonds from an oxygen atom are expected to resonate upfield from 30 ppm. In particular, this includes the methylenes bonded to the ester carbons. Thus, six out of 24 methylenes, or 25% of the methylene signal, are expected to resonate at < 30ppm, which is in good agreement with the spectrum of Figure 5.3.

The ester ^{13}C signals of the ^{13}COO-labeled polymer exhibit a distinct fine structure as seen in spectrum (c). A ^{1}H $T_{1\rho}$-filtered ^{13}COO spectrum, which retains predominantly the signal of the crystalline segments, shows a slight but clear reduction of intensity on the right-hand side of the spectrum, which is thus identified as partially non-crystalline. The static CP powder spectrum of the ester groups, as depicted in spectrum (d), shows no signs of a major mobile component. The principal values determined for polyester 22,4 are 106, 143, and 271 ppm. The isotropic chemical shift for the ester groups is 173.3 ppm.

5.3.2.3 ^{13}C DP/MAS Spectra: Determination of Crystallinity

In order to determine the crystallinity of polyester 22,4, a series of ^{13}C DP spectra with varying recycle delays were recorded.[11] Torchia CP/T_1 experiments show that the longest recycle delay of 3000 seconds (about $4 \cdot T_{1,C}$) provides a 93% relaxed crystalline signal intensity in the DP/MAS spectrum. The 7% missing intensity is easily corrected for in the quantitative analysis. The spectra with short recycle delays and more scans allow for deconvolution of the amorphous signals and quantification by comparison. The heteronuclear nuclear Overhauser effect (NOE) has been suppressed by a 10-s delay

before ^{13}C saturation pulses and the nominal recycle delay. The series of spectra with varying recycle delays is depicted in Figure 5.4.

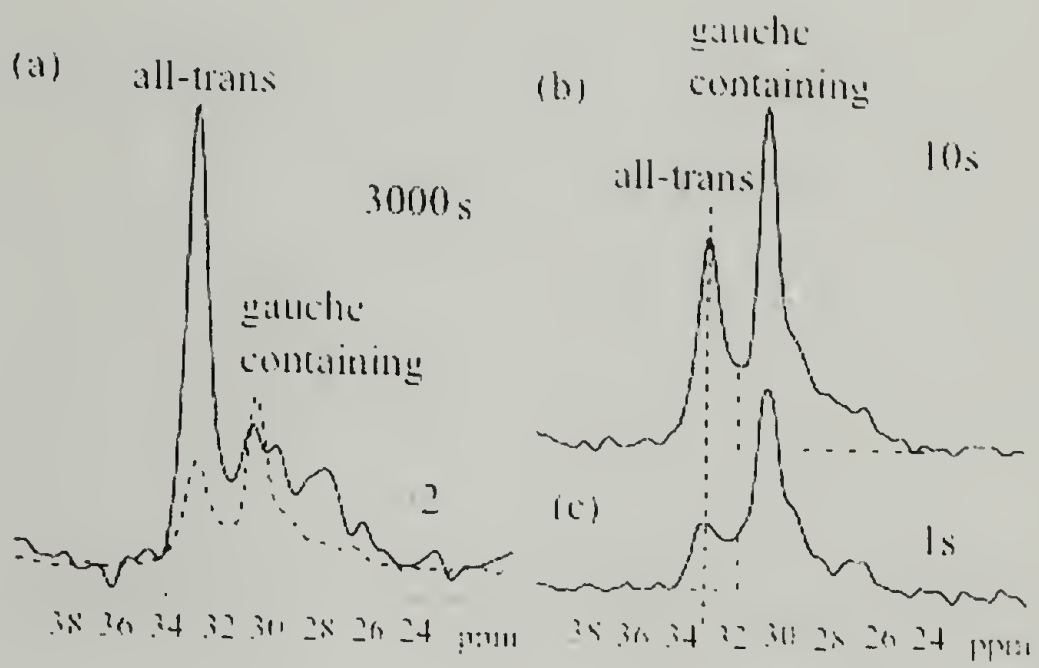

Figure 5.4 DP/MAS ^{13}C NMR for crystallinity determination with recycle delays of (a) 3000 s; (b) 10 s; (c) 1 s. Dash-dotted lines demarcate the spectral areas of the non-crystalline components.

After the short recycle delays, the main peak of the amorphous fraction is clearly observed at 30.5 ppm. It is relatively narrow compared to the amorphous peak in polyethylene at the same temperature, indicating relatively high and uniform mobility. The signal is seen to rise with the recycle delay up to 10 s; a further rise is excluded based on the match with the 3000-s spectrum.

The small 33-ppm band observed in the 1-second spectrum is clearly distinct from the crystal peak, in terms of peak position, width, and relaxation time, and is therefore considered as part of the non-crystalline components. It accounts for 5% of all segments.

The area of the peaks at 30.5 and 33 ppm relative to that of the fully relaxed signal in Fig. 5.4(a) yields a mass-based crystallinity of 70%, which is in good agreement with the volume crystallinity obtained from SAXS. The two quantities are related through the ratio of the crystal and sample densities.

In SAXS, the amorphous regions show contrast due to their reduced physical and scattering density, while NMR characterizes them based on segmental mobility and non-crystalline chain conformations. While SAXS yields a volume crystallinity, $f_{c,V}$, NMR measures the relative number of segments in crystalline and amorphous regions, which gives the slightly larger mass-based crystallinity, $f_{c,m}$. The two quantities are related through the ratio of the crystal and sample densities, ρ_c/ρ_{sample}, by equation 5.1

$$f_{c,m} = f_{c,V} \ \rho_c/\rho_{sample} \qquad (5.1)$$

In the preceding paragraph, we showed that the ratio of crystal thickness to long period, estimated by our analysis of the SAXS correlation function, amounts to $f_{c,V} = 0.7$. This converts to $f_{c,m} = 0.72$, using density estimates based on polyethylene values, ρ_c = 1.0 g/cm^3 and ρ_a = 0.9 g/cm^3. Note that an inaccuracy of a few percent in the densities has only a minimal effect on the ρ_c/ρ_{sample} conversion factor.

5.3.2.4 ^{1}H Spin Diffusion: Distribution of Ester Groups in the Polymer Morphology

In the preceding section, it was concluded that a crystal thickness of about 54 Å, as observed by SAXS, can only be achieved by deeply burying carbonyl segments in the crystal, as it consists of two repeat units. In order to gain information on domain size and

on the exact location of specific functional groups in the polymer morphology, ^{1}H spin diffusion with ^{13}C detection was performed. It allows for the localization of ester groups with respect to the amorphous and crystalline phases.

The technique measures diffusion of ^{1}H nuclear magnetization, which arises due to ^{1}H-^{1}H dipole-dipole interactions, between domains of a solid polymer. In the Goldman-Shen experiment, ^{1}H magnetization in the mobile amorphous regions can be selected exclusively through a $T_{2,H}$ filter, which dephases the magnetization in the more rigid crystalline and interfacial regions.[12] After flipping the magnetization back to the z-direction, its ^{1}H spin diffusion through the intermediate interfacial regions into the crystallites can be observed after ^{13}C cross polarization. Figure 5.5 depicts the fine structure of the ester resonance with increasing spin diffusion time.

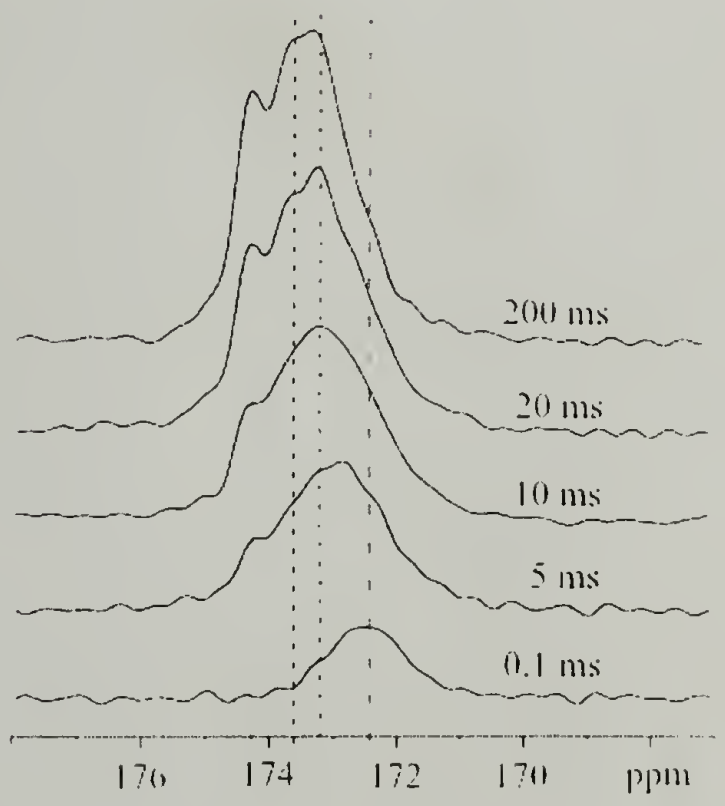

Figure 5.5 ^{13}COO spectra after ^{1}H T_2 selection of 15 μs duration and ^{1}H spin diffusion of the indicated durations.

The amorphous COO resonance is easily identified based on the longer T_2 relaxation time of the nearby protons and gives rise to the signal at around 172.5 ppm shown at the bottom of Figure 5.5 after a 100 μs spin diffusion time. It accounts for 19% of the CP spectrum; this is found based on comparison of Fig. 5.5 top and bottom. In the latter spectrum, the intensity is enhanced by $1/f_{amorphous}$ = 3-fold. Thus, this signal accounts for 6.3% of the regular CP spectrum. In the spectra of Fig.5.5, there are indications of a second non-crystalline band slightly shifted downfield, centered around 173.3 ppm. It is polarized quickly by spin diffusion, which indicates its location close to the interface. The intensity fraction of this component is estimated at 15%. Being suppressed by the ^1H T_2 filter, it must be associated with less mobile segments and is therefore expected to cross-polarize similar to the other segments. The spin diffusion behavior suggests 2/3 of all ester groups are near the crystalline-amorphous interface, while 1/3 of esters are buried deeply inside the polyester crystals.

5.3.2.5 DOQSY Spectra: Chain Conformation and Packing

In order to gain information on the polymer chain conformations and packing and to assess similarities to and differences from polyethylene chain packing, double quantum spectra (DOQSY) of polyester 22,4 with varying amounts and placement of ^{13}C-labels were recorded.

DOQSY NMR measures the relative orientation of pairs of ^{13}C-labeled segments that are close in space, by correlating their chemical-shift anisotropies.[13] This allows for distinction between all-trans conformations and other structures. If ^{13}COO groups on neighboring chains are sufficiently close in space, chain packing can be characterized

with high angular resolution. The coherence transfer between the ^{13}C spins is modulated by the distance- and orientation-dependent ^{13}C-^{13}C dipolar coupling, which provides additional structural information.

The experimental DOQSY spectrum of 100% doubly labeled polyester 22,4 as well as the simulated spectrum and its three components are shown in Figure 5.6.

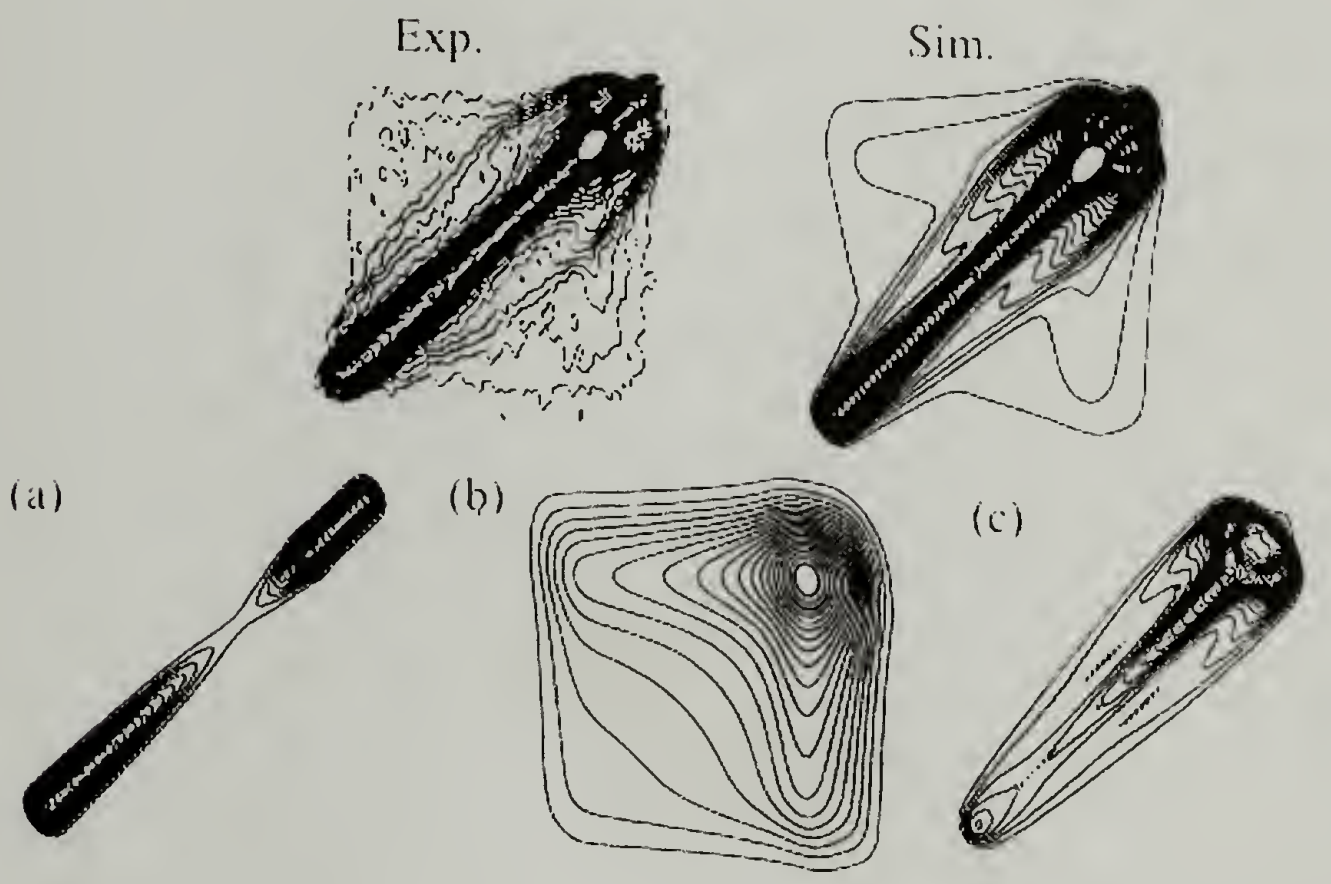

Figure 5.6 DOQSY NMR spectrum of 100% doubly ^{13}COO-labeled polyester 22,4. 3 components of simulated spectrum: (a) intrasegmental correlation in all-trans chains in the crystallites (b) random relative orientations in the non-crystalline segments (c) interchain correlations in the crystallites.

The pattern exhibits three discernible spectral patterns. The simulations for each one of these components individually are shown at the bottom of Figure 5.6 individually. First, there is a straight ridge on the diagonal as seen in simulation (a), characteristic of the intramolecular correlation for an all-trans conformation.

Here, correlations of ester groups within the same succinic acid moiety are termed intramolecular/intrachain, while correlations arising from neighboring ester groups are referred to as intermolecular/interchain. Note, however, that this convenient nomenclature is not strictly speaking accurate, as ester groups in neighboring chain stems in the crystal, which are termed intermolecular here, can be part of the same polymer chain.

Secondly, there is a low and broad pattern spread over a wide range of the 2D plane, simulated in spectrum (b). This is characteristic for a random relative orientation of ester groups. Thirdly, intensity near the diagonal that tapers at the left end of the spectrum is observed, and the pattern simulated in spectrum (c). This was attributed to inter- rather than intramolecular correlations of neighboring chains, which are close enough in space as esters are packed in layers.

In order to confirm this decomposition into three patterns and to assign them unambiguously, first a DOQSY spectrum of 100% monolabeled polyester 22,4 was recorded. The ^{13}C-labels along the chain in the crystallites are separated by at least 28 Å, which results in a corresponding ^{13}C-^{13}C dipolar coupling of less than 1 Hz, rendering intrachain double-quantum coherences negligible. The spectrum of the singly ^{13}COO-labeled polyester 22,4 shows a surprisingly high DOQSY intensity, despite the lack of

intramolecular correlation partners. Figure 5.7 shows the DOQSY spectrum and its simulations for monolabeled polyester 22,4.

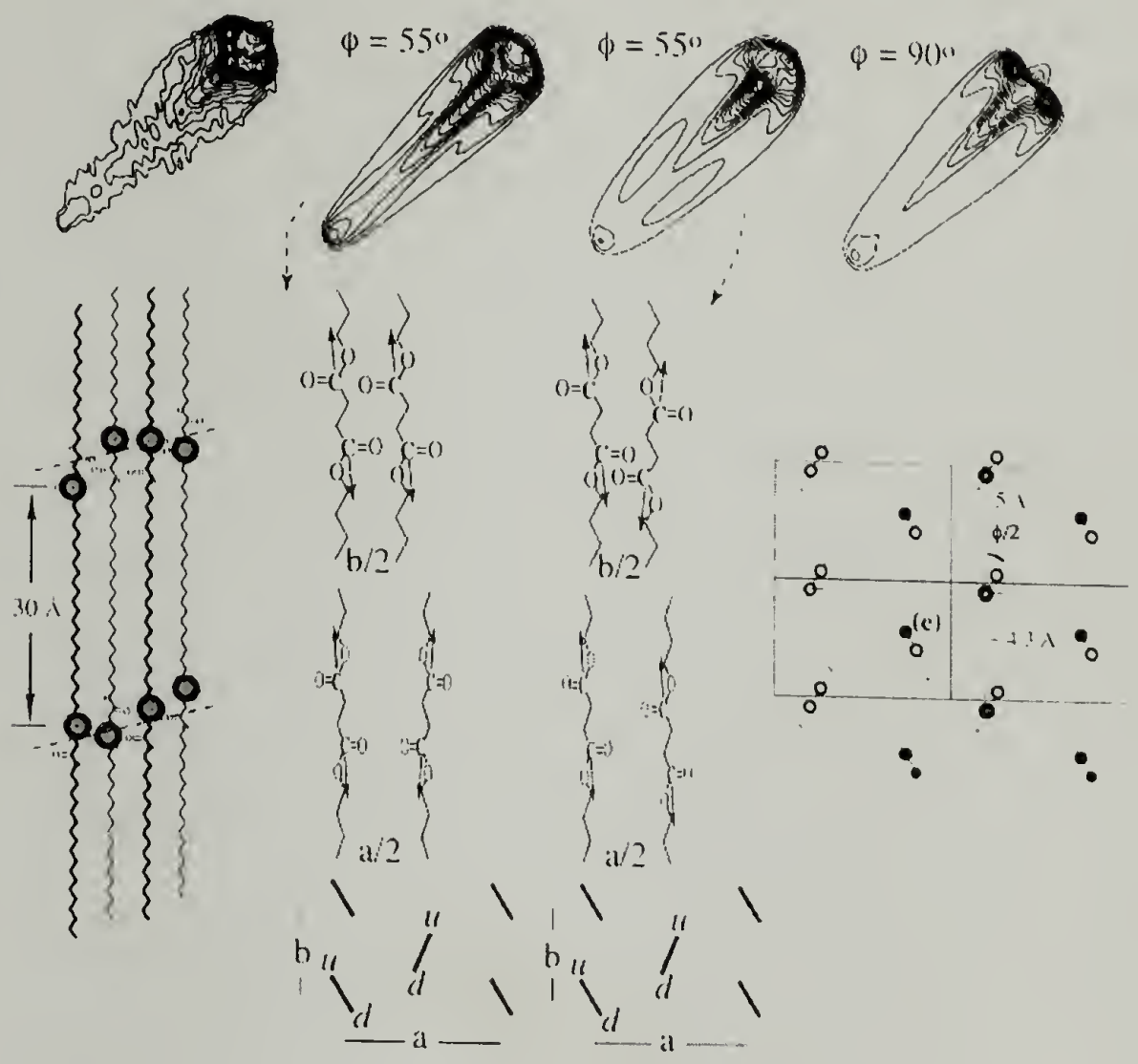

Figure 5.7 Experimental DOQSY spectrum of singly ^{13}COO-labeled polyester 22,4 and simulations for different ester group orientations in the O'⊥ structure with an angle of 55° and O⊥ structure with an angle of 90°. Schematics for the large ^{13}C-^{13}C intramolecular distance and a representation of the crystal structure with definition of the angle ϕ and intermolecular distances.

The observed strong intermolecular correlation signal indicates that ^{13}COO groups in neighboring chains are preferentially close, rather than randomly distributed along the

chains within the crystal. This indicates that the COO groups in the crystal are clustered in double-layers, a conclusion that is fully consistent with the SAXS data. The clear DOQSY pattern can be used to elucidate the chain packing in the unit cell.

As discussed previously, the boat-shaped DOQSY pattern for ml-22,4 must be attributed solely to interchain correlations. The specific spectral pattern provides reliable information on the interchain ester distances and the relative orientation of the ester planes.

The experimental DOQSY of ml-22,4 shows two main contributions: first, there is off-diagonal intensity that is most pronounced in the upper right-hand corner of the spectrum and must be due to correlations between nonequivalent chains. Secondly, there is a diagonal ridge that must arise from correlations between parallel chains in neighboring unit cells. The intensity distribution of the off-diagonal pattern reflects the relative orientation of the ester groups. The observed absence of significant exchange intensity near the σ_{11} (lower left) end of the spectrum is expected: This principal value corresponds to a direction close to the chain axis, and the chain axes in the crystal are all parallel. Therefore, the frequencies ω_A and ω_B in this spectral region will be similar, i.e. close to the diagonal.

The most reliable and nontrivial quantity derived from this spectrum is the angle between the normals of the ester planes of the two nonequivalent chains in the unit cell. This measurement requires knowledge of the orientation of the ^{13}COO chemical-shift tensor with respect to the chemical bonds. As will be described in the following, correlation with the H-H internuclear vector in the nearby CH_2 groups confirms that here,

as in almost all other ester groups studied to date, the σ_{33} principal axis is along the normal to the plane of the ester group.

Figure 5.7 shows a best-fit simulation with an angle of 55° between the planes of non-equivalent chains. The six nearest-neighbor chains in the crystal structure have been included in the simulation, using the double-quantum spin-pair approximation, which is appropriate for these weak dipolar couplings. The angle of 55° deviates significantly from that in polyethylene, where the chains are essentially perpendicular, i. e. $\phi = 90°$. Spectra simulated with this angle show a straight ridge perpendicular to the main diagonal near the upper right-hand corner of the spectrum, as depicted in the last simulation in Figure 5.7. This is clearly different from the elliptical broadening observed in the experimental spectrum.

While the "shape" of the diagonal ridge in the spectrum is prescribed and does not provide new geometric information, the intensity distribution along the diagonal reflects the angle between the plane of the chain and the C-C interchain vector connecting neighboring equivalent chains. This angle is directly related to the angle ϕ discussed above. The intensity-modulation of the diagonal can resolve ambiguities that remain with the off-diagonal pattern from the inequivalent-chain correlation.

In a given chain, the ester group can adopt two different orientations. The transition from one to the other is achieved by a 180° rotation around the chain axis (and displacement by one CH_2 unit, if the rest of the chain structure should remain unchanged). Two possible relative orientations of ester groups within the given O'$\perp$ sublattice are shown below their corresponding simulations in Figure 5.7. The CSA tensor orientation does not change strongly by this 180° rotation; in particular, the

orientation of the σ_{33} principal axis is unchanged. Nevertheless, the orientation of the σ_{11} axis changes by at least 15° (actually 22° according to the tensor orientation found here), which is significant enough to result in distinct spectral patterns. The simulations indicate that the ester groups in neighboring nonequivalent chains are closer to parallel (smaller angles between the C-O bonds in the two nonequivalent chains).

SAXS had shown an angle of 34° of the chain axis with the normal of the layers of ester groups, which means that ester groups in neighboring chains are displaced relative to each other along the chain. The NMR spectrum depends on the glide plane arrangement, since the length and direction of the ^{13}C-^{13}C internuclear vectors change for different glide planes, resulting in a variation of the dipolar modulation of the double quantum spectrum.

The fit used in the simulation for ml-22,4 is consistent with the SAXS-derived displacement of ester groups along the a and the b axis in an $\alpha\beta_{22}$ glide plane. Each neighboring chain is displaced by c = 2.54 Å. It is noteworthy that the relative intensity of the intrachain diagonal ridge and the crystalline off-diagonal interchain correlation pattern is not a free parameter, but is determined by the internuclear distances in the crystal structure. Due to the presence of two ester groups separated by 3.9 Å in each repeat unit, even with displacements on the order of 3 Å along neighboring chains, at least two out of the four ester groups in a pair of neighboring chains will be spatially close.

In order to confirm the decomposition of the DOQSY spectrum for dl-22,4 and to convincingly assign them, three DOQSY spectra of samples with varying labeling content were recorded and are plotted with comparable contour levels in Figure 5.8.

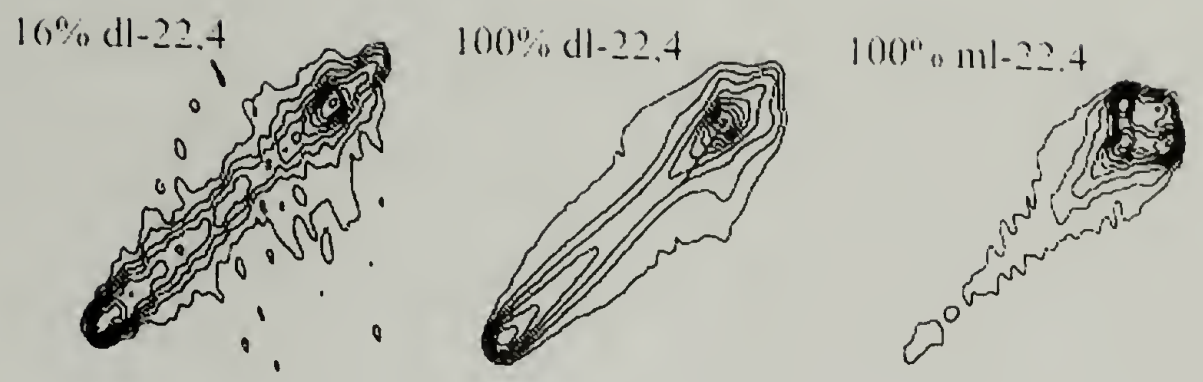

Figure 5.8 DOQSY NMR spectra of differently labeled polyester 22,4, processed and plotted comparably.

In summary, it was found that the angle between chains is 55° ± 20° with the error margin including uncertainties in the tensor orientation discussed below. This structural finding requires an O'⊥ crystal structure. The simulations with the crystalline packing parameters provided good fits for the experimental DOQSY spectra of both, doubly and singly labeled polyester 22,4, indicating that the majority of ester groups are in a crystalline environment.

5.3.2.6 HH/CSA Correlation: Chemical Shift Tensor Orientation

In order to use the ^{13}C CSA of the ester groups as a reliable orientational probe, knowledge about the ^{13}C chemical-shift tensor orientation with respect to the chemical bonds is required. Generally, the tensor orientation of COO groups has been found to reflect the invariance of the local electron distribution under a reflection with respect to the ester plane, i.e. the plane containing the four atoms of the C-(C=O)-O moiety. The corresponding invariance of the chemical shift can only be achieved if a principal axis of the chemical shift tensor is perpendicular to the ester plane. In almost all esters studied to

date, this axis is associated with the σ_{33} principal value. Given that a PE-like all-trans chain has the same symmetry, this symmetry principle is expected to apply to a good approximation to the esters in our sample. For measuring the relative orientation of the normals of the two inequivalent chains in the unit cell, the orientation of the σ_{33} chemical-shift principal axis is particularly important.

In order to confirm this aspect of the tensor orientation experimentally, the correlation between the ^{13}C chemical-shift anisotropy and the H-H dipolar coupling was measured. In an all-trans structure, the H-H vectors connecting geminal protons are perpendicular to the ester plane. The HH/CSA experiment therefore measures the components of the chemical shift tensor perpendicular to the plane of the chain with particular sensitivity. Without sample rotation, an undecoupled ^{1}H dipolar evolution (t_1) is followed by relatively short Lee-Goldburg cross polarization to ^{13}C, which prevents long-range C-H or H-H transfers. The ^{13}C chemical-shift frequency is detected during t_2 under standard proton decoupling.[14] Figure 5.9 shows the HH/CSA correlation for determination of ^{13}COO chemical-shift tensor orientation.

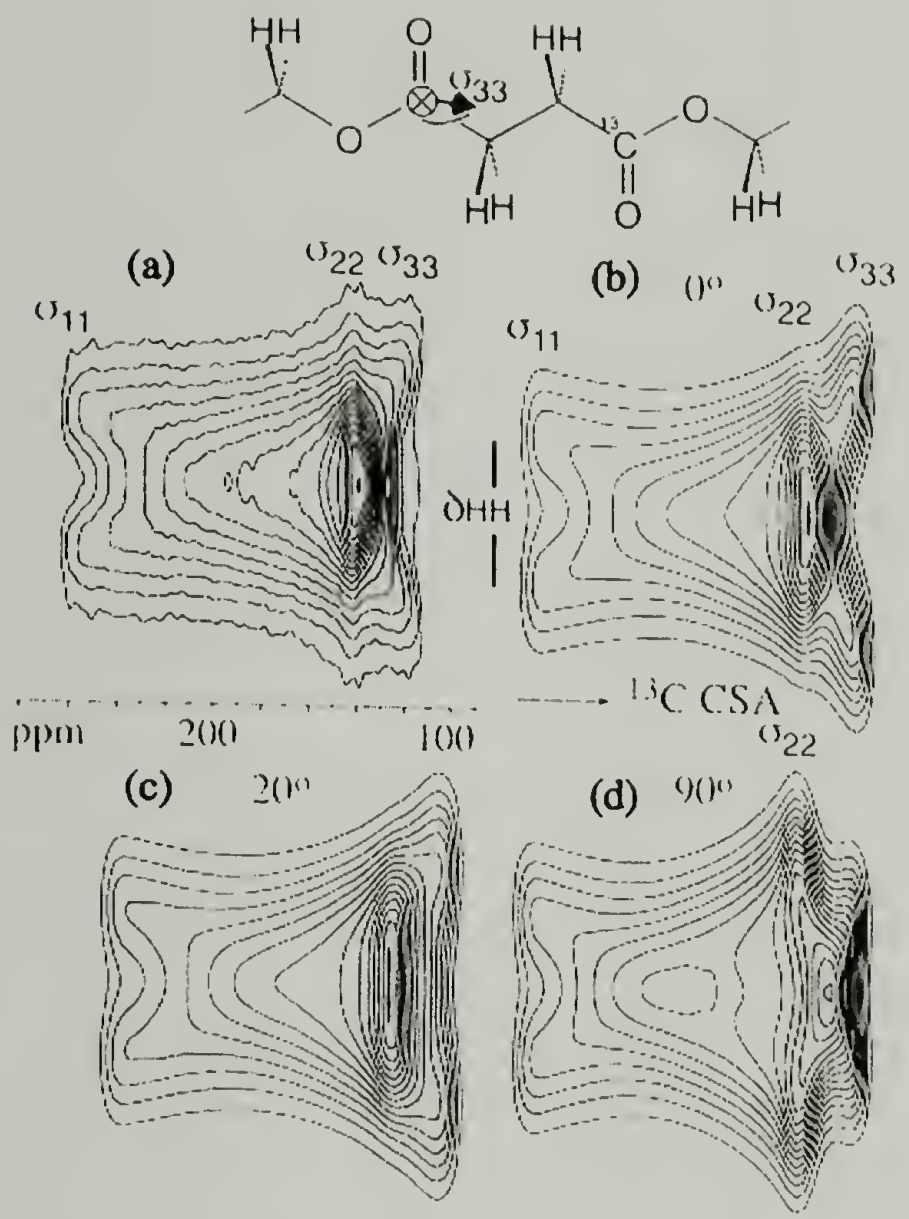

Figure 5.9 HH/CSA correlation for determining the ^{13}COO chemical-shift tensor orientation in the crystallites of 22,4, by correlation of ^{13}C CSA with the ^{1}H-^{1}H dipolar coupling in neighboring CH_2 groups. The relevant diester segment and the chemical-shift tensor are indicated at the top of the figure. (a) Experimental spectrum. ^{1}H spin diffusion during CP has been suppressed by employing magic-angle-spinlock (Lee-Goldburg) cross polarization. (b) Best-fit simulated spectrum with the canonical tensor orientation that reflects the reflection symmetry with respect to the ester plane, for a trans conformation. (c) Simulated spectrum for a chemical-shift tensor whose σ_{33} axis makes an angle of 20° with the normal to the ester plane. (d) Simulated spectrum with the orientation of the σ_{22} and σ_{33} axes interchanged relative to (a).

The geminal H-H dipolar coupling is an order of magnitude stronger than the other H-H interactions of the methylene protons nearest to the ester group. Therefore, the spectral pattern is dominated by the geminal coupling, with more or less uniform linebroadening from the large number of weaker intersegmental H-H couplings. The spectrum has no or little sensitivity to the small angle between the σ_{11} axis and the chain axis.

The spectrum shows strong dipolar modulation near σ_{33}, indicating unambiguously that the σ_{33} axis is close to parallel to the H-H internuclear vector, i. e. normal to the plane of the chain. Comparison with simulations shown in Figure 5.9 (b) through (d) for varying symmetries confirms the canonical tensor orientation that reflects the local symmetry with respect to the O-C=O plane, and excludes a ~20° deviation of the σ_{33} axis from the chain normal.

5.3.2.7 Detailed Structural Model

Figure 5.10 summarizes many of the specific structural features deduced from the NMR and SAXS data. The excellent quality and consistency of the data, combined with the high regularity and long repeat unit of the polymer, permit the analysis to extend almost seamlessly from segmental (0.3-nm) to morphological (10-nm) length scales.

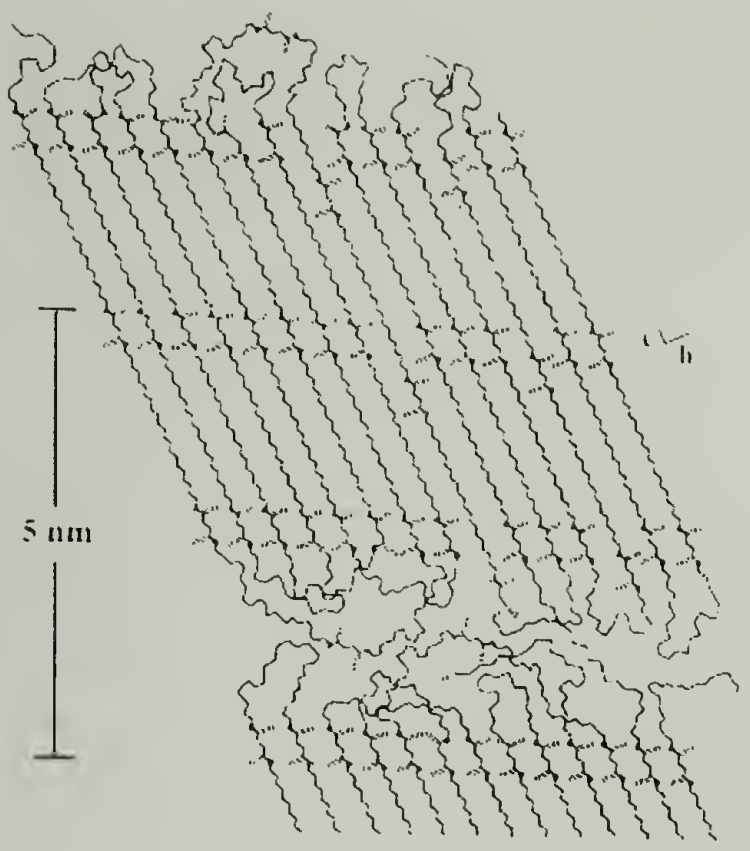

Figure 5.10 Molecular and phase structure of aliphatic polyester 22,4 according to NMR and SAXS. It consists of 5-nm thick crystallites, 2.5-nm thick amorphous layer made up mostly of $(-CH_2-)_{22}$ chain loops, a diester layer in the center of the crystallite, and a partially disordered diester layer at each crystallite surface. Occasional displaced chains in the crystallite, as suggested by $T_{1\rho}$ relaxation, are also indicated.

Based on the measured crystallinity, the crystallite thickness, and the chain tilt relative to the crystal surface, all of which are indicated in Figure 5 10, the average number of repeat units in the amorphous and crystalline phases was determined. Two $(CH_2)_{22}O_2CC_2H_4CO_2$ repeat units, with the expected all-trans conformation, form a crystalline stem, while the $(CH_2)_{22}$ portion of a third repeat unit produces a highly mobile loop in the amorphous region.

The ester groups form three double-layers in the crystallite: one in the center and two at the crystalline-amorphous interfaces. This is indicated by the absence of a

significant fraction of highly mobile ester groups and by the complete SAXS correlation functions. DOQSY NMR shows that the majority, but not all, of the interfacial ester groups exhibit crystalline conformational and packing order.

Two smaller-scale features determined by DOQSY NMR, which are not displayed in Fig. 5.10, are the 55° angle between the ester planes of the two chains in the unit cell, and the relative orientation of the C=O bonds.

5.3.2.8 Relaxation Time Measurements: Chain Dynamics

The detailed studies performed by solid state NMR, namely through CP and DP spectra, DOQSY NMR, and spin diffusion summarized in the detailed structural model of Figure 5.10, allow for an in-depth analysis of structural features and polymer morphology of polyester 22,4. In order to see the effects of the ester layering on the polymer dynamics, especially in comparison with polyethylene, further NMR studies, concentrating on relaxation times, were performed. In polyethylenes, the chains have been shown to undergo 180° flips coupled with displacements by one methylene unit. Depending on the crystallite thickness, the jump rate at ambient temperature is 1 – 1000 s^{-1}. It increases steeply with increasing temperature and decreasing crystallite thickness. The crystallite-thickness dependence and strong temperature dependence observed in polyethylenes have been explained by chain diffusion between crystalline and amorphous regions.[4]

As an additional comparison, relaxation times were also determined for polyester 32/12,4, a structural isomer of 22,4 with slightly randomized placement of ester groups through random incorporation of both 1,12-dodecanol and 1,32-dotriacontanediol in the

polyesterification. The extent of rate decrease exerted by the ester groups on the chain flips in the crystallites was compared to polyethylene; these dynamics have important effects on creep as well as ultradrawability.[11] The more regular the ester placement, the more pronounced the cooperative effects of the ester groups are expected to be.

5.3.2.8.1 $T_{1\rho}$ Relaxation of ^1H Magnetization

The relaxation time of spin-locked magnetization, $T_{1\rho}$, contains information on the motion of CH_2 groups in the 10-1000 kHz region.[15] The ^1H $T_{1\rho}$ values of the crystalline regions of 22,4 and 32/12,4 were measured with ^{13}C-detection after 1 ms of regular CP at various temperatures. They are shown in Figure 5.11 and compared to linear low-density polyethylene with an average crystallite thickness of ~7 nm.

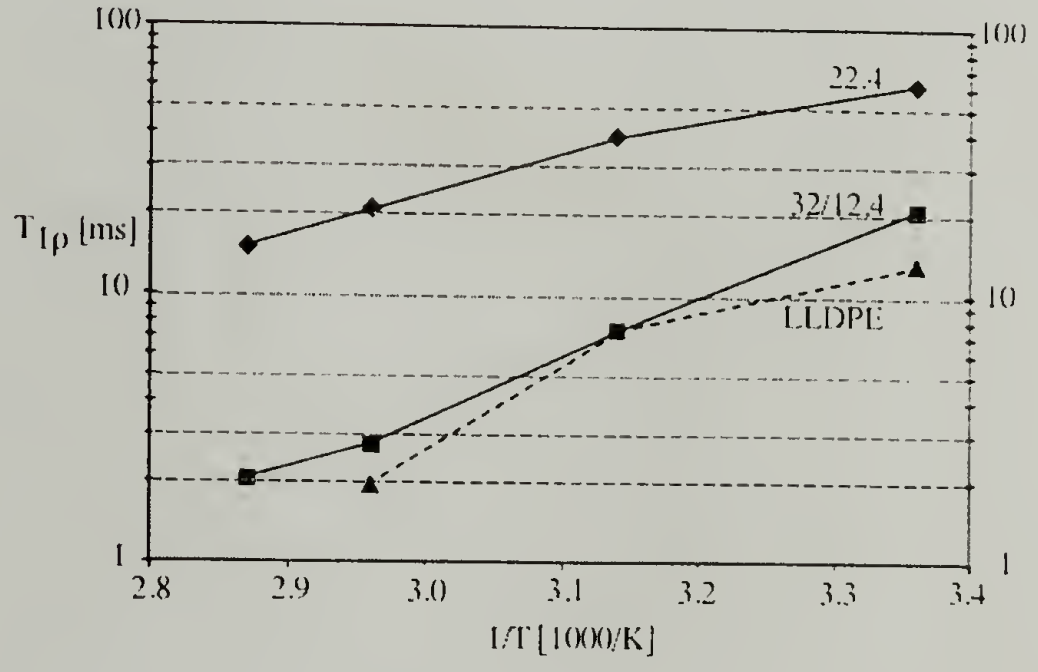

Figure 5.11 Arrhenius plot of the temperature dependence of ^1H $T_{1\rho}$ of crystalline regions for 22,4, 32/12,4, and a quenched linear low-density polyethylene (LLDPE) of ca. 7 nm crystallite thickness.

It is found that although the ester functionalities only account for about 15% of sample mass, they induce significant deviations from polyethylene dynamics. While the polyethylene studied here exhibits fast $T_{1\rho}$ relaxation driven by the 180° chain flips, this motion is suppressed in polyester 22,4. This can be attributed to the layering of the ester groups requiring cooperative motion of chains. Chain flips with similar rates as in the LLDPE occur in polyester 32/12,4, which possesses intermediate character between complete layering of esters and purely aliphatic polyethylene.

The reduction in ^{1}H $T_{1\rho}$ with increasing temperature indicates that even in 22,4 some chain motion still occurs. It can be speculated that at any given time, a small fraction of ester groups are out of register. This would permit the corresponding chains to undergo fast chain flips, until the ester groups are moved back into register.

5.3.2.8.2 $T_{1,C}$ Relaxation

The longitudinal ^{13}C relaxation was measured using the sensitive Torchia method with a phase-cycled z-storage of magnetization after CP.[6] Compared to saturation or inversion recovery, this method also has the great advantage of a well-defined final magnetization value of zero. The $T_{1,C}$ relaxation in polyethylene has been found to be strongly non-exponential and crystal-thickness dependent.[16] These unusual properties and the observed strong temperature dependence have been explained by chain diffusion from amorphous into the crystalline regions.[4] In this process, magnetization is transported into the crystalline regions by diffusing with the chain segments from the fast-relaxing amorphous regions. The $T_{1,C}$ relaxation curves for polyesters 22,4 and 32/12,4 at room temperature as well as 65°C are depicted in Figure 5.12.

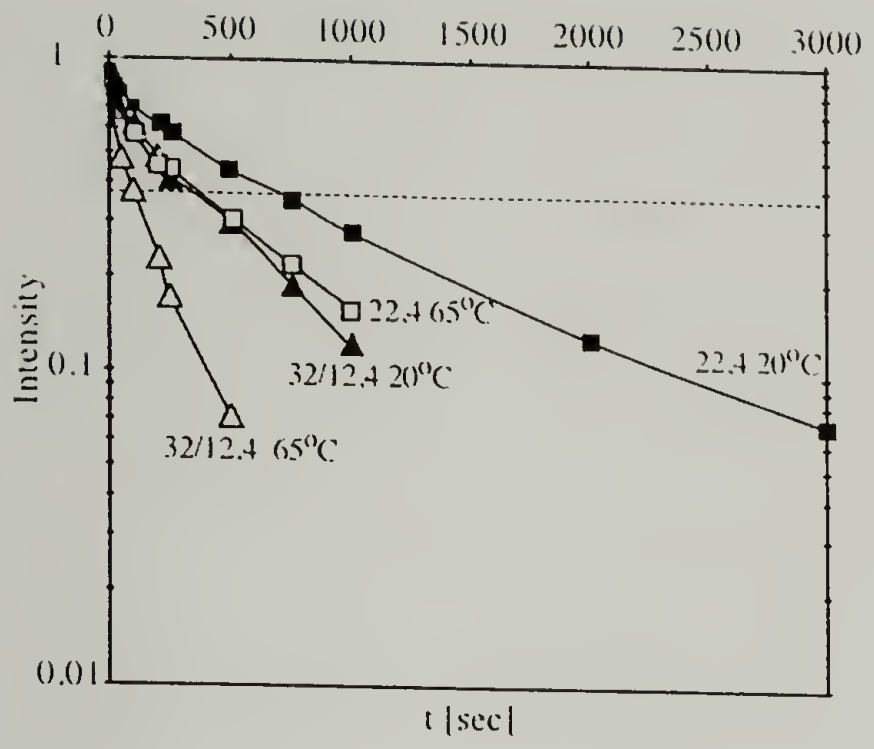

Figure 5.12 $T_{1,C}$ relaxation curves of CH_2 signals of unlabeled polyesters 22,4 and 32/12,4 at variable temperatures.

The $T_{1,C}$ relaxation curves of the crystalline CH_2 peak heights of 22,4 and 32/12,4 at ambient temperature measured using the Torchia method exhibit a significant non-exponentiality, as also found in polyethylenes. The straight final portion for polyester 22,4 evaluated as described by Axelson et al.[16] has a $T_{1,C} > 700$ ms. In polyethylenes, the ^{13}C longitudinal relaxation time $T_{1,C}$ depends strongly on the crystallite thickness, predominantly due to the chain diffusion between amorphous and crystalline regions.[16] Thus, $T_{1,C}$ for a known crystallite thickness can provide some insight into the rates of chain flips and chain diffusion. A polyethylene of comparable crystallite thickness of about 5 nm is expected, according to Axelson, to exhibit a $T_{1,C}$ of 50-60 ms.[16]

The strong deviation of the data for 22,4 from the PE data supports the conclusion that chain flips are suppressed by the ester-ester interactions.

Again, the observed decrease in $T_{1,C}$ with an increase in temperature is potentially due to a small fraction of ester groups being out of register, allowing those chains to undergo fast chain flips to move back into register.

5.3.2.8.3 PUREX NMR

In order to characterize potential segmental reorientations on the millisecond to second time scale, the pure exchange (PUREX) method was used.[17] The goal of this experiment is the detection of potential chain flips or other slow motions in the crystallites of the polyesters. Figure 5.13 depicts the temperature dependence of PUREX exchange NMR for 16% doubly labeled polyester 22,4 and 100% monolabeled polyester 32/12,4.

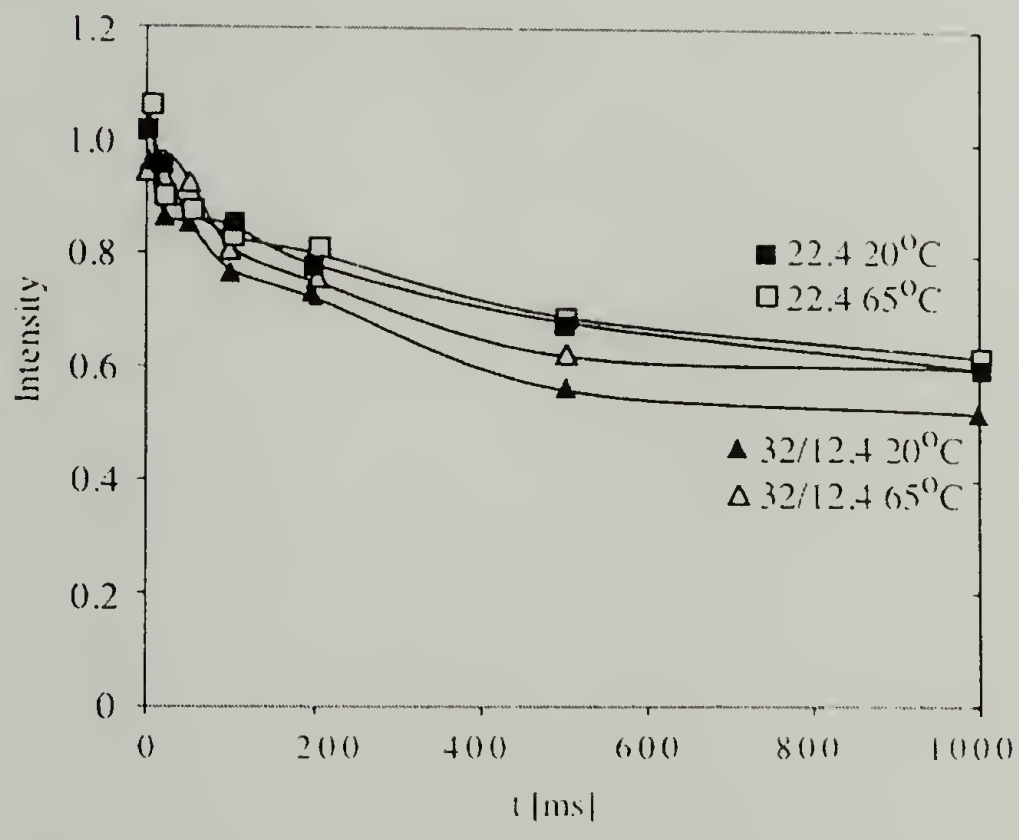

Figure 5.13 Temperature dependence of PUREX exchange NMR ^{13}COO signals of polyesters 16 % doubly labeled 22,4 and 100 % monolabeled 32/12,4.

It can be seen that the exchange intensity is low and nearly temperature independent. This indicates that ^{13}C dipolar spin exchange is dominant, rather than segmental reorientation. This finding is consistent with the earlier structural findings that there is no significant population of flipped ester groups.

5.3.2.8.4 Wideline Separation (WISE) Spectrum: Mobility of Various Sites

To gain insight into the dynamics of specific sites of polyester 22,4, a ^{1}H-wideline separation spectrum (WISE) was recorded. Figure 5 14 displays the ^{1}H wideline spectrum of PE22,4 and ^{1}H wideline cross sections for the carbonyl, crystalline methylene, and amorphous methylene segments taken from a WISE spectrum obtained with 0.5 ms of LGCP.

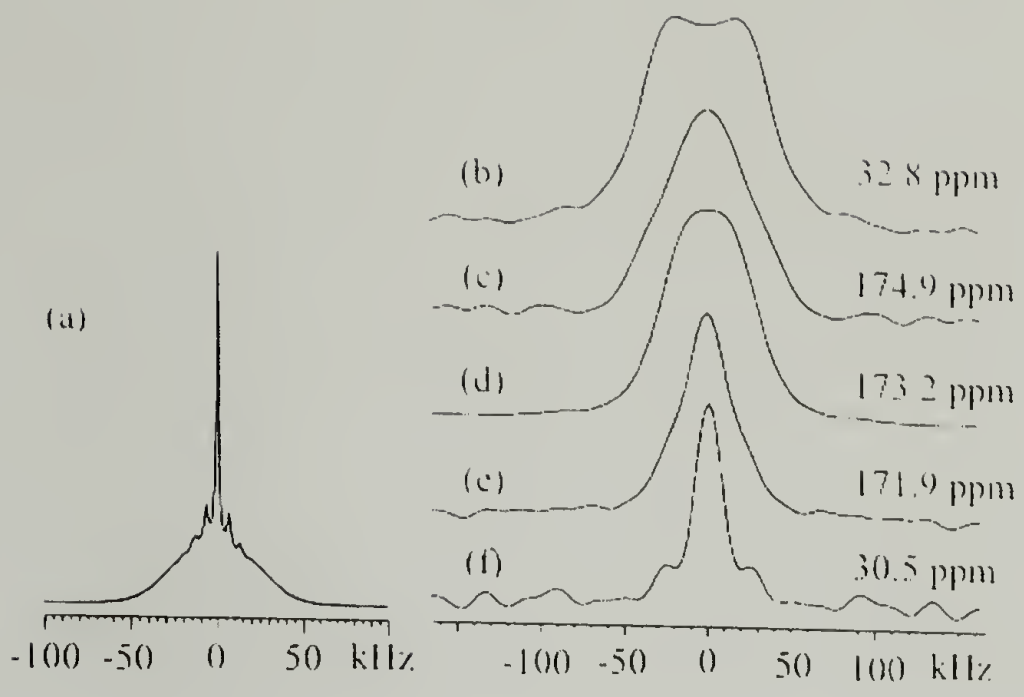

Figure 5.14 ^{1}H wideline traces of doubly ^{13}COO-labeled PE22,4. (a) Regular ^{1}H wideline spectrum without sample rotation. (b-f) Cross sections taken from a 2D WISE spectrum at various resonance positions in the ^{13}C dimension: (b) crystalline CH_2 at 32.6 ppm, (c) COO at 174.9 ppm, (d) COO at 173.2 ppm, (e) COO at 171.9 ppm, and (f) amorphous CH_2 at 30.5 ppm.

From the similar widths of the cross sections for carbonyl and crystalline methylene segments and the significantly narrower amorphous segment cross section, it can be deduced that the carbonyl segments possess a mobility comparable to that of the crystalline methylene segments. This indicates that the carbonyl segments are incorporated into the crystal.

5.4 Conclusions

Through state-of-the-art solid-state NMR and SAXS, a detailed picture of the aliphatic polyester 22,4 with widely but regularly placed ester groups along the polymer

backbone was obtained, varying in length scales from the molecular level up to 10-nm morphological structures. Both SAXS and NMR found a mass crystallinity of 70 %. This high crystallinity was confirmed by ^{13}C and ^{1}H-CP MAS spectra. DOQSY NMR confirmed an all-trans conformation of the succinate units between the ester groups. The DOQSY NMR of a singly ^{13}COO-labeled sample proved intermolecular correlations, as detected by SAXS, due to the layering of ester groups. The observed NMR intensity pattern, reflecting the relative orientation of neighboring chains, identified the crystal structure as an O'$\perp$ crystal modification with a 55° angle between the planes of the chains. The ^{13}COO chemical shift tensor orientation was confirmed by correlation with the geminal H-H dipolar coupling of neighboring CH_2 groups. The above mentioned high crystallinity, found consistently from ^{13}C-NMR and SAXS, along with the long period of 7.7 nm obtained from SAXS required the incorporation of two repeat units into the crystalline regions alternating with a non-crystalline loop consisting of a $-(CH_2)_{22}-$ unit. SAXS as well as NMR through spin diffusion and WISE experiments showed very strong evidence of three ester double-layers in the crystal, of which two are at the surface and one is in the center of the crystal.

Measurements of relaxation times $T_{1\rho}$ and $T_{1,C}$ as well as PUREX NMR confirmed that in spite of the small fraction of ester groups along the poly(methylene) chains, fast 180° chain flips as observed in polyethylene are suppressed. Comparison with linear low-density polyethylene of comparable crystal thickness and with polyester 32/12,4, which introduces a controlled amount of randomness into the ester placement, revealed that layering of ester groups cooperatively controlled the dynamics of the chains in the crystallites.

Providing very detailed structural information on one specific long-chain aliphatic non-branched polyester, it was shown that a few ester groups, placed perfectly regularly into an otherwise purely aliphatic backbone are sufficient to gain partial control of the morphology of a polyethylene-like polymer. It was found that strong intermolecular forces such as H-bonds as found in polyamides and polyurethanes are not essential to achieve quantization of crystal thickness and length of folds.

The crystal structure obtained is polyethylene-like, rendering polyesters valid models for the study of polyethylene crystallization after introduction of defects at perfectly regular distances along the polymer backbone. The observed reduction of chain dynamics may result in a significant modification of mechanical properties, such as reduced creep.

5.5 References

(1) Ehrenstein, M.; Sikorski, P.; Atkins, E.; Smith, P. *J. Polym. Sci., Polym. Phys. Ed.* **2002**, *40*, 2685-2692.

(2) Mandelkern, L.; Alamo, R. G. *Polymer Data Handbook*; Oxford University: Oxford, 1999.

(3) Fuller, C. S. *Chem. Rev.* **1940**, *26*, 143-167.

(4) Schmidt-Rohr, K.; Spiess, H. W. *Macromolecules* **1991**, *24*, 5288-5293.

(5) Bennett, A. E.; Rienstra, C. M.; Auger, M.; Lakshmi, K. V.; Griffin, R. G. *J. Chem. Phys.* **1995**, *103*, 6951-6958.

(6) Torchia, D. A. *J. Magn. Reson.* **1978**, *30*, 613.

(7) Abrahamson, S.; Dahlén, B.; Löfgren, H.; Pascher, I. *Progress in the Chemistry of Fats and Other Lipids*; Pergamon: London, 1978; Vol. 16.

(8) Lee, K.-S.; Wegner, G.; Hsu, S. L. *Polymer* **1987**, *28*, 889.

(9) Liau, W.-B.; Boyd, R. H. *Macromolecules* **1990**, *23*, 1531-1539.

(10) Le Fevere de Ten Hove, C. Ph. D., Université Catholique de Louvain, 2001.

(11) Hu, W.-G.; Schmidt-Rohr, K. *Polymer* **2000**, *41*, 2979-2987.

(12) Goldman, M.; Shen, L. *Phys. Rev.* **1966**, *144*, 321.

(13) Schmidt-Rohr, K. *Macromolecules* **1996**, *29*, 3975-3981.

(14) Dunbar, M. G.; Sandström, D.; Schmidt-Rohr, K. *Macromolecules* **2000**, *33*, 6017-6022.

(15) Schmidt-Rohr, K.; Spiess, H. W. *Multidimensional Solid-State NMR and Polymers*; 1st ed.; Academic Press: London, 1994.

(16) Axelson, D. E.; Mandelkern, L.; Popli, R.; Mathieu, P. *J. Polym. Sci., Polym. Phys. Ed.* **1983**, *21*, 2319-2335.

(17) deAzevedo, E. R.; Bonagamba, T. J.; Schmidt-Rohr, K. *J. Magn. Reson.* **2000**, *142*, 86-96.

CHAPTER 6

SOLID-STATE NMR CHARACTERIZATION OF BRANCHED LONG-CHAIN POLYESTERS

6.1 Introduction

With the advance of metal catalysis from conventional Ziegler-Natta systems to metallocene catalysts over the past decade, an increasing control over regularity of branching in polyethylene has been gained.[1] However, branches are still randomly spaced along the polymer backbone resulting in a distribution of crystal thicknesses attainable from LLDPE.[2-4] In the model polyesters studied here, control over lamellar thickness is achieved through incorporation of aliphatic and aromatic side branches at perfectly regular distances along a polyethylene-like backbone.

It is the goal of this chapter to establish the influence, upon polymer microstructure and chain folding, of diester moieties bearing branches too large to be accommodated in a polyethylene-like orthorhombic crystal structure placed regularly along the polymer backbone. A variety of different sizes of diacid moieties and side branches are probed to prove the general applicability of the concept used here: to force tight chain folding at controlled distances through exclusion of defects into the amorphous regions. A further goal is to smooth a path for crystalline/amorphous interface functionalization through incorporation of functionalized defects. Through the placement of ^{13}C-labels in the diester units along the backbone, sophisticated solid-state NMR experiments are enabled, elucidating polymer crystallization, morphology, and dynamics of these otherwise polyethylene-like polymers. SAXS yields information on

the length scale of a few nanometers, measuring crystal thickness as well as long period. On a smaller length scale of a few tenths of nanometers, interchain distances and the conformations adopted by the diacid units can be probed through DOQSY NMR.

6.2 Experimental

6.2.1 X-Ray Scattering

Small-angle X-ray scattering (SAXS) measurements were obtained with a Kratky camera (Anton-Paar KKK) using a Braun OED 50 M proportional position sensitive detector and Ni-filtered Cu K_α radiation. The data were smoothed, then desmeared using a variant of Glatter's algorithm, furthermore parasitic scattering and background were subtracted, and the Lorentz correction was applied. Fourier transforming the Lorentz-corrected desmeared experimental data multiplied by an apodization function yielded the corresponding correlation functions.

6.2.2 Solid-State NMR Parameters

Solid-state NMR experiments were conducted using either a Bruker DSX-300 or a Bruker DSX-400 spectrometer in a magnetic field of 7 or 9.4 T, respectively. Measurements under static as well as magic angle spinning (MAS) conditions were performed at ambient temperature. For all MAS experiments, 4-mm diameter zirconia rotors with Kel-F caps were used to hold the samples. For measurements on the Bruker DSX-300 spectrometer, a 5-kHz spinning speed and decoupling with two-pulse phase modulation[5] (TPPM) at $\gamma B_1/2\pi = 63$ kHz were utilized. Measurements on the Bruker DSX-400 were performed at a spinning speed of 6.5 kHz to avoid overlap of CH_2 peaks

with spinning side bands of the ester signals. The ^{1}H spectra were obtained with a ^{1}H 90° pulse length of 3 μs, for ^{13}C cross-polarization (CP) measurements, a ^{1}H 90° pulse length of 4 μs and a contact time of 1 ms were applied.

For the direct polarization experiments (DP) to determine crystallinity, ^{13}C magnetization was excited by a single 90° pulse. To obtain the fully relaxed polymer signals, spectra with a recycle delay of 500 s and 24 or 32 scans were acquired. Signals for the non-crystalline all-trans and gauche containing regions were obtained with recycle delays of 1 and 10 s, respectively; 2048 or 3072 scans were added up.

Spin diffusion measurements were carried out using the Goldman-Shen pulse sequence with ^{13}C detection. Lee-Goldburg cross-polarization (LG CP) of 0.5 ms duration was used to prevent spin diffusion during CP. The crystalline signal will vanish after the dephasing time of ca. 15 μs, whereas most of the amorphous signal is retained and can undergo spin diffusion to the crystallites. In all MAS experiments the chemical shift calibration is based on a chemical shift of 32.8 ppm for crystalline HDPE.

The two-dimensional wideline separation (WISE) spectra were recorded with ^{13}C decoupling during evolution, 128 t_1 increments, a t_1 dwell time of 5 μs, and a Lee-Goldburg cross-polarization contact time of 0.5.

In the static measurements (without MAS), the sample was inserted as a cylindrical block of 4-mm diameter wrapped in Teflon tape into the 4.5-mm coil of a stationary Bruker double-resonance probe. The measurements were carried out at 298 K without sample rotation. The ^{1}H- and ^{13}C 90° pulse lengths were 2.8 μs. In the DOQSY experiments, cross-polarization time was 1.6 ms. A recycle delay of 3 s, an acquisition time of 3.12 ms, and a dwell time of 3 μs were used. The DQ excitation and

reconversion delays, τ_{DQ} = 0.7 ms, each contained two cycles of the xy-16 pulse sequence.

The $T_{1\rho,H}$ relaxation time in the crystallites were measured with a pulse sequence consisting of a variable ^{1}H spin-lock, cross-polarization to ^{13}C, a 10 second phase-cycled z-filter to suppress signal from the non-crystalline regions, and ^{1}H-decoupled ^{13}C detection. The cross polarization time was 0.5 ms.

^{13}C spin lattice relaxation times, $T_{1,C}$, were measured by the cross-polarization method developed by Torchia. 90° Pulse lengths of 4 μs for both, ^{13}C and ^{1}H, were used with a cross-polarization time of 0.5 ms.

6.3 Results and Discussion

6.3.1 X-Ray Scattering

The wide-angle x-ray diffraction patterns observed for branched polyesters have been described in chapter 4. Generally, it was found that a diol segment length of 22 methylene units lead to small or disordered crystals. A diol segment length of at least 32 methylene units was found to be required to achieve polyethylene-like crystallization in an orthorhombic unit cell for branched polyesters.

Benoit de Meersman at the Université Catholique de Louvain in Belgium performed the small-angle x-ray scattering experiments on branched polyesters. In a detailed study for polyesters 32,5-3 and 32,5-ph, crystallization time as well as crystallization temperature was varied. The resulting SAXS correlation functions are shown in Figure 6.1.

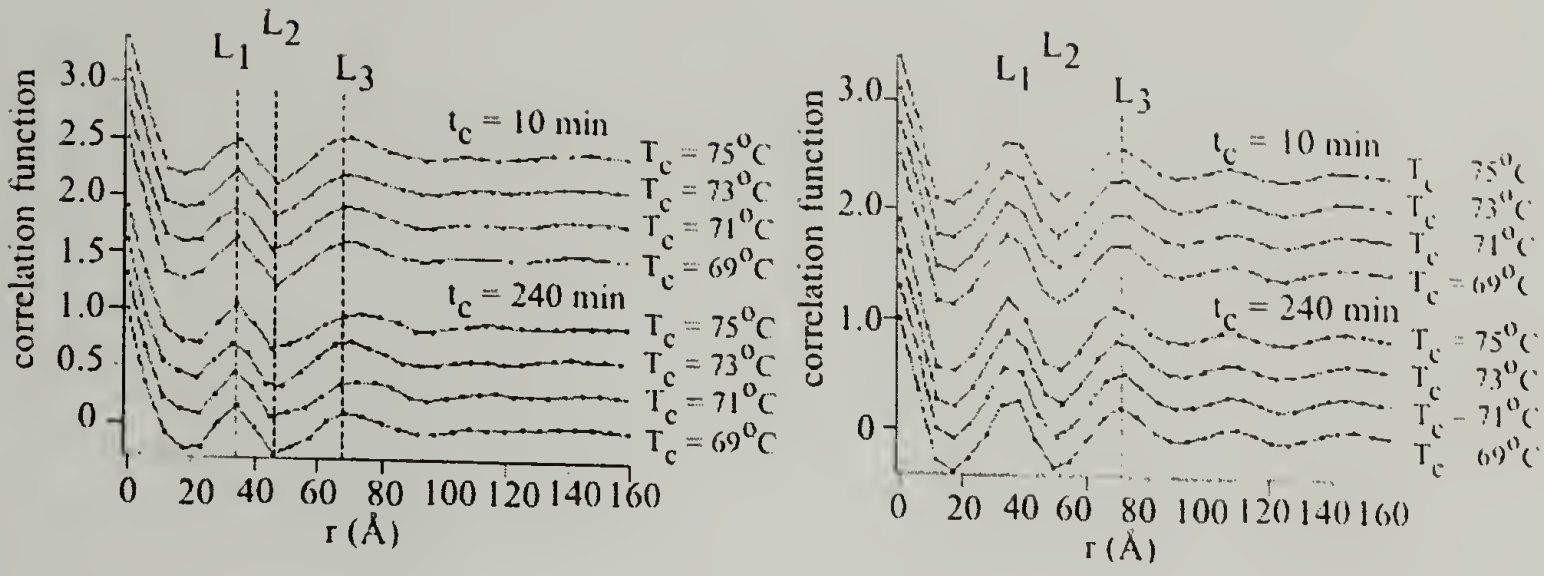

Figure 6.1 SAXS correlation functions for polyesters 32,5-3 and 32,5-ph obtained at varying crystallization times and temperatures.

It was found that the first peak observed in the correlation functions, here labeled as L_1, was invariable under varying crystallization conditions, and also showed no thickening upon annealing. The interpretation of this peak, however, is not unambiguous, and will be discussed below. SAXS diffractograms were also obtained for three annealed branched polyesters, and correlation functions were computed. The example of the correlation function for polyester 32,phac and the observed peaks for all three branched polyesters are shown in Figure 6.2.

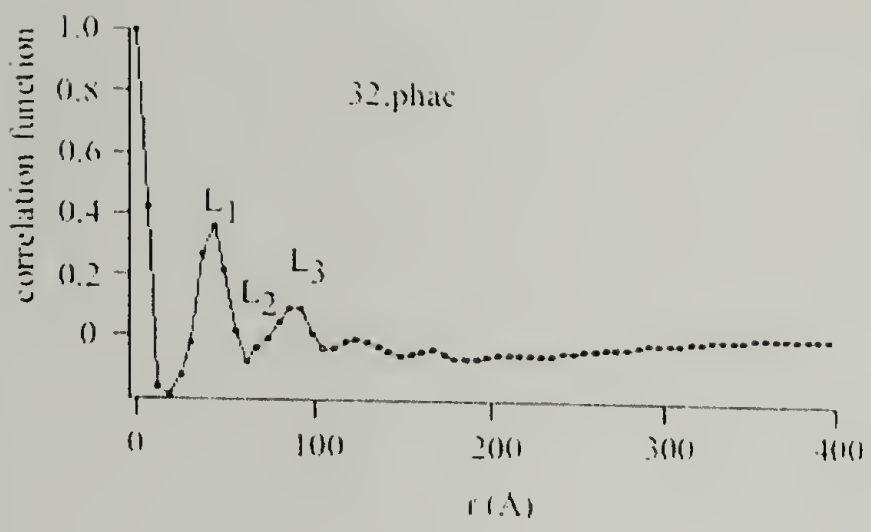

Polyester	L_1	L_3
32.phac	43 Å	88 Å
32.3-ph	42 Å	102 Å
32.3-6	37Å	62Å

Figure 6.2 SAXS correlation function for branched polyester 32,phac and peak positions derived from correlation functions for branched polyesters.

As mentioned briefly above, the physical meaning of the peak, L_1, either being the crystal thickness, L_c, or the long period, L_p, is somewhat ambiguous, and not as clear as expected. Assuming L_1 or L_2 to correspond to the crystal thickness and L_3 to represent the long period L_p, the crystallinities obtained for branched polyesters here are found to be around 50 %. This is in contradiction to crystallinities measured well above 50 % by CP and DP NMR. In addition to that, interpreting L_1 to correspond to the crystal thickness in some cases such as 32,phac yields thicknesses too high to correspond to one diol segment length. Considering that even the formation of tight folds will require some use of diol segment length in the formation of the fold, this is physically unfeasible.

Alternatively, L_1 can be interpreted as the long period, L_p, with L_3 being $2 \cdot L_p$. This interpretation will yield high crystallinities in accordance with the results found by solid-state NMR and suggests crystals to be indeed formed by one diol segment with tight chain folds consisting of the diacid units. In either case, the invariance of the peak

position of L_1 with varying crystallization conditions suggests control over lamellar thickness and chain folding by chemical means.

6.3.2 Solid-State NMR

X-ray scattering, as shown above, suggested single lamellar thicknesses for branched polyesters, invariable under varying crystallization conditions or annealing. The question arising from this observation is the nature of chain folded structures formed by these polyesters, particularly the nature of the chain folds and the placement of the ester moieties. Two models of chain folding, tightly and loosely folded, are considered here. In these models, the crystalline lamellae are formed by the crystallizable polymethylene $[\text{-}CH_2\text{-}]_n$ sequences, with connecting loops of different lengths. Figure 6.3 shows schematics of the two chain folding models proposed here, consisting (i) of tight folds by adjacent reentry of chains or (ii) of loose folds in a switchboard model.

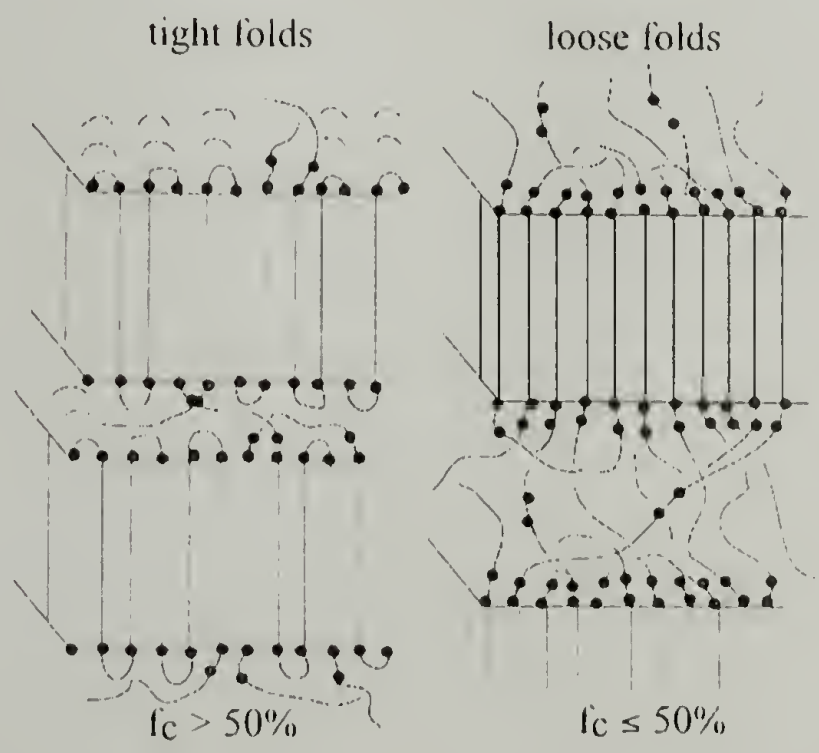

Figure 6.3 Models of chain folding in single lamellar thickness branched polyesters.

In the tight-folding model, folds consisting only of the diacid defects connect the crystallizable segments; this results in a high crystallinity > 50 % if the folds do not sequester too many CH_2 groups of the crystallizable polymethylene segment. In the loose-folding model, the crystallizable segments along one chain are alternately part of the crystalline and the amorphous regions; adoption of this structure must result in crystallinities below 50 %. In a combination model, the crystallinity may be near 50 %. In other words, crystallinities well above 50 % prove a predominance of tight chain folding. The presence of the regularly spaced non-crystallizable defects results in quantization of the fold length; it can only consist of integer (0,1,2,3,...) numbers of diol segments. In this description, a fold of 0 diol segments consists only of the diacid segments with a possibility for sequestering of a few diol methylene units to form a stable tight fold. The folding described for polyester 22,4 in chapter 5 constitutes a fold length of 1 diol unit in the description used here. In the following, a number of experiments probing crystallinity are described to assess the applicable model for the branched polyesters studied here.

6.3.2.1 Proton Wideline MAS Spectra

Qualitative information on the amount of crystalline *versus* amorphous regions, and on the mobility of branched polyesters can be gained through their proton spectra. The ^1H wideline MAS spectra of a number of branched polyesters with diol segment lengths of 32 or 46 methylenes are depicted in Figure 6.4.

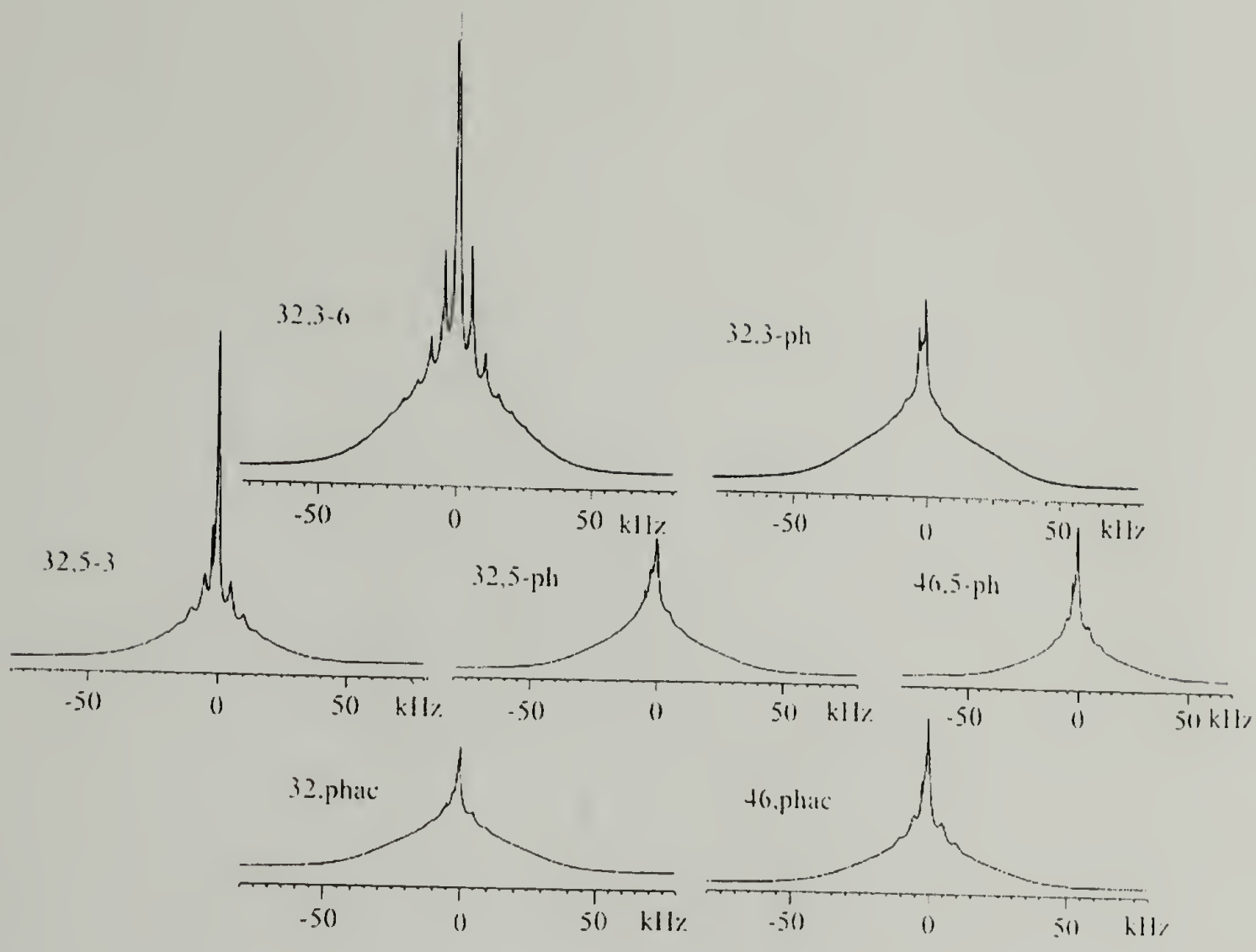

Figure 6.4 ^{1}H wideline MAS NMR spectra of branched polyesters at a spinning speed of 5 kHz.

The spectra consist predominantly of broad peaks due to rigid crystalline regions. Secondly, in the polyesters carrying an aliphatic branch, a narrow signal due to those mobile branch segments in the amorphous regions is observed. The large area fractions of broad crystalline bands generally indicate high crystallinities, with no significant amount of mobile diol segments in the amorphous regions and exclusion of branches into the amorphous regions. This favors the tightly folded model of Figure 6.3.

6.3.2.2 ^{13}C CP Spectra

In order to gain a qualitative measure of crystallinity and chain mobility, CP spectra under magic angle spinning as well as static spectra of the branched polyesters were recorded. Figure 6.5 shows a few examples for the CH_2 crystalline signals of branched polyesters.

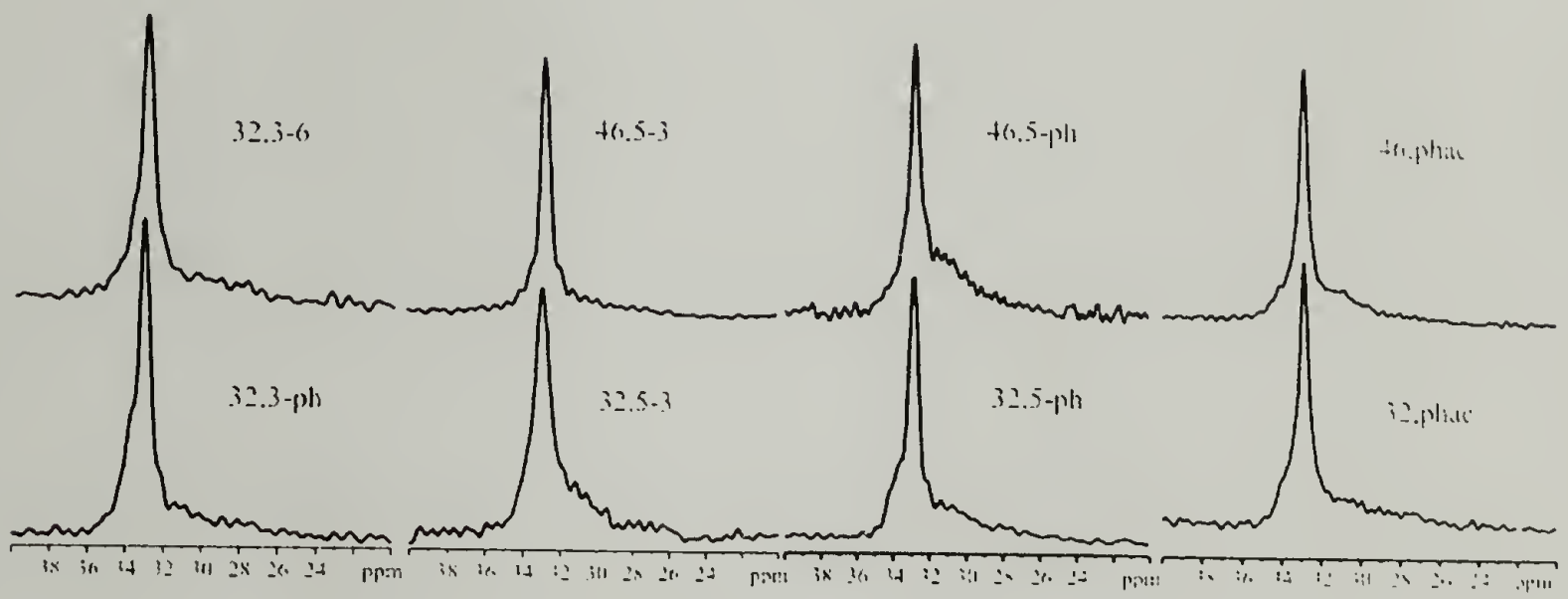

Figure 6.5 ^{13}C CP/MAS NMR spectra of doubly ^{13}COO-labeled branched polyesters.

Generally, the aliphatic regions of the ^{13}C CP/MAS spectra of branched polyesters are dominated by the crystalline $[-CH_2-]_n$ peak centered at 32.8 ppm and very little amorphous contribution. In some cases, a shoulder of the crystalline resonance observed slightly downfield from the peak at 32.8 ppm is observed. By annealing the polyesters at a small undercooling, this shoulder can be minimized or even completely eliminated. As no significant $[-CH_2-]_n$ signal stemming from amorphous regions upfield from the crystalline peak at 32.8 ppm is observed, the chain folding in tight loops seems preferred.

In static ^{13}C-CP spectra of ^{13}COO-labeled branched polyesters the mobility of ester groups can be assessed through the motional narrowing of the ^{13}COO powder spectra. Figure 6.6 depicts several examples.

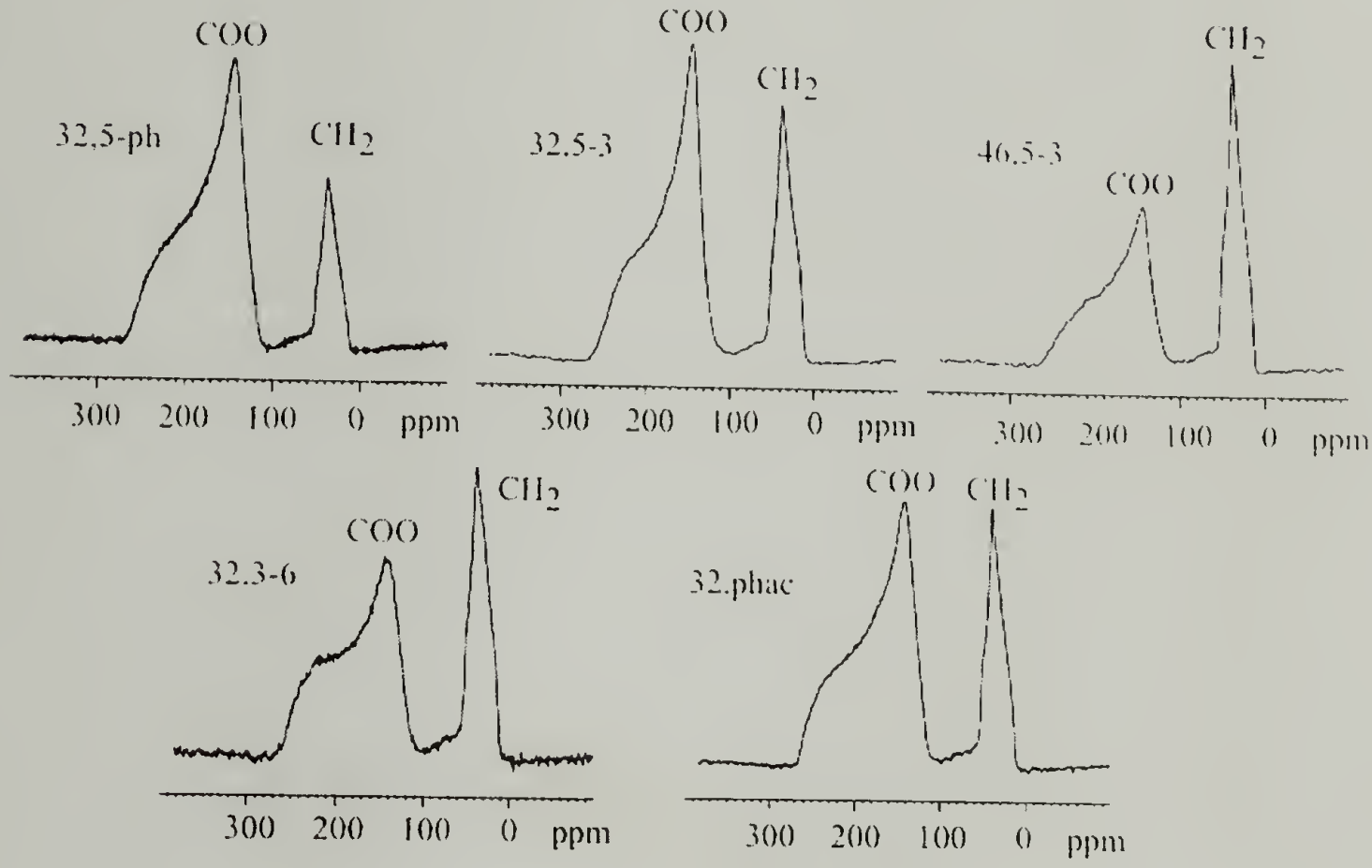

Figure 6.6 ^{13}C CP static NMR spectra of doubly ^{13}COO-labeled branched polyesters.

The ^{13}COO powder patterns show edges that are not sharp but rather gradually rising. This indicates partial motional narrowing of the powder patterns, which can be attributed to some "wiggling" motion of the carbonyl groups in the loops. The patterns observed here are indicative of interfacial ester groups as they neither show well defined sharp powder patterns as observed for crystalline regions nor strong motional narrowing as expected for COO groups in the center of the amorphous regions.

6.3.2.3 ^{13}C DP/MAS Spectra: Determination of Crystallinity

Quantitatively, crystallinities of the branched polyesters were determined, as described for polyester 22,4 in chapter 5, by a series of ^{13}C DP spectra with varying recycle delays.[6] Torchia CP/T_1 experiments[7] performed prior to crystallinity measurements showed that the longest recycle delay of 500 seconds accounts for 5-10·$T_{1,C}$, and so provides quantitative peak areas in the DP spectrum when integrated between 34.8 and 25.0 ppm. The amorphous signals were deconvoluted through two spectra with shorter recycle delays of 10 and 1 second and aquired with more scans. They were quantified by comparing the integrated signals per scan. The heteronuclear nuclear Overhauser effect (NOE) in the 1 second recycle delay spectrum has been suppressed by a 10-s delay before ^{13}C saturation pulses and the nominal recycle delay.[6]

In the determination of crystallinities for polyesters bearing aliphatic side chains, 32,5-3, 46,5-3, and 32,3-6, the exclusion of aliphatic branches into the amorphous regions was taken into account. The contribution of signal from the branch CH_2 groups to the measured amorphous content is subtracted from the amorphous signal. This subtraction yields what will be termed the "backbone" crystallinity for these branched polyesters. All samples were annealed overnight at an undercooling of 10°C prior to crystallinity determination. Figure 6.7 shows the DP spectra obtained for polyester 32,5-ph as an example.

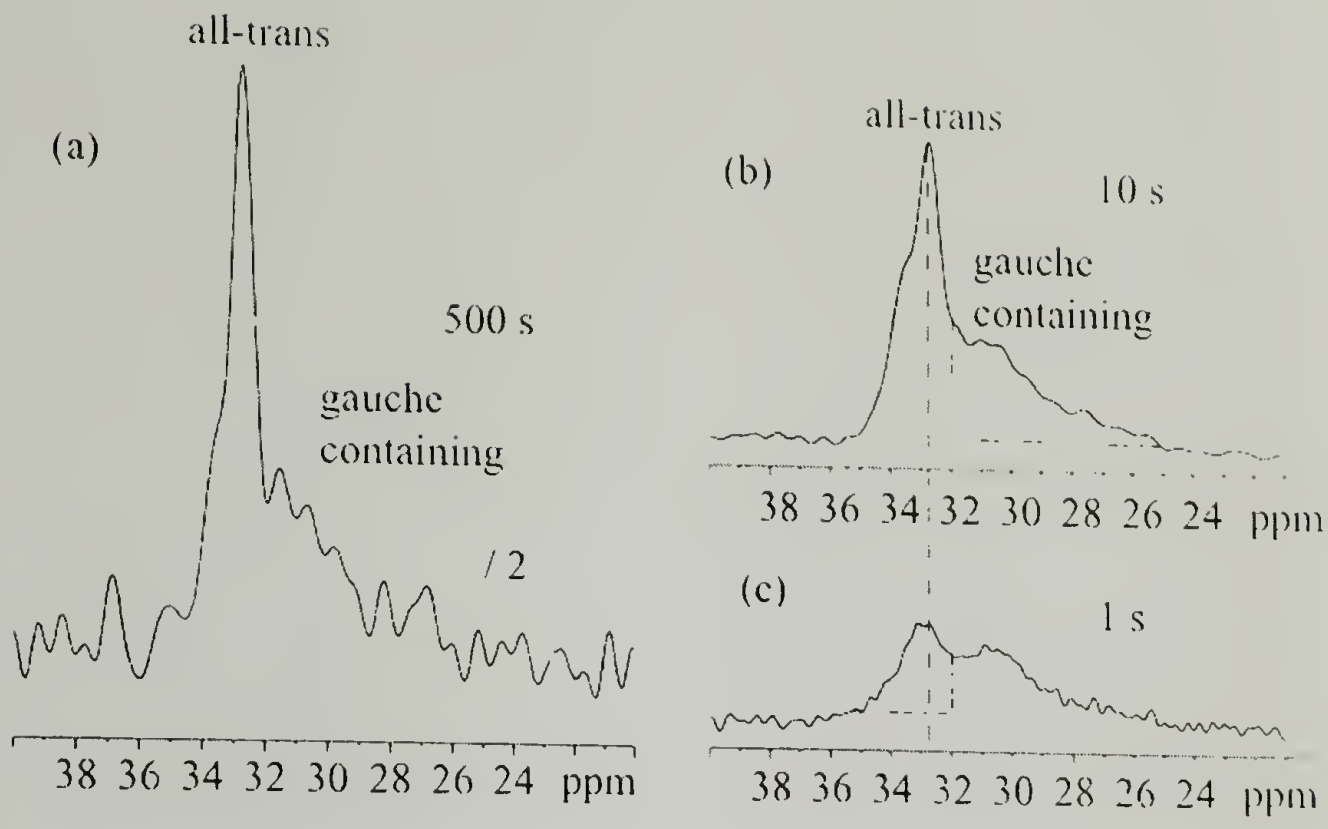

Figure 6.7 DP/MAS ^{13}C NMR for crystallinity determination exemplified by polyester 32,5-ph: (a) 500 s recycle delay (b) 10 s (c) 1 s.

At the short recycle delays, the gauche-containing amorphous fraction is observed at 30.5 ppm. The small 33-ppm band observed in the 1-second spectrum is clearly distinct from the crystal peak, in terms of peak position, width, and relaxation time, and is therefore considered as part of the non-crystalline components.

The areas of the peaks between 34.8 and 32.0 ppm in the 1-s recycle delay spectrum and 32.0-25.0 ppm in the 10-s recycle delay spectrum relative to that of the fully relaxed signal in Fig. 6.7 (a) yield a mass-based crystallinity of 54% for this particular polyester.

In the case of polyesters derived from 1,46-hexatetracontanediol, a large difference in crystallinities measured was observed. Figure 6.8 shows the series of DP spectra for polyester 46,5-ph which possesses a relatively low crystallinity of 45 %, even

after annealing repeatedly at a supercooling of 10°C. In the 10 second recycle delay spectrum, a large fraction of gauche containing amorphous region upfield from the crystalline peak at 32.8 is clearly visible, while the amount of mobile all-trans observed in the 1 second recycle delay spectrum downfield from the crystalline resonance at 32.8 ppm is relatively small.

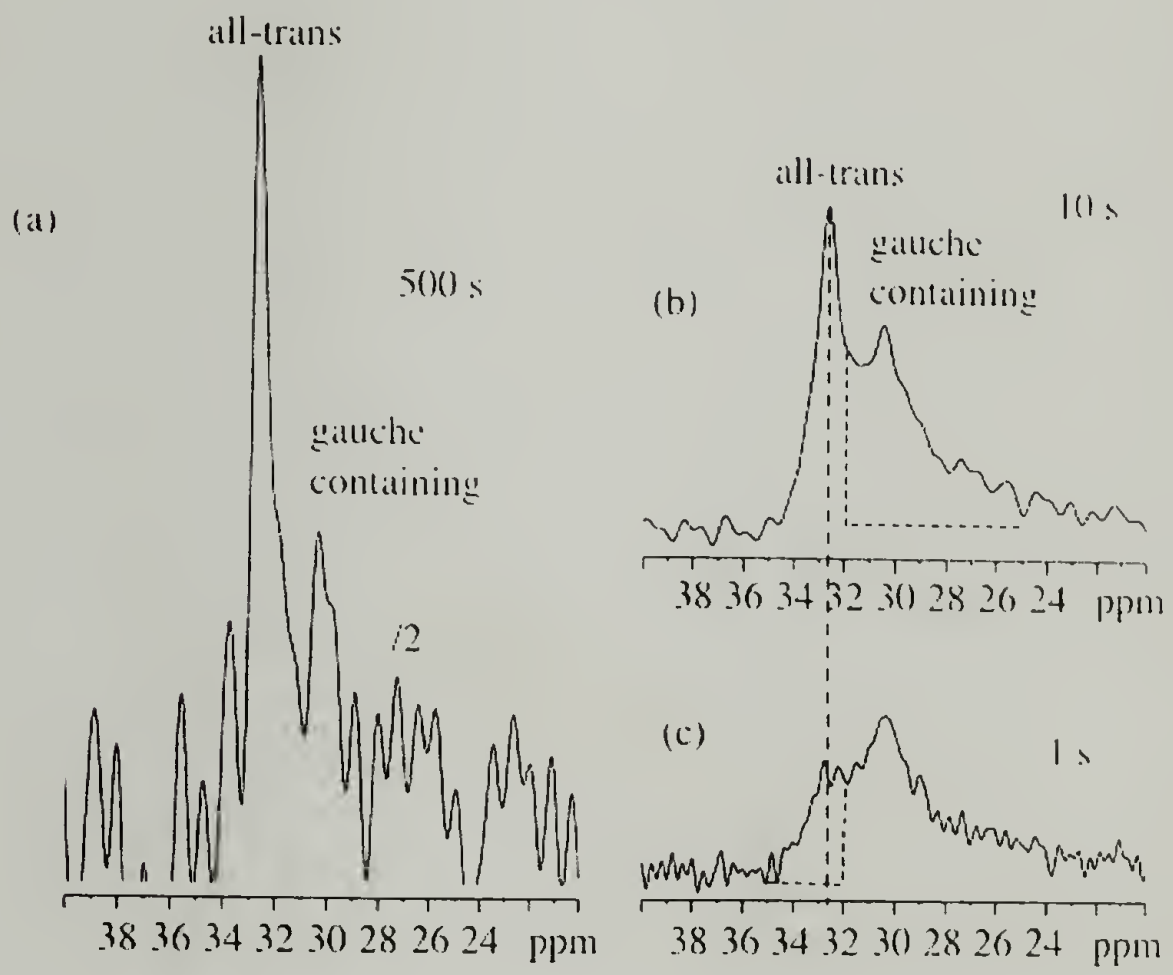

Figure 6.8 DP/MAS ^{13}C NMR for crystallinity determination exemplified by polyester 46,5-ph: (a) 500 s recycle delay (b) 10 s (c) 1 s.

In contrast to 46,5-ph, polyester 46,5-3 shows a high backbone crystallinity of 71 % after the contribution of the aliphatic branch to the amorphous fraction is subtracted.

Figure 6.9 shows the series of DP spectra for polyester 46,5-3 in which only minor contributions from the amorphous regions are detectable.

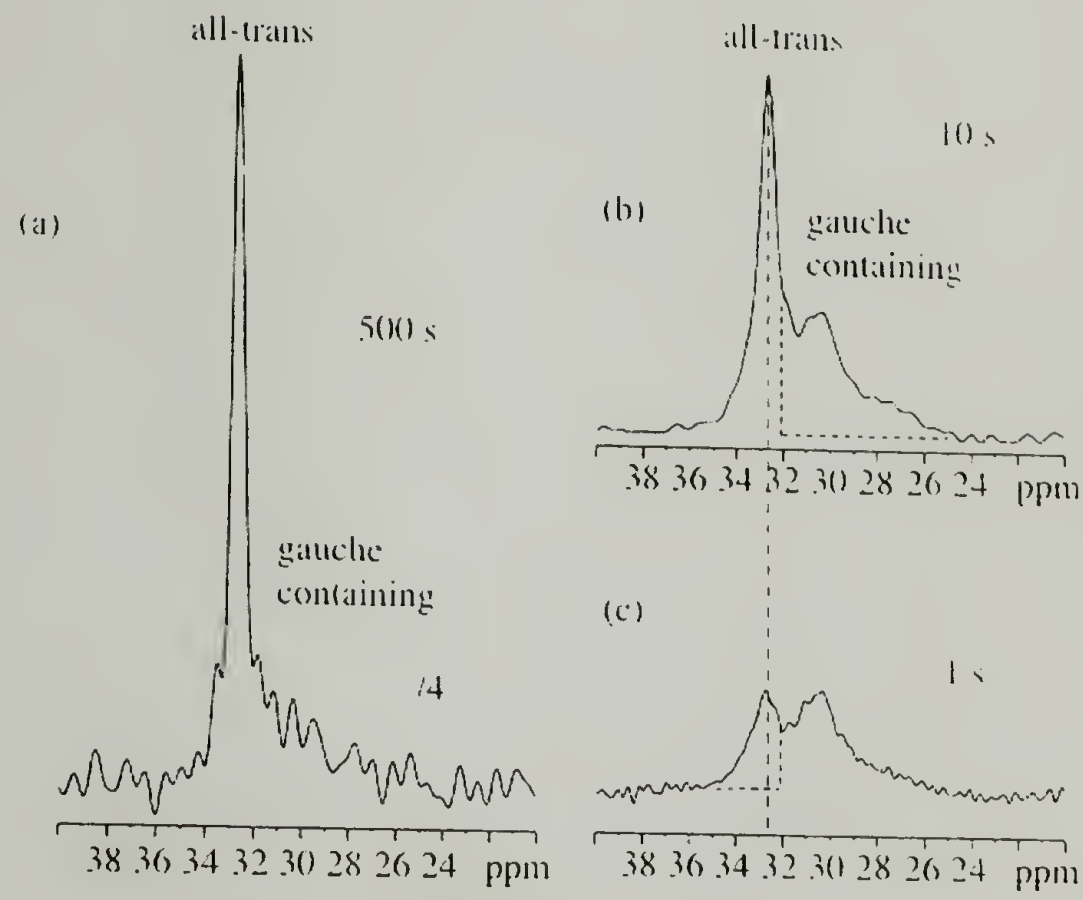

Figure 6.9 DP/MAS ^{13}C NMR for crystallinity determination exemplified by polyester 46,5-3: (a) 500 s recycle delay (b) 10 s (c) 1 s.

Crystallinities for branched polyesters 22,3-6 and 22,3-ph were determined as well and were 31 and 33 %, respectively. However, as these systems showed only small or disordered crystals in the WAXS patterns, they are assumed to adopt a liquid-crystalline-like structure and were not characterized in detail as done for branched polyesters with methylene segment length ≥32. Figure 6.10 shows the DP series for

polyester 22,3-ph, were a major contribution to the mobile all-trans peak attributed to the amorphous regions can be observed.

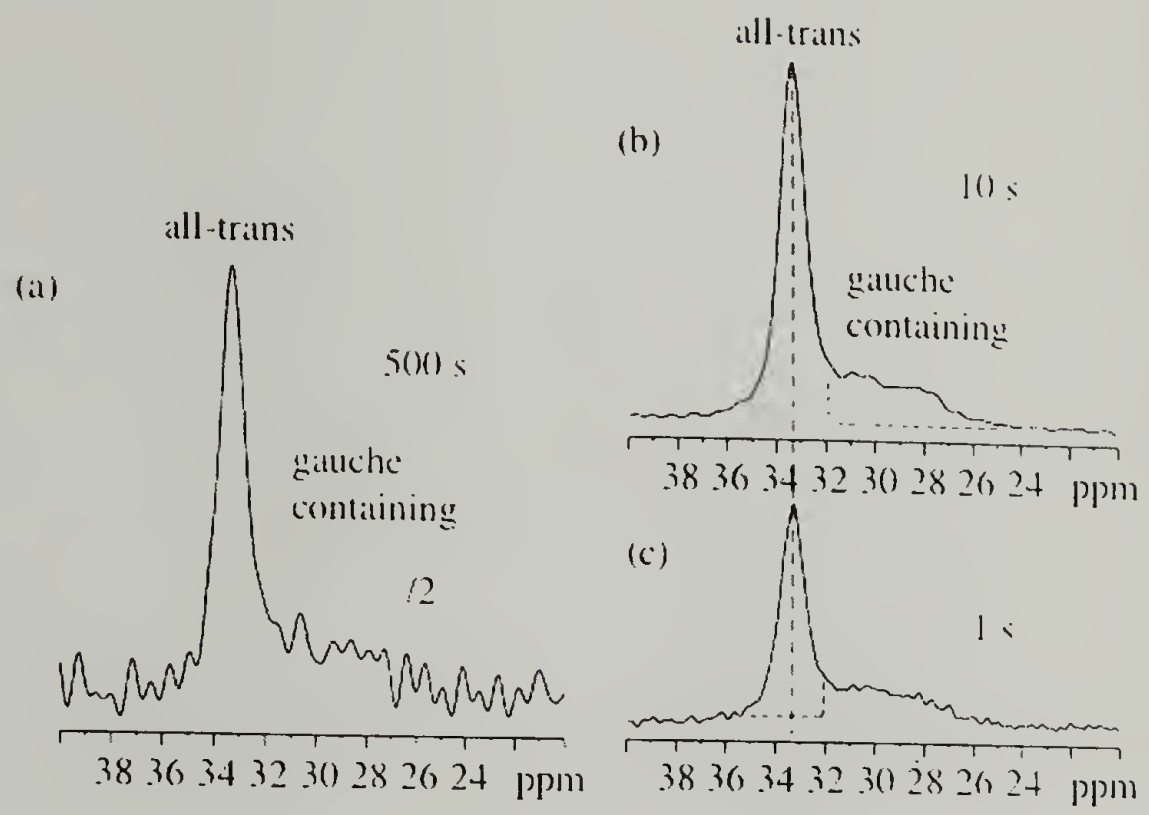

Figure 6.10 DP/MAS ^{13}C NMR for crystallinity determination exemplified by polyester 22,3-ph: (a) 500 s recycle delay (b) 10 s (c) 1 s.

Table 6.1 summarizes the measured backbone crystallinities for branched polyesters with a diol segment length of 32 methylene units or more.

Table 6.1 Backbone crystallinities of branched polyesters as determined by DP/MAS ^{13}C NMR

Polyester	mobile all-trans fraction of amorphous	Backbone Crystallinity
46,5-3	28 %	71 %
32,5-3	35 %	62 %
32,3-6	25 %	66 %
32,3-ph	28 %	64 %
32,phac	29 %	59 %
46,phac	18 %	48 %
32,5-ph	25 %	54 %
46,5-ph	18 %	45 %

Backbone crystallinities for branched polyesters measured here, with the exception of 46,5-ph and 46,phac, lie well above 50 %. This observation, combined with the findings of ^{1}H- and ^{13}C CP/MAS and static spectra proves the polymers to predominantly adopt tight chain folds, consisting of the diacid segment under exclusion of branches into the amorphous regions. The crystal thickness is then roughly given by the diol segment length, which is determined by SAXS.

The reduced crystallinity in 46,5-ph and 46,phac systems may be due to sequestering of CH_2 units out of the crystals into the fold, which is more "affordable" given the longer crystallizable diol segment. Attempts on increasing the order in these systems by reannealing did not improve the crystallinity measured.

6.3.2.4 ^{1}H Spin Diffusion: Distribution of Ester Groups in the Polymer Morphology

After proving that the polymers fold according to the tightly chain folded model, the next question that arose is the placement of the ester groups in the polymer microstructure. Depending on the length and flexibility of the diacid segment and potentially the diol length, ester groups are either located at the crystal/amorphous interface or are pulled out into the amorphous regions. Figure 6.11 shows the tightly chain folded model with either decoration of crystalline/amorphous interface with ester groups, or ester groups being pulled out into the amorphous regions.

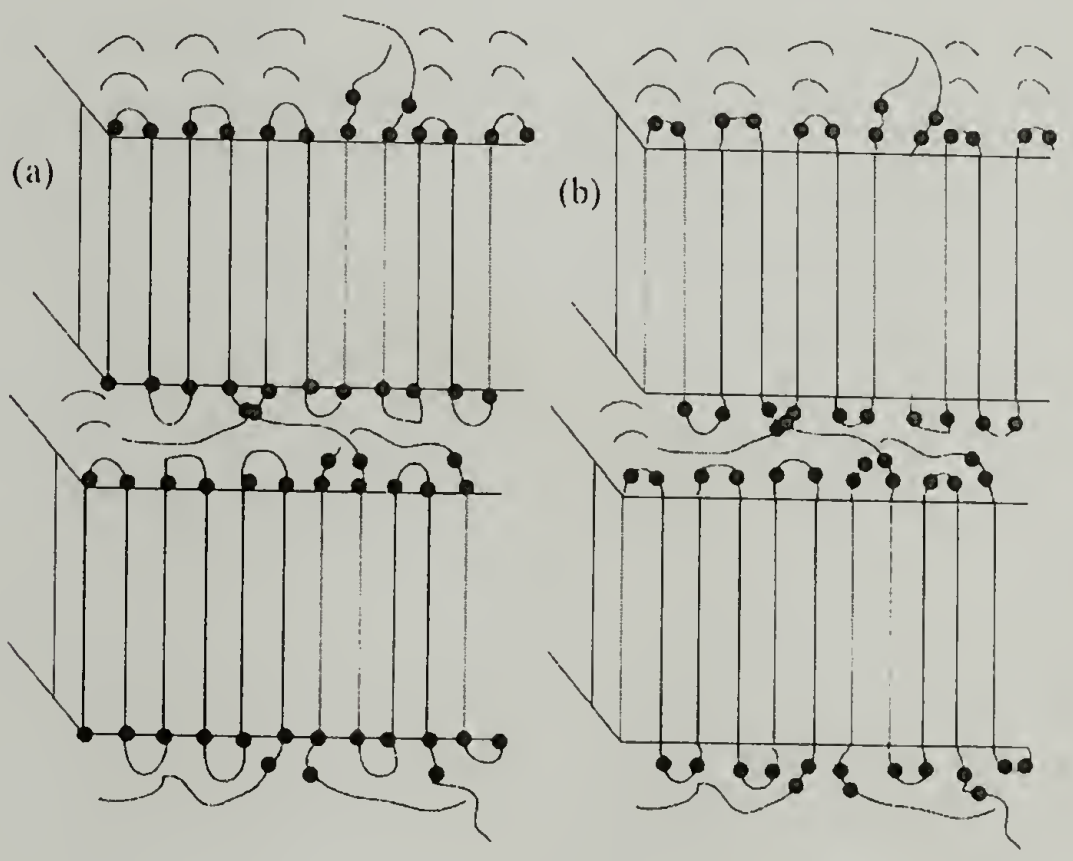

Figure 6.11 Placement of ester groups in a tightly chain folded polymer microstructure: (a) at the crystal/amorphous interface (b) in the amorphous regions.

Determination of the ^{13}COO-labeled defects location and measurements of lamellar size by solid-state NMR were performed through ^{13}C-detected ^{1}H-spin diffusion experiments.[8] In the Goldman-Shen experiment[9], the magnetization of the mobile amorphous segments is selected through a $T_{2,H}$ filter, while crystalline magnetization is dephased. After varying mixing times, cross polarization from ^{1}H to ^{13}C is performed. The rise of the CH_2 crystalline signal- indicative of the lamellar thickness- and the ^{13}COO signal- indicative of defect location- are then observed.

Figure 6.12 shows the spin diffusion behavior of polyester derived from branched glutarates and phenylene diacetate.

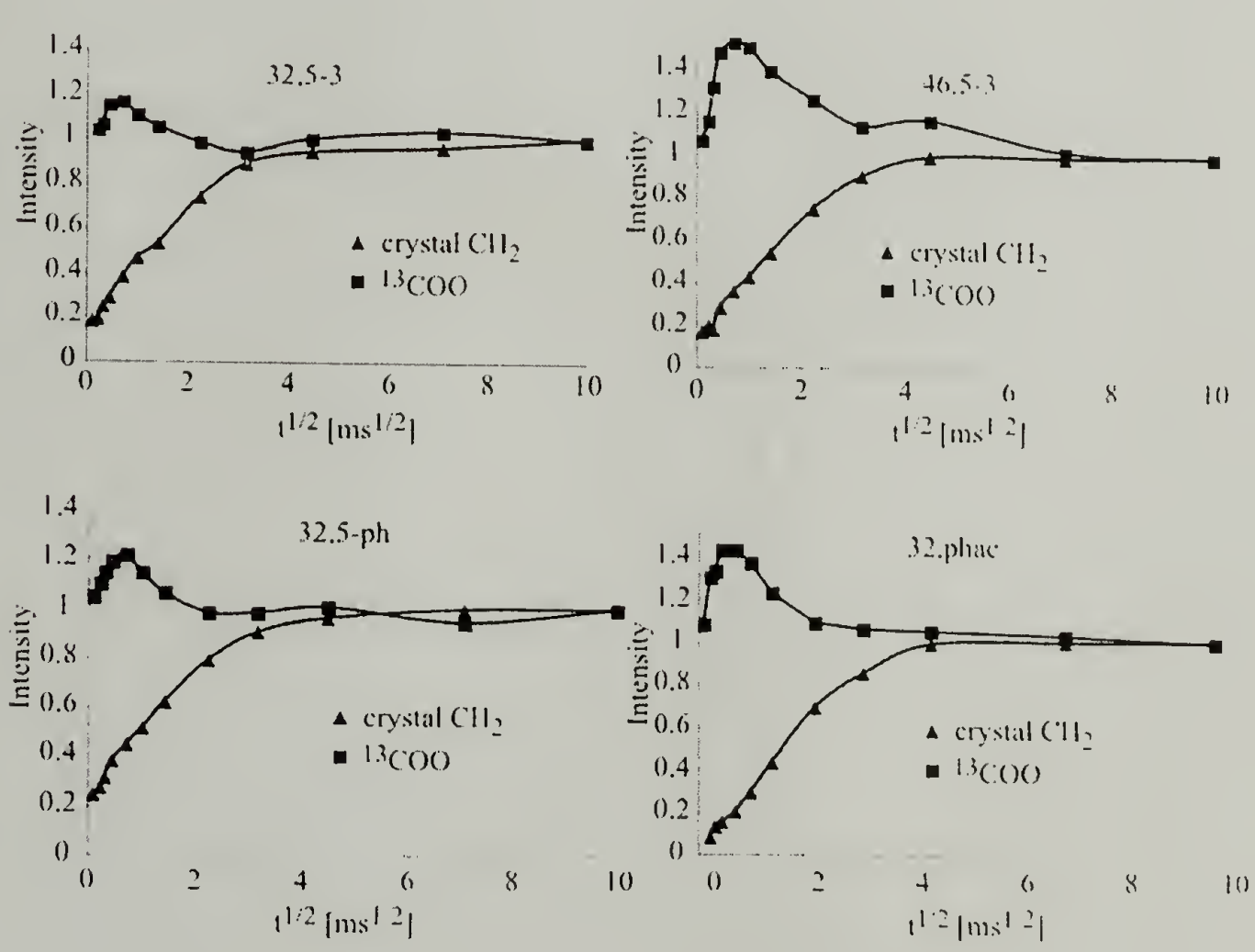

Figure 6.12 Crystalline CH_2 and ^{13}COO-spin diffusion after ^{1}H T_2 selection of 15 μs duration for polyesters 32,5-3, 46,5-3, 32,5-ph, and 32,phac.

As opposed to the gradual rise of intensity in the signal of ester moieties seen for polyester 22,4 described in chapter 5, all polyesters shown here exhibit an early maximum in the spin diffusion curves for ^{13}COO sites. This is a strong indication of exclusion of the diacid segments from the crystal to the interfacial regions as depicted in Figure 6.8 (a). The maximum in the spin diffusion curve is typical of interfacial components in a system of > 50 % crystallinity.

A third, different spin diffusion behavior is observed for polyesters bearing malonate units as the defects. The spin diffusion curves for labeled polyesters 32,3-6 and 44,3 are shown in figure 6.13.

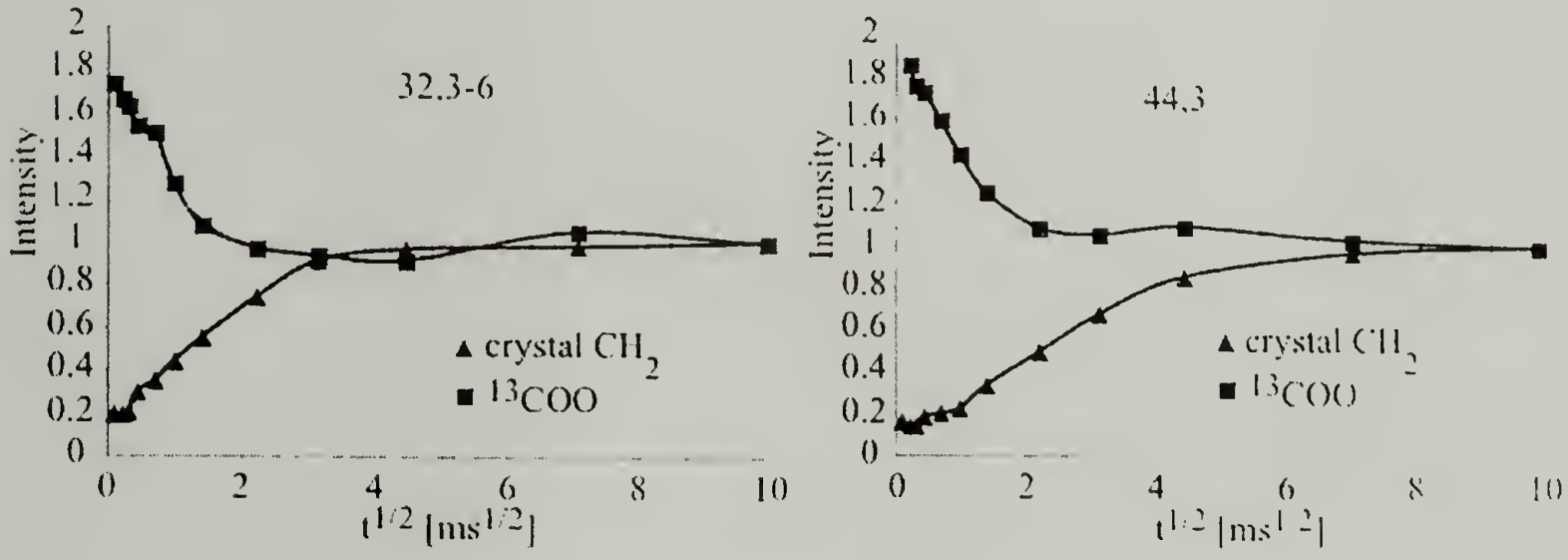

Figure 6.13 Crystalline CH_2 and ^{13}COO-spin diffusion after ^1H T_2 selection of 15 μs duration for polyesters 32,3-6, and 44,3.

Again, the rise in the CH_2 crystal signal is proportional to the crystal thickness and can be converted to a crystal thickness, if the magnetization diffusion coefficient is known. The constant and steady decrease in signal intensity for the ^{13}COO sites is

indicative of their location in the amorphous regions. The ester moieties are immediately reached by spin diffusion from the proton magnetization in the amorphous regions, indicating their location near those mobile segments. The magnetization then diffuses further into the crystalline regions, resulting in a decrease in ^{13}COO signal. As can be expected, the malonate unit consisting of only three carbon atoms is too small to form even a tight chain fold. This lack of carbon atoms to form a fold results in the sequestering of a few methylene units from the diol segment into the fold, which forces the ester moieties to be located in the amorphous regions.

As mentioned above, crystal thicknesses can be estimated from the initial slope of the crystalline CH_2 spin diffusion curves, if the diffusion coefficient for the ^1H magnetization is known. Figure 6.14 shows a qualitative comparison of CH_2 spin diffusion curves for the polyesters incorporating malonate units as the defect.

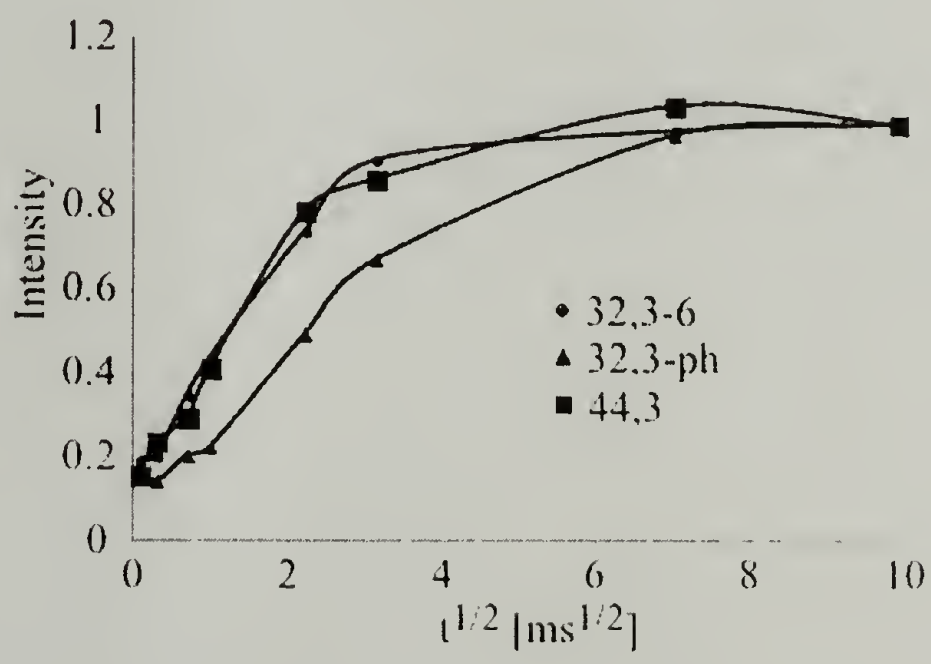

Figure 6.14 Comparison of the crystalline CH_2 spin diffusion for polyesters 32,3-6, 32,3-ph, and 44,3.

Polyesters 32,3-6 and 32,3-ph show a similar steeper rise in the CH_2 signal, when compared to polyester 44,3. This steeper slope indicates thinner crystals formed from 32,3-6 and 32,3-ph then from 44,3. This observation is expected when comparing a 32 diol segment versus a 44 methylene unit segment length, assuming the polyesters will possess similar magnetization diffusion coefficients.

6.3.2.5 Wideline Separation Spectra: Mobility of Various Sites

In order to confirm the information on ester moiety location in the polymer morphology obtained from ^1H spin diffusion measurements, wideline separation spectra of ^{13}COO-labeled branched polyesters were recorded. In WISE NMR, the widths of proton lines arising from homonuclear ^1H-^1H-dipolar couplings are employed as indicators of rigidity.[10] Rigid segments in the polymer microstructure will show broad ^1H-lines, while in mobile segments the static homonuclear ^1H-^1H dipolar couplings couplings will be partially averaged out, yielding a reduction in linewidth.[11] Figure 6.15 shows the WISE cross sections taken for the ^{13}COO-segments and the crystalline and amorphous methylene segments of polyester 32,phac.

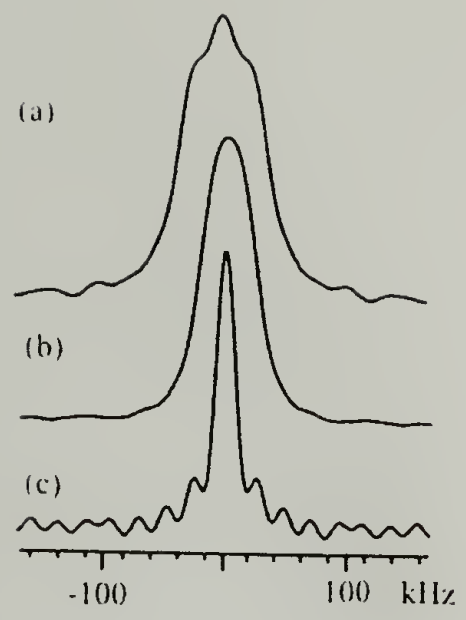

Figure 6.15 Cross sections of the WISE spectrum for polyester 32,phac: (a) crystalline CH_2 resonance at 32.8 ppm, (b) ^{13}COO resonance at 172.0 ppm, (c) amorphous CH_2 resonance at 30.9 ppm.

As can be seen from the width of the cross section of ^{13}COO-labeled sites compared with the CH_2 crystalline and amorphous signals, the width is intermediate between those two, indicative of intermediate site mobility. This suggests placement of the ester groups at the crystalline/amorphous interface, as found by ^{1}H spin diffusion experiments. This placement of ester groups is generally found in the WISE cross sections for the branched glutarates and phenylene diacetates. The WISE cross sections taken for the ^{13}COO-labeled polyesters 32,5-ph, 32,5-3, and 46,5-3 are shown in Figure 6.16.

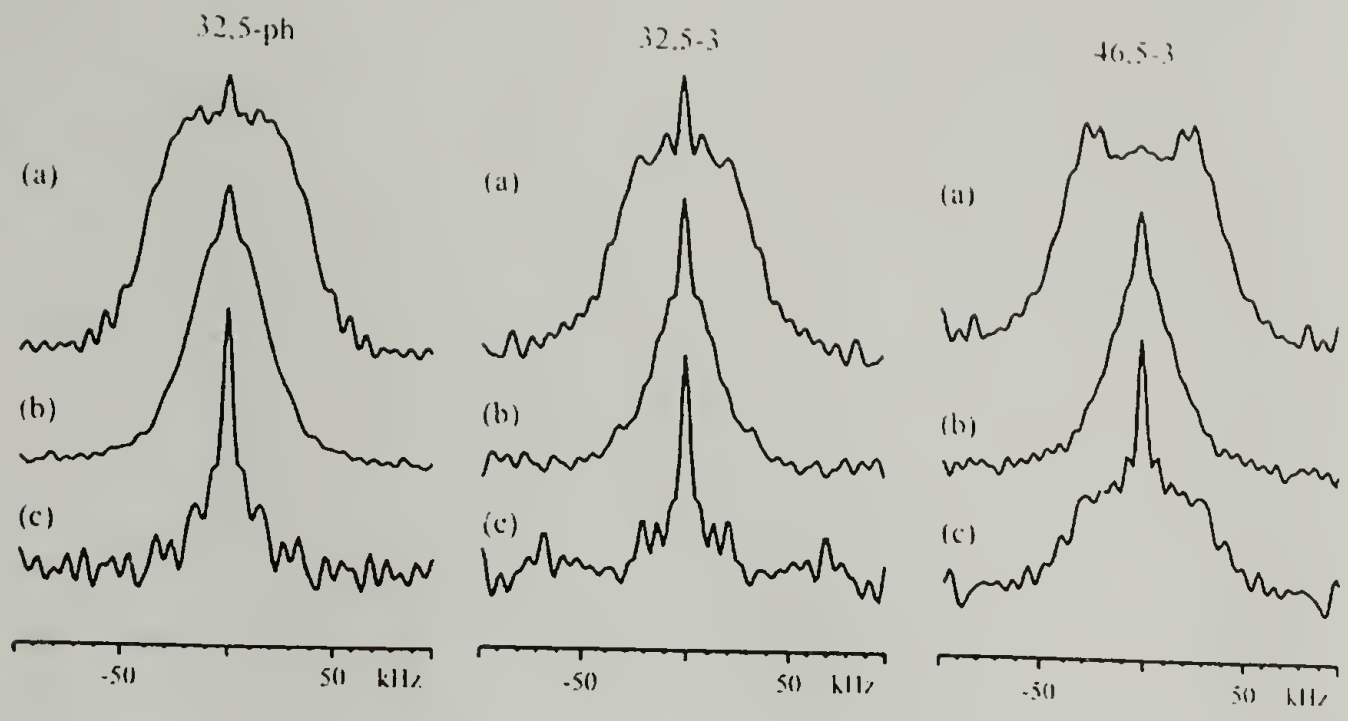

Figure 6.16 Cross sections of the WISE spectrum for polyesters 32,5-ph, 32,5-3, and 46,5-3: (a) crystalline CH_2 resonances at 32.9 ppm, (b) ^{13}COO resonances at 172.6 ppm, (c) amorphous CH_2 resonances at 31.1 ppm.

As mentioned above, in all three cases the ^{13}COO-line widths are intermediate between crystalline and amorphous methylene units, confirming the placement of ester groups at the interface, as was found by ^{1}H spin diffusion.

From the ^{1}H spin diffusion experiments, malonates were found to place ester moieties in the amorphous regions. Figure 6.17 shows the WISE cross sections taken for the ^{13}COO-segments as well as the crystalline and amorphous methylene segments of polyester 32,3-6.

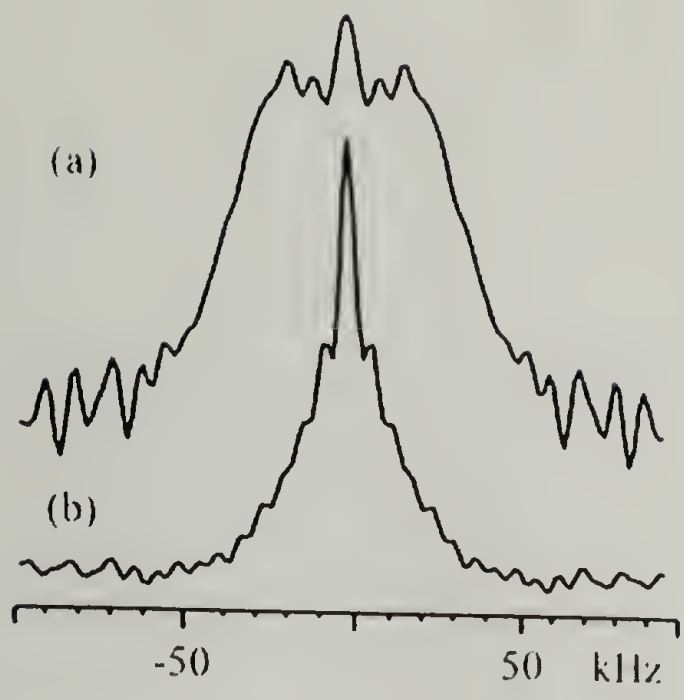

Figure 6.17 Cross sections of the WISE spectrum for polyester 32,3-6: (a) crystalline CH_2 resonance at 32.6 ppm, (b) ^{13}COO resonance at 169.0 ppm.

The linewidth of the ^{13}COO sites is significantly narrower than the width observed for the crystalline segments. It is also significantly narrowed compared to the branched glutarates and phenylene diacetate, indicating a location of ester moieties near mobile segments, most likely in the amorphous regions. The same is observed for non-branched polyester 44,3, whose WISE cross sections are displayed in Figure 6.18.

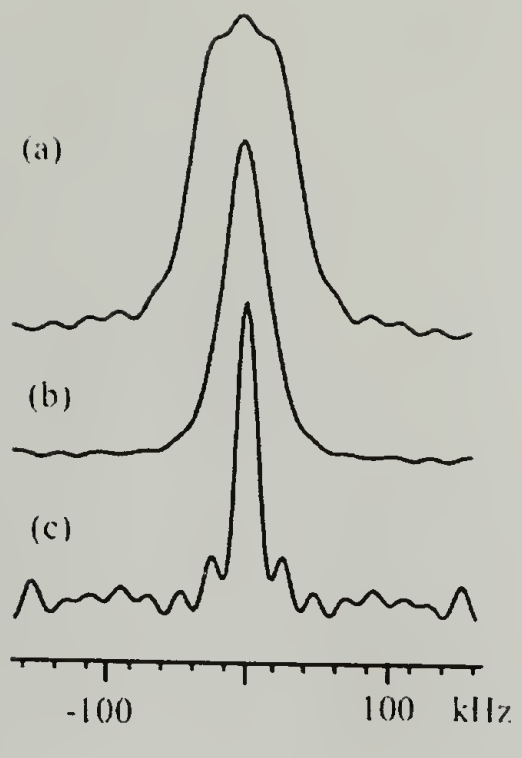

Figure 6.18 Cross sections of the WISE spectrum for polyester 44,3: (a) crystalline CH_2 resonance at 33.0 ppm, (b) ^{13}COO resonance at 167.7 ppm, (c) amorphous CH_2 resonance at 30.8 ppm.

6.3.2.6 DOQSY Spectra: Chain Conformation and Packing

In order to gain information on the polymer chain conformations and packing, DOQSY NMR spectra of ^{13}COO-labeled polyester 44,3 and branched polyesters were recorded. As described in detail in chapter 5, DOQSY NMR measures the relative orientation of pairs of ^{13}C-labeled segments that are close in space, by correlating their chemical-shift anisotropies.[12] This allows for distinction between conformations sometimes at the level of a few degrees.

In the DOQSY spectrum for non-branched 44,3 it was found that the chains adopt a specific conformation that is non-trans in nature. As opposed to non-branched polyester 22,4, exhibiting predominantly all-trans conformations, non-branched polyester

44,3 showed a tendency for a deviation from all-trans conformation, although no obvious driving force for a chain fold, e. g. a large side branch to be excluded into the amorphous regions, was provided. Figure 6.19 shows the experimental DOQSY spectrum and the best fit simulation.

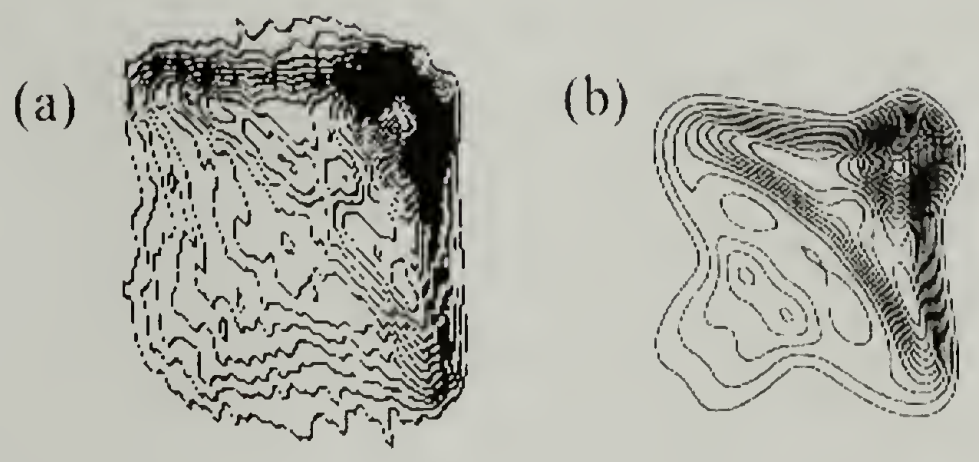

Figure 6.19 DOQSY NMR spectrum of 100% doubly ^{13}COO-labeled polyester 44,3: (a) experimental spectrum, (b) simulated spectrum incorporating 2/3 of 105° and -105° angles and 1/3 all trans conformations.

The malonates are relatively simple systems to simulate DOQSY patterns, as the relative orientation of the ^{13}COO segments is only dependent on the two torsion angles in the malonate unit. Based on the relative chemical shift anisotropy orientations determined from the non-trans DOQSY pattern (containing a ~72° angle between unique principal axes), possible torsion-angle combinations could be determined. Figure 6.20 shows the torsion angle map with the gray dots marking the best solutions found when the DOQSY modulation is considered.

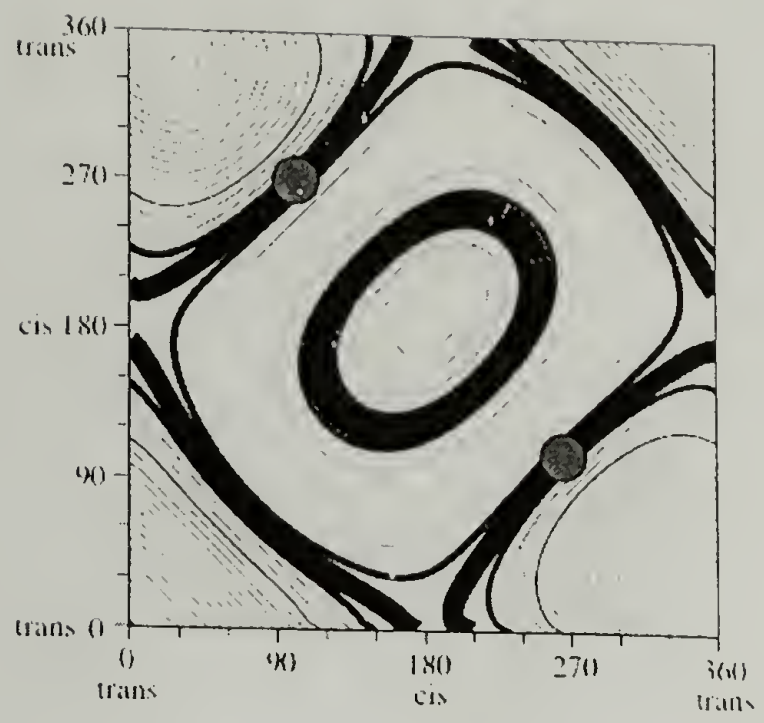

Figure 6.20 Torsion angle map for polyester 44,3 computed from the non-trans DOQSY pattern and the approximately uniaxial chemical shift anisotropy tensor.

These findings were translated into potential folded structures incorporating two 105° angles. The loop can be completed by two gauche bonds on either side of the defect separated by no more than one trans bond. Figure 6.21 shows these potential chain folded structures for polyester 44,3.

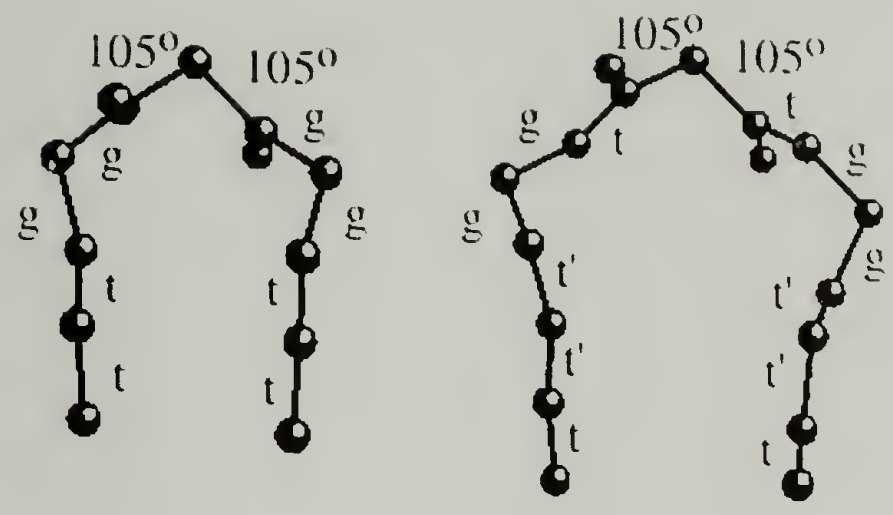

Figure 6.21 Potential chain folded structures as obtained from DOQSY NMR of non-branched polyester 44,3.

Since the results for polyester 44,3 showed the malonates to be a very promising system to be preorganized to fold even in non-branched systems, branched malonate systems were examined in more detail. Here, the incorporation of a branch sufficiently large to not be incorporated into the crystal structure was expected to result in a perfectly tightly chain folded structure. Its crystal thickness was expected to be determined by the diol length employed. Again, the conformation and packing was to be determined by DOQSY. Figure 6.22 shows the DOQSY spectrum obtained for polyester 32,3-6 and simulations taking a variety of torsion angle combinations into account.

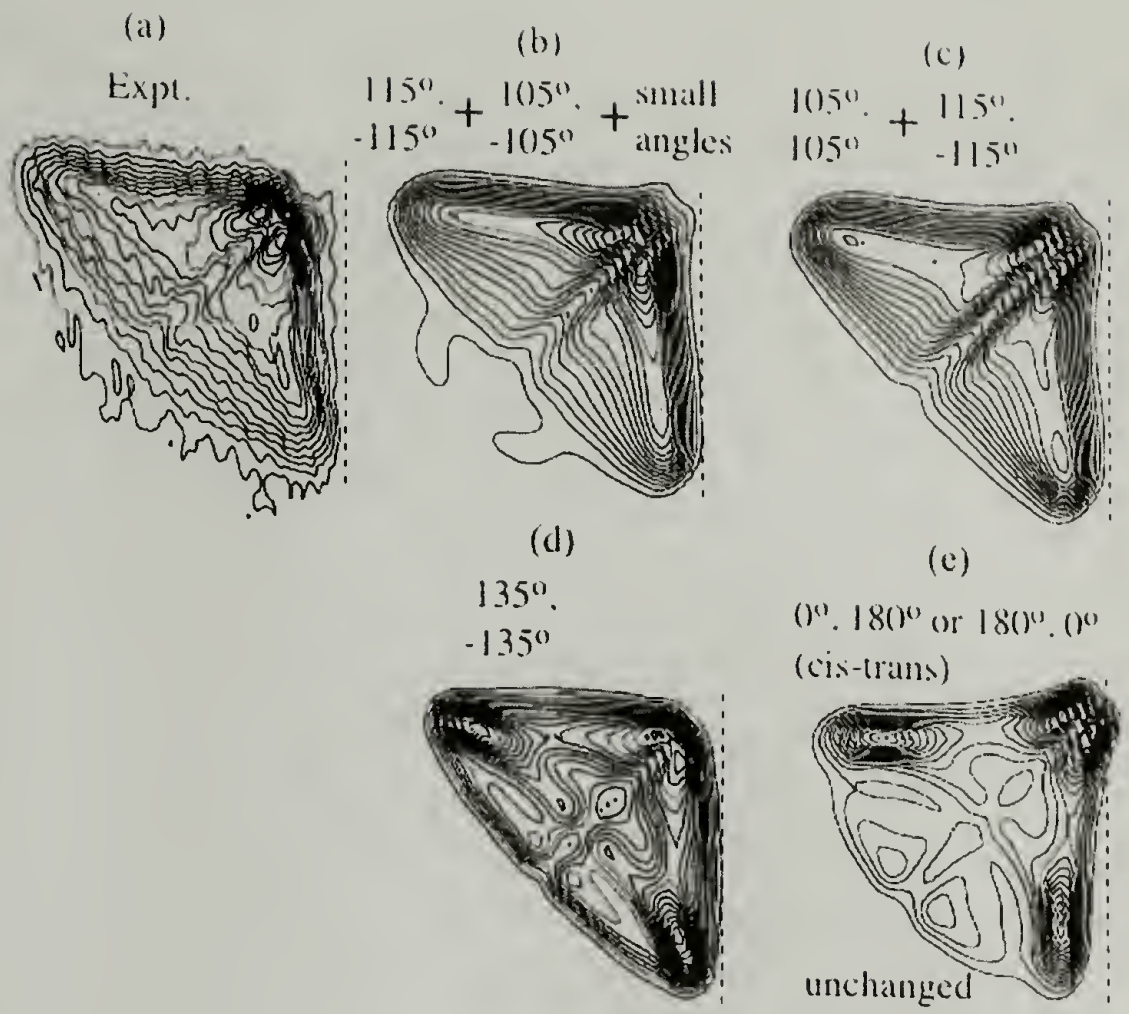

Figure 6.22 DOQSY NMR spectrum of 100% doubly ^{13}COO-labeled polyester 32,3-6: (a) experimental spectrum, (b) simulated spectrum incorporating 105° and 115° angles as well as small angles, (c) simulated spectrum incorporating 105° and 115° angles without small angles, (d) simulated spectrum using 135° angles, (e) simulated spectrum with cis/trans conformation of malonate unit.

As was observed for polyester 44,3, the best fit in the simulations for polyester 32,3-6 is found when the angles of the malonate units are around 105-115°. This angle combination, again, can be pictured as seen in Figure 6.18 adopting a tight chain folded structure. A combination of a cis and a trans bond in the malonate unit is excluded by the shape and modulation of the DOQSY pattern. Even more pronounced than for polyester

44,3 is the absence of a diagonal ridge indicative of an all-trans conformation. The observed DOQSY pattern here is compatible with a predominantly tightly chain folded poiymer microstructure with exclusion of branches and malonate unit into the amorphous regions.

DOQSY spectra were also recorded for other branched polyesters that were synthesized with ^{13}COO labels in both ester groups, which had shown single lamellar thicknesses by SAXS. Figure 6.23 shows the DOQSY spectra for a series of branched glutarates.

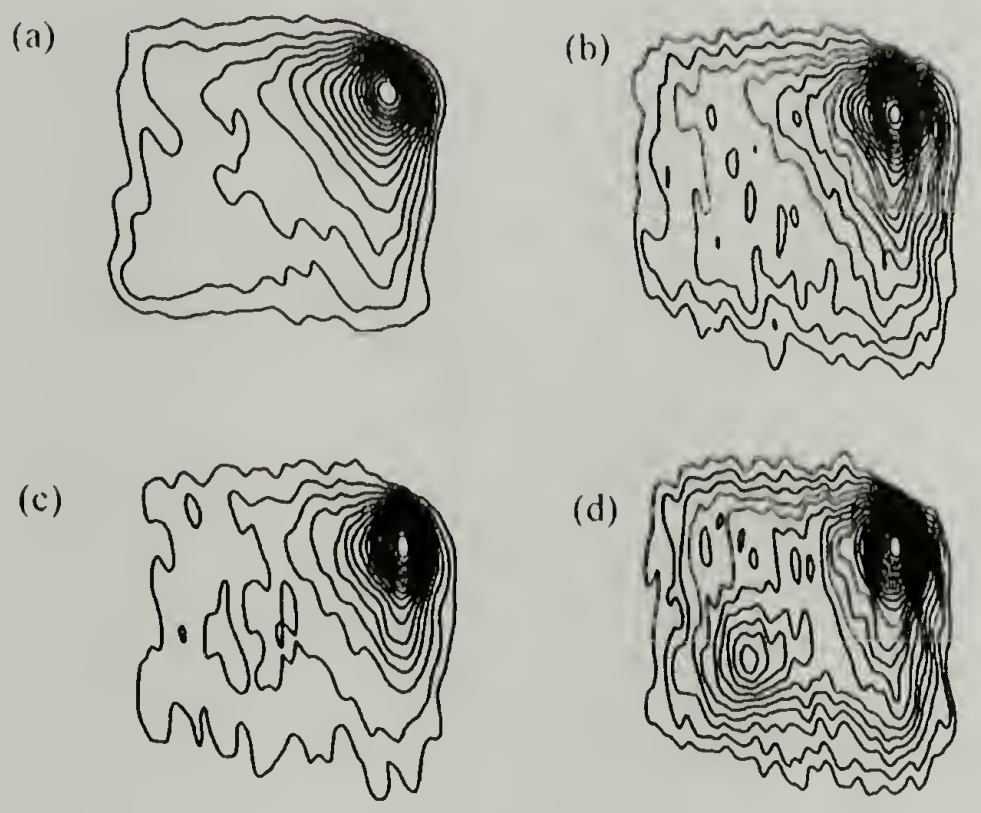

Figure 6.23 DOQSY experimental spectra for branched polyesters: (a) 32,phac, (b) 32,5-ph, (c) 32,5-3, and (d) 46,5-3.

The patterns observed here for the branched glutarates are compatible, again, with a tightly chain folded polymer microstructure under exclusion of branches from the

crystal into the amorphous regions. The 2D patterns are distinct and dominated by off-diagonal intensity. The pronounced peaks observed in all four spectra clearly indicate a non-random relative orientation with an estimated angle of about 40° between σ_{11} principal axes. However, to exactly determine the angle, simulations of the DOQSY patterns are needed.

6.3.2.7 Relaxation Time Measurements

In order to study the effects of single lamellar thickness, tight chain folding, and elimination of ester group layering on the polymer dynamics, relaxation time measurements on the branched polyesters were performed. As has been described in chapter 5, the relaxation time of spin-locked magnetization, $T_{1\rho}$, contains information on the motion of CH_2 groups in the 10-1000 kHz region.[10] For the branched polyesters investigated here, it was found that they exhibit $T_{1\rho}$ relaxation times much shorter than non-branched polyesters 22,4 and 32/12,4, and even the LLDPE described in chapter 5. It is speculated that one reason for these significantly shorter relaxation times is the lack of ester layering allowing for motion of the crystalline segments a few units in and out of the amorphous regions, as opposed to the suppression of chain flips by ester layering in non-branched polyesters.

In Figure 6.24, the relaxation times $T_{1\rho}$ and T_2 are correlated to explore relationships between defect nature and effect of diol and diacid segment lengths on relaxation behavior.

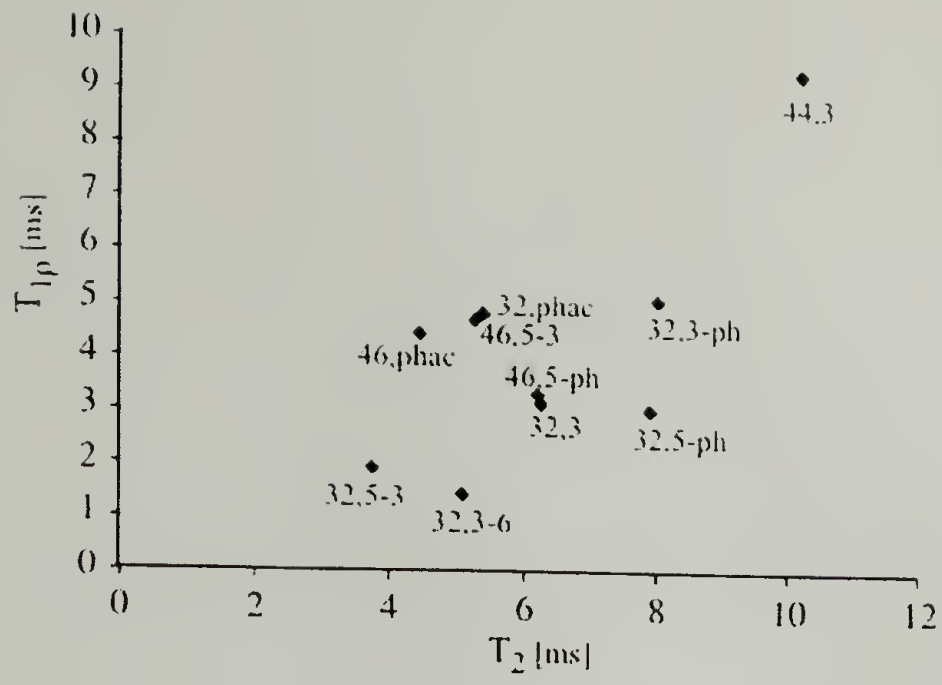

Polyester	$T_{1\rho}$ *[ms]*	T_2 *[ms]*
32.3-6	1.44	5.09
32.3-ph	5.08	8.05
32.5-3	1.93	3.75
46.5-3	4.70	5.28
32.5-ph	3.03	7.92
46.5-ph	3.31	6.22
32.phac	4.82	5.40
46.phac	4.44	4.46
32.3	3.14	6.26
44.3	9.37	10.27

Figure 6.24 $T_{1\rho}$ *versus* T_2 relaxation times for crystalline methylene segments.

It was found that $T_{1\rho}$ and T_2 relaxation times are generally shorter for aliphatic side branched polyesters as compared to aromatic side branched ones. A further correlation was difficult to establish. Some of the polyesters studied here exhibit $T_{1\rho}$ relaxation times close to the minimum, which is observed when the rate of motion is approximately equal to the characteristic frequency. Cooling or heating should then increase the $T_{1\rho}$ relaxation time.

6.4 Conclusions

The state-of-the-art solid-state NMR and SAXS measurements performed for a variety of branched polyesters have resulted in a detailed structural picture of a quite regularly folded single lamellar thickness polymer microstructures obtained upon crystallization. It was found that polyethylene-like crystallization is achieved for 32 or

more methylene units. Polyesters derived from only 22 carbon atoms in the diol segment resulted in small or disordered crystals, manifested by a diffuse WAXS diffractogram and low crystallinities, whereas polyesters derived from diols of 32 and 46 methylene units showed polyethylene-like WAXS diffractograms and crystallinities well above 50 %.

The high crystallinities found in branched polyesters studied here proved the polymer chains to be tightly chain folded, with exclusion of the side-chain bearing diacid units into the amorphous regions. The placement of ester moieties in the polymer microstructure as probed by ^{1}H spin diffusion and WISE NMR experiments indicated that for sufficiently long diacid segments, the ester groups are located at the crystalline/amorphous interface, whereas for shorter diacids the defects are pulled out into the amorphous regions. DOQSY NMR provided some insight into the conformations adopted by the diacid segments, showing distinct patterns compatible with tight chain folds of a quite specific conformation that is not all-trans.

Relaxation time measurements showed surprisingly low values for crystalline $T_{1\rho}$ and T_2 relaxation times. The exact correlation between structural defects and resulting relaxation times is not well understood yet. However, as ester groups are located outside the crystal in the chain folds, either at the crystalline/amorphous interface or the amorphous regions, diester layering in the crystal as observed for polyester 22,4 can be eliminated. The lack of diester layering, which for polyester 22,4 led to suppression of chain flips, may result in higher chain mobility for the branched polyesters studied here, explaining the significantly shorter relaxation times compared to those found for non-branched polyesters 22,4 and 32/12,4.

By securing detailed structural information on a wide variety of branched long-chain aliphatic polyesters, it was shown that the introduction of sufficiently large side branches placed at regular intervals along an otherwise purely aliphatic backbone is sufficient to gain control over the chain folding and crystal thickness of those polyethylene-like polymers. Finally it was demonstrated that strong intermolecular interactions such as H-bonds as typical of polyamides and polyurethanes are not essential to achieve quantization of crystal thickness and fold length.

6.5 References

(1) Failla, M. D.; Lucas, J. C.; Mandelkern, L. *Macromolecules* **1994**, *27*, 1334-1337.

(2) Alamo, R. G.; Viers, B. D.; Mandelkern, L. *Macromolecules* **1993**, *26*, 5740-5747.

(3) Lu, L.; Alamo, R. G.; Mandelkern, L. *Macromolecules* **1994**, *27*, 6571-6576.

(4) Stribeck, N.; Alamo, R. G.; Mandelkern, L.; Zachmann, H. G. *Macromolecules* **1995**, *28*, 5029-5036.

(5) Bennett, A. E.; Rienstra, C. M.; Auger, M.; Lakshmi, K. V.; Griffin, R. G. *J. Chem. Phys.* **1995**, *103*, 6951-6958.

(6) Hu, W.-G.; Schmidt-Rohr, K. *Polymer* **2000**, *41*, 2979-2987.

(7) Torchia, D. A. *J. Magn. Reson.* **1978**, *30*, 613.

(8) Clauss, J.; Schmidt-Rohr, K.; Spiess, H. W. *Acta Polymer.* **1993**, *44*, 1-17.

(9) Goldman, M.; Shen, L. *Phys. Rev.* **1966**, *144*, 321.

(10) Schmidt-Rohr, K.; Spiess, H. W. *Multidimensional Solid-State NMR and Polymers*; 1st ed.; Academic Press: London, 1994.

(11) Schmidt-Rohr, K.; Clauss, J.; Spiess, H. W. *Macromolecules* **1992**, *25*, 3273-3277.

(12) Schmidt-Rohr, K. *Macromolecules* **1996**, *29*, 3975-3981.

CHAPTER 7

CONCLUSIONS AND PERSPECTIVE

7.1 Conclusions

Polyethylene-like polymers were synthesized in this study as model systems to study differences in structure and properties of random versus regularly branched polyethylenes. Randomly branched polyethylenes form ordered crystalline regions made of polymethylene segments organized into lamellae of varying thicknesses and separated by disordered amorphous regions containing the branches. This study aimed at preparing structures that would lead to single lamellar thicknesses controlled by regularity of branch substitution. The polymers synthesized in our work were expected to lead to unique properties resulting from this obtained independence from crystallization conditions or annealing.

It was known that a wide range of densities and crystallinities can be obtained for polyethylene through the variation of branch distribution and content. While branches are only a minor component in high-density polyethylene, linear low-density polyethylene contains a higher branch content due to controlled comonomer inclusions. Despite improvements in catalyst design, the placement of branches is far from regular even in controlled copolymerization of ethylene and α-olefins, leading to a statistical distribution of branches or "defects" along the backbone that has a pronounced influence on achievable crystal thicknesses and crystallinities. This study demonstrated that the synthesis of regularly branched polyethylene-like polymers with relatively high branch content could be achieved, while maintaining high crystallinities.

The required perfectly regular placement of structural "defects" was achieved by step-growth polymerization. To this effect, long-chain aliphatic α,ω-diols were copolymerized with short-chain diacids. The first component in the resulting polyesters acted as perfectly monodisperse telechelic oligomers of polyethylene, while the second one was used as a linker bearing branches designed to be too large to be incorporated into a polyethylene unit cell.

Long-chain α,ω-diols were synthesized according to well-established literature procedures. Despite specific limitations of these reactions associated with decreasing solubility with increasing methylene numbers, the diols were produced in sufficiently high yield due to the development of an improvement in the limiting step of enamine couplings. In order to facilitate and enable sophisticated solid-state NMR measurements, a number of ^{13}COO-labeled diacids were synthesized according to slight modifications of established literature procedures. Polyesterifications were performed under standard conditions. In the case of malonates, another procedure was necessary as direct polymerization would have resulted in decarboxylation. Instead of direct esterification, transesterification was used to synthesize the desired polymers. The synthesized polyesters showed molecular weights between 5.0 and 30.0 $\cdot 10^3$ g/mol and polydispersities around two, as was expected for polymers synthesized by step-growth polymerization.

It can be expected that a certain critical number of methylene units in the aliphatic segment is needed in order to obtain a polyethylene-like crystal structure for these polyesters. It was found by WAXS that 22 methylene units between defect sites was too short, and yielded small and disordered crystals. Increasing the segment length to 32 and

later 46 carbon atoms allowed for the recovery of polyethylene-like crystal structures as demonstrated by the WAXS signature.

The structure and dynamics of a model polyester containing 22 methylene units in the diol segment and a succinic acid moiety as the "defect" was studied in detail by SAXS and a variety of solid-state NMR techniques. This non-branched model system was used in order to establish the influence of "normal" esters on the polyethylene-like character of polyesters containing low concentrations of ester units. It was found that the crystal structure in polyester 22,4 is indeed polyethylene-like, exhibiting an orthorhombic dense packing that with the exception of a layering between esters located on neighboring chains, conserve the structural characteristic features of polyethylene crystals. Although no branches were introduced on this polyester, some quantized control over the lamellar thickness was achieved *via* the above diester layering, which was also found to have a pronounced influence on polymer dynamics. The stacked diester layers in the crystal were found to hinder chain diffusion from the crystalline to the amorphous regions as is observed for polyethylene.

Control over chain folding and lamellar thickness was achieved by introducing branches at regular distances along the polymer backbone. Using aliphatic as well as aromatic side groups sufficiently large to be excluded from the polyethylene unit cell, polyesters were synthesized that exhibited single lamellar thicknesses of dimensions defined by the number of methylene units in the starting diol monomers. This self-organization into lamellae of controlled dimensions was not affected by crystallization conditions.

In order to establish the nature of chain folded structures adopted by the branched polyesters, a variety of solid-state NMR techniques were employed, probing structural features on variable length scales. High crystallinities were found from direct polarization experiments as well as ^{1}H-MAS and ^{13}C-CP/MAS spectra, proving the chain folds to be tight in nature. The locations of ester groups as well as crystal thicknesses were probed by spin diffusion experiments. Ester moieties were shown to be either located at the crystalline/amorphous interface or in the amorphous regions, depending on the length of both the diacid and diol segments. The mobility, and therefore the location, of ester groups was also probed by WISE experiments, which confirmed the spin diffusion results. The nature of chain folds on a smaller length scale was then probed by DOQSY NMR, which showed that specific conformations were adopted by the "defect" moieties, in agreement again with a predominance of tightly chain folded crystal structures. A combination of all the X-ray and NMR techniques employed during our investigation indicate that regularly branched polyesters adopt a tightly chain folded lamellar structure if (a) the branches are sufficiently large to be rejected from the crystal into the amorphous regions, and (b) the diol segments are sufficiently long.

In conclusion, this study has demonstrated that model polyesters with tailored architectures accurately mimic polyethylene crystal structures and introduce tight chain folding. Ester moieties, while having a pronounced influence on polymer dynamics, still allow for polyethylene-like crystallization, enabling direct comparison of long-chain aliphatic polyesters with polyethylenes. The introduction of chain folds at regular distances resulted in single lamellar thicknesses solely controlled by the initial structure of repeat units, not by specific processing techniques. It was found that the introduction

of branches so large as to be excluded from the polyethylene unit cell are a sufficient driving force to control lamellar thickness and the nature of chain folds. High crystallinities could be obtained by this strategy despite high branch contents. Finally, it was shown that the above concept can be extended to a wide variety of "defects", and does not require strong intermolecular forces such as hydrogen bonding.

7.2 Perspective

Further investigation of the mechanical properties of the obtained model polyesters would be desirable. This study has shown that while the structure of the obtained polyesters is polyethylene-like, the chain dynamics differ significantly from those observed for polyethylene. This can be expected to have a strong influence on mechanical properties such as drawability and strength, a feature that should be probed in more detail.

While it was shown that the introduction of sufficiently large branches still yields highly crystalline structures, it would also be of interest to study a wider variety of branch structures and architectures. A next logical step would be the incorporation of functional groups (as long as compatible with the polymerization chemistry). For example, introduction of a double bond would be of interest to probe the possibilities of crosslinking the amorphous regions and further locking in the polymer microstructure. The crystal/amorphous interface could also be decorated with polar groups or TEM contrast-enhancing atoms such as iodine to investigate the structures in more detail by electron microscopy without any need for external staining.

It would be of interest to synthesize structures that are even structurally closer to polyethylene, eliminating entirely the ester groups and their influence on crystallization. This would make a comparison between regularly and randomly branched structures even more meaningful. ADMET polymerization of α,ω-dienes containing side-chains in the middle of the monomer can be viewed as the logical solution to this challenge. The synthesis of α,ω-diene monomers with sufficiently long spacers (more than 32 methylene units as suggested by this study) may prove challenging though.

BIBLIOGRAPHY

Abrahamson, S.; Dahlén, B.; Löfgren, H.; Pascher, I. *Progress in the Chemistry of Fats and Other Lipids*; Pergamon: London, 1978; Vol. 16.

Abrahamson, S. S.-S., S.; Stenhagen, E., Ed. *Progress in the Chemistry of Fats and Other Lipids*; Pergamon: London, 1963; Vol. 7.

Adams, K. R.; Beonnett, R. *Phytochemistry* **1971**, *10*, 1885.

Adkins, H. *Organic React.* **1954**, *8*, 1.

Adkins, H.; Billica, H. *J. Am. Chem. Soc.* **1948**, *70*, 3121.

Alamo, R. G.; Domszy, R. C.; Mandelkern, L. *J. Phys. Chem.* **1984**, *88*, 6587.

Alamo, R. G.; Mandelkern, L. *Macromolecules* **1989**, *22*, 1273.

Alamo, R. G.; VanderHart, D. L.; Nyden, M. R.; Mandelkern, L. *Macromolecules* **2000**, *33*, 6094-6105.

Alamo, R. G.; Viers, B. D.; Mandelkern, L. *Macromolecules* **1993**, *26*, 740.

Alamo, R. G.; Viers, B. D.; Mandelkern, L. *Macromolecules* **1993**, *26*, 5740-5747.

Alamo, R. G.; Viers, B. D.; Mandelkern, L. *Macromolecules* **1995**, *28*, 3205-3213.

Armelin, E.; Casas, M. T.; Puiggali, J. *Polymer* **2001**, *42*, 5695-5699.

Axelson, D. E.; Mandelkern, L.; Popli, R.; Mathieu, P. *J. Polym. Sci., Polym. Phys. Ed.* **1983**, *21*, 2319-2335.

Aylwin, P. A.; Boyd, R. H. *Polymer* **1984**, *25*, 323-329.

Baker, A. M. E.; Windle, A. H. *Polymer* **2001**, *42*, 651.

Baker, A. M. E.; Windle, A. H. *Polymer* **2001**, *42*, 667.

Baker, A. M. E.; Windle, A. H. *Polymer* **2001**, *42*, 681.

Barbiroli, G.; Lorenzetti, C.; Berti, C.; Fiorini, M.; Manaresi, P. *European Polymer Journal* **2003**, *39*, 655-661.

Becker, H. G. O. *Organikum*; 19 ed.; Barth Verlagsgesellschaft mbH: Leipzig, 1993.

Bennett, A. E.; Rienstra, C. M.; Auger, M.; Lakshmi, K. V.; Griffin, R. G. *J. Chem. Phys.* **1995**, *103*, 6951-6958.

Berzelius, J. *Rapp. Ann.* **1847**, 26.

Birch, A.; Williamson, D. *Org. React.* **1976**, *24*, 1.

Boyd, R. H.; Aylwin, P. A. *Polymer* **1984**, *25*, 330-339.

Boyd, R. H.; Aylwin, P. A. *Polymer* **1984**, *25*, 340-346.

Boyd, R. H.; Hasan, A. A. *Polymer* **1984**, *25*, 347-356.

Breslow, D. S.; Newburg, N. R. *J. Am. Chem. Soc.* **1957**, *79*, 5072.

Brooke, G. M.; Burnett, S.; Mohammed, S.; Proctor, D.; Whiting, M. C. *J. Chem. Soc.-Perkin Trans.* 1 **1996**, 1635-1645.

Brown, H.; Zweifel, G. *J. Am. Chem. Soc.* **1959**, *81*, 5832.

Brown, R. D.; Godfrey, P. D.; Elmes, P. S.; Rodler, M.; Tack, L. M. *J. Am. Chem. Soc.* **1985**, *107*, 4112-4115.

Carothers, W. H. *J. Am. Chem. Soc.* **1930**, *52*, 711.

Carothers, W. H. *J. Am. Chem. Soc.* **1932**, *54*, 1559.

Carothers, W. H.; Arvin, J. A. *J. Am. Chem. Soc.* **1929**, *51*, 2560.

Chum, S. P.; Knight, G. W.; Ruiz, J. M.; Phillips, P. J. *Macromolecules* **1994**, *27*, 656.

Clauss, J.; Schmidt-Rohr, K.; Spiess, H. W. *Acta Polymer.* **1993**, *44*, 1-17.

Crist, B.; Howard, P. R. *Macromolecules* **1999**, *32*, 3057.

deAzevedo, E. R.; Bonagamba, T. J.; Schmidt-Rohr, K. *J. Magn. Reson.* **2000**, *142*, 86-96.

Doak, K. W.; Schrage, A. In *Crystalline Olefin Polymers Part 1*; Raff, R. A. V., Doak, K. W., Eds.; Interscience: New York, 1965.

Duhamel, L. *Ann. Chim.* (Paris) **1963**, *8*, 315.

Dunbar, M. G.; Sandström, D.; Schmidt-Rohr, K. *Macromolecules* **2000**, *33*, 6017-6022.

Eckman, R. R.; Henrichs, P. M.; Peacock, A. J. *Macromolecules* **1997**, *30*, 2474-2481.

Ehrenstein, M.; Dellsperger, S.; Kocher, C.; Stutzmann, N.; Weder, C.; Smith, P. *Polymer* **2000**, *41*, 3531-3539.

Ehrenstein, M.; Sikorski, P.; Atkins, E.; Smith, P. *J. Polym. Sci., Polym. Phys. Ed.* **2002**, *40*, 2685-2692.

Failla, M. D.; Lucas, J. C.; Mandelkern, L. *Macromolecules* **1994**, *27*, 1334-1337.

Fischer, E. W. *Z. Naturforsch.* **1957**, *12a*, 753.

Flory, P. J. *J. Am. Chem. Soc.* **1962**, *84*, 2857.

Flory, P. J.; Yoon, D. Y. *Nature* **1978**, *272*, 226-229.

Friedman, L.; Shechter, H. *J. Org. Chem.* **1960**, *25*, 877.

Fuller, C. S. *Chem. Rev.* **1940**, *26*, 143-167.

Fuller, C. S.; Erickson, C. L. *J. Am. Chem. Soc.* **1937**, *59*, 344-351.

Fuller, C. S.; Frosch, C. J. *J. Am. Chem. Soc.* **1939**, *61*, 2575.

Fuller, C. S.; Frosch, C. J.; Pape, N. R. *J. Am. Chem. Soc.* **1942**, *64*, 154-160.

Glotin, M.; Mandelkern, L. *Macromolecules* **1981**, *14*, 1394.

Goldman, M.; Shen, L. *Phys. Rev.* **1966**, *144*, 321.

Graham, J. T.; Alamo, R. G.; Mandelkern, L. *J. Poly. Sci., Polym. Phys. Ed.* **1997**, *35*, 213-223.

Hadjoudis, E.; Pulima, I. *Mol. Cryst. Liq. Cryst.* **1986**, *137*, 29-36.

Hagemann, H.; Snyder, R. G.; Peacock, A. J.; Mandelkern, L. *Macromolecules* **1989**, *22*, 3600.

Hakkarainen, M. In *Degradable Aliphatic Polyesters*, 2002; Vol. 157, pp 113-138.

Hartzell, C. J.; Pratum, T. K.; Drobny, G. *J. Chem. Phys.* **1987**, *87*, 4324-4331.

Hoffman, J. D. *SPE Transactions* **1964**, 315.

Hoffman, J. D. *Polymer* **1982**, *23*, 656.

Hoffman, J. D. *Polymer* **1983**, *24*, 3.

Hoffman, J. D.; Davis, G. T.; Lauritzen, J. I. In *Treatise on Solid State Chemistry*; Hannay, N. B., Ed.; Plenum: New York, 1976; Vol. 3.

Hoffman, J. D.; Lauritzen, J. I. *J. Res. Nat. Bur. Stand. Sect. A. Phys. Chem.* **1961**, *65A*, 297.

Holden, G. In *Encyclopedia of Polymer Science and Engineering*; Kroschwitz, J. I., Ed.; Wiley: New York, 1986; Vol. 5, p 426.

Holmes, D. L.; Lightner, D. A. *Tetrahedron* **1996**, *52*, 5319-5338.

Hu, W.-G.; Schmidt-Rohr, K. *Polymer* **2000**, *41*, 2979-2987.

Hu, W.-G.; Zimmermann, H.; Schmidt-Rohr, K. *Appl. Magn. Reson.* **1999**, *17*, 197-209.

Hünig, S.; Buysch, H. *Chem. Ber.* **1967**, *100*, 4010.

Hünig, S.; Hoch, H. *Tetrahedron Lett.* **1966**, *42*, 5215-5220.

Hünig, S.; Lendle, W. *Chem. Ber.* **1960**, *93*, 913.

Hünig, S.; Lücke, E. *Chem. Ber.* **1959**, *92*, 652.

Hünig, S.; Lücke, E.; Brenninger, W. *Org. Synth. Coll. Vol.* **1973**, *5*, 533-539.

Irwin, R. S. *Macromolecules* **1993**, *26*, 7125-7133.

Isasi, J. R.; Haigh, J. A.; Graham, J. T.; Mandelkern, L.; Alamo, R. G. *Polymer* **2000**, *41*, 8813-8823.

Ito, M.; Serizawa, H.; Tanaka, K. *Polym. J.* **1978**, *10*, 215.

Iwata, M. Jpn. J. *Appl. Phys.* **2001**, *40*, 1352.

Janimak, J. J.; Stevens, G. C. *Polymer* **2000**, *41*, 4233.

Jourdan, N.; Deguire, S.; Brisse, F. *Macromolecules* **1995**, *28*, 8086-8091.

Kanamoto, T. *J. Polym. Sci., Polym. Phys. Ed.* **1974**, *12*, 2535.

Kanamoto, T.; Tanaka, K. *J. Polym. Sci.: Part A-2* **1971**, *9*, 2043.

Kapitza, H.; Zentel, R. *Macromol. Chem. Phys.* **1988**, *189*, 1793.

Keith, H. D. *Macromolecules* **1982**, *14*, 114.

Keller, A. *Philos. Mag.* **1957**, *2*, 1171.

Kobayashi, H.; Nakamura, N. *Cryst. Res. Technol.* **1995**, *30*, 495-500.

Kobler, H. *Liebigs Ann. Chem.* **1978**, 1946-1962.

Koenig, J. L. *Spectroscopy of Polymers*; American Chemical Society: Washington D.C., 1992.

Koleske, J. V. In *Polymer Blends*; Paul, D. R., Ed.; Academic Press: New York, 1978; Vol. 2, p 369.

Kraut, K. *Liebigs Ann. Chem.* **1869**, *150*, 1.

Krejchi, M. T.; Atkins, E. D. T.; Waddon, A. J.; Fournier, M. J.; Mason, T. L.; Tirrell, D. A. *Science* **1994**, *265*, 1427.

Kubik, S. *Angew. Chem. Int. Ed.* **2002**, *41*, 2721.

Kumar, S. K.; Yoon, D. Y.; Dill, K. A. *Macromolecules* **1989**, *22*, 3458.

Le Fevere de Ten Hove, C. Ph. D., Université Catholique de Louvain, 2001.

Lee, K.-S.; Wegner, G.; Hsu, S. L. *Polymer* **1987**, *28*, 889.

Liau, W.-B.; Boyd, R. H. *Macromolecules* **1990**, *23*, 1531-1539.

Lokey, R. S.; L., I. B. *Nature* **1995**, *375*, 303.

Lotz, B. *Eur. Phys. J. E* **2000**, *3*, 185.

Loudon, G. M. *Organic Chemistry*; 2nd ed.; Benjamin/Cummings: Menlo Park, 1988.

Lu, L.; Alamo, R. G.; Mandelkern, L. *Macromolecules* **1994**, *27*, 6571-6576.

Luderwald, I. In *Developments in Polymer Degradation*; Grassie, N., Ed.; Applied Science: London, 1979; Vol. 2, p 77.

Malek, J. *Org. React.* **1988**, *36*, 249.

Mandelkern, L. *Chemtracts (Macromol. Chem.)* **1992**, *3*, 347.

Mandelkern, L.; Alamo, R. G. In *Polymer Data Handbook*; Oxford University: Oxford, 1999.

Mandelkern, L.; Alamo, R. G. In *Polymer Data Handbook*; Oxford University: Oxford, 1999, p 493.

Mandelkern, L.; Peacock, A. J. In *Stud. Phys. Theor. Chem.*; Lacher, R. C., Ed.; Elsevier Science B. V.: Amsterdam, 1988; Vol. 54, pp 201-227.

Mandelkern, L.; Price, J. M.; Gopalan, M.; Fatou, J. G. *J. Polym. Sci., A-2* **1966**, *4*, 385.

McKiernan, R. L. Ph. D., University of Massachusetts, 2002.

Minke, R.; Blackwell, J. *J. Macromol. Sci., Phys.* **1979**, *B16*, 407-417.

Miyata, T.; Masuko, T. *Polymer* **1998**, *39*, 1399-1404.

Mowery, D. M.; Schmidt-Rohr, K. *Polymeric Materials: Science & Engineering* **2001**, *85*, 35.

Mowry, D. T. *Chem. Rev.* **1948**, *42*, 189-284.

Murray, K. E.; Schoenfeld, R. *Aust. J. Chem.* **1955**, *8*, 432.

Musgrave, O. C.; Stark, J.; Spring, F. S. *J. Chem. Soc.* **1952**, 4393.

Muthukumar, M. *Eur. Phys. J. E* **2000**, *3*, 199.

Odian, G. *Principles of Polymerization*; 3rd ed.; John Wiley: New York, 1991.

Ogawa, Y.; Nakamura, N. *Bull. Chem. Soc. Jpn.* **1999**, *72*, 943-946.

Patwardhan, S. A. *Org. Prep. Proced. Int.* **1994**, *26*, 645-670.

Petragnani, N.; Yonashiro, M. *Synthesis* **1982**, 521-578.

Pilati, F. In *Comprehensive Polymer Science*; Pergamon: Oxford, 1989; Vol. 5, pp 275-317.

Polyakova, M.; Belov, V. *Zh. Obshch. Khim.* **1964**, *34*, 565.

Prasad, A. In *Polymer Data Handbook*; Oxford University: Oxford, 1999, p 518.

Prasad, A. In *Polymer Data Handbook*; Oxford University: Oxford, 1999, p 508.

Prasad, A. In *Polymer Data Handbook*; Oxford University: Oxford, 1999, p 529.

Rathore, O.; Sogah, D. Y. *J. Am. Chem.Soc.* **2001**, *123*, 5231-5239.

Reck, B.; Ringsdorf, H. *Makromol. Chem., Rapid Commun.* **1985**, *6*, 291.

Rusanova, E. E.; Sebyakin, Y. L.; Volkova, L. V.; Evstigneeva, R. P. *Zh. Org. Khim.* **1984**, *20*, 279-282.

Saotome, K.; Komoto, H.; Yamazaki, T. *Bull. Chem. Soc. Japan* **1966**, *39*, 480.

Schall, J. D. Ph.D., University of Massachusetts, 2001.

Schlosser, M.; Bossert, H. *Tetrahedron* **1991**, *47*, 6287-6292.

Schmidt-Rohr, K. *Macromolecules* **1996**, *29*, 3975-3981.

Schmidt-Rohr, K. *J. Magn. Reson.* **1998**, *131*, 209-217.

Schmidt-Rohr, K.; Clauss, J.; Blumich, B.; Spiess, H. W. *Magn. Reson. Chem.* **1990**, *28*, S3-S9.

Schmidt-Rohr, K.; Clauss, J.; Spiess, H. W. *Macromolecules* **1992**, *25*, 3273-3277.

Schmidt-Rohr, K.; Spiess, H. W. *Macromolecules* **1991**, *24*, 5288-5293.

Schmidt-Rohr, K.; Spiess, H. W. *Multidimensional Solid-State NMR and Polymers*; 1st ed.; Academic Press: London, 1994.

Segerman, E. *Acta Crystallographica* **1965**, *19*, 789.

Shimizu, Y.; Harashina, Y.; Sugiura, Y.; Matsuo, M. *Macromolecules* **1995**, *28*, 6889.

Sieber, G.; Stehfest, I. *J. Prakt. Chem.* **1961**, *15*, 118.

Signer, R.; Sprecher, P. *Helv. Chim. Acta* **1947**, *30*, 1001.

Small, D. M. *Handbook of Lipid Research*; Plenum Press: New York, 1986; Vol. 4.

Smith, J. A.; Brezezinska, K. R.; Valenti, D.; Wagener, K. B. *Macromolecules* **2000**, *33*, 3781.

Soga, K. *Macromol. Symp.* **1996**, *101*, 281.

Soo, P. L.; Luo, L. B.; Maysinger, D.; Eisenberg, A. *Langmuir* **2002**, *18*, 9996-10004.

Spaleck, W. *Organometallics* **1994**, *13*, 954.

Spiess, H. W. *Chemical Reviews* **1991**, *91*, 1321-1338.

Stack, G. M.; Mandelkern, L.; Voigt-Martin, I. G. *Polym. Bull.* **1982**, *8*, 421.

Stribeck, N.; Alamo, R. G.; Mandelkern, L.; Zachmann, H. G. *Macromolecules* **1995**, *28*, 5029-5036.

Strobl, G. R. *Eur. Phys. J. E* **2000**, *3*, 165.

Till, P. H. *J. Polym. Sci.* **1957**, *24*, 301.

Torchia, D. A. *J. Magn. Reson.* **1978**, *30*, 613.

Trollsås, M.; Hedrick, J.; Mecerreyes, D.; Jérôme, R.; Dubois, P. *J. Polym. Sci., Polym. Chem. Ed.* **1998**, *36*, 3187-3192.

Trollsås, M.; Hedrick, J. L.; Mecerreyes, D.; Dubois, P.; Jérôme, R.; Ihre, H.; Hult, A. *Macromolecules* **1997**, *30*, 8508-8511.

Trollsås, M.; Hedrick, J. L.; Mecerreyes, D.; Dubois, P.; Jérôme, R.; Ihre, H.; Hult, A. *Macromolecules* **1998**, *31*, 2756-2763.

Turner-Jones, A.; Bunn, C. W. *Acta Crystallogr.* **1962**, *15*, 105.

Ueda, A. S.; Chatani, Y.; Tadokoro, H. *Polym. J.* **1971**, *2*, 387.

Vand, V. *Acta Crystallographica* **1951**, *4*, 104.

Vanden Eyde, S.; Mathot, V. B. F.; Koch, M. H. J.; Reynaers, H. *Polymer* **2000**, *41*, 4889.

VanderHart, D. L.; Perez, E. *Macromolecules* **1986**, *19*, 1902.

Voigt-Martin, I. G.; Alamo, R. G.; Mandelkern, L. *J. Polym. Sci., Polym. Phys. Ed.* **1986**, *24*, 1283.

Voigt-Martin, I. G.; Mandelkern, L. *J. Polym. Sci., Polym. Phys. Ed.* **1984**, *22*, 1901.

von Braun, J.; Kruber; Danziger *Chem. Ber.* **1916**, *49*, 2647.

Wagener, K. B.; Boncella, J. M.; MNel, J. G. *Macromolecules* **1991**, *24*, 2649.

Wagener, K. B.; Valenti, D.; Hahn, S. F. *Macromolecules* **1997**, *30*, 6688.

Whinfield, J. R. *Nature (London)* **1946**, *158*, 930.

Wilfong, R. E. *J. Polym. Sci.* **1961**, *54*, 385-410.

Yoo, E. S.; Im, S. S.; Ihn, K. J. *Bull. Korean Chem. Soc.* **1997**, *18*, 350.

Young, R. J.; Lovell, P. A. *Introduction to Polymers*; 2nd ed.; Chapman & Hill: London, 1991.

Yurev, Y.; Mikhailovskii, G.; Shapiro, S. *Zh. Obshch. Khim.* **1949**, *19*, 2217.

Zhang, X.; Li, Z.; Lu, Z.; Sun, C. *Macromolecules* **2002**, *35*, 106.

Zilm, K. W.; Grant, D. M. *J. Am. Chem. Soc.* **1981**, *103*, 2913-2922.

Zweifel, G.; Brown, H. *Organic React.* **1963**, *13*, 1.